(2)

TRANSPORT PROPERTIES OF PLASMAS IN MICROWAVE ELECTROTHERMAL THRUSTERS

By

Scott Stanley Haraburda

A THESIS

Submitted to
Michigan State University
in partial fulfillment of the requirements
for the degree of

MASTER OF SCIENCE

Department of Chemical Engineering

1990

SECURITY CLASSIFICATION OF THIS PAGE

REPORT DOCUMENTATION PAGE

Form Approved
OMB No 0704-0188
Exp Date Jun 30, 1986

1a REPORT SECURITY CLASSIFICATION	1b RESTRICTIVE MARKINGS
2a SECURITY CLASSIFICATION AUTHORITY	3 DISTRIBUTION / AVAILABILITY OF REPORT
2b DECLASSIFICATION / DOWNGRADING SCHEDULE	
4 PERFORMING ORGANIZATION REPORT NUMBER(S)	5 MONITORING ORGANIZATION REPORT NUMBER(S)
6a NAME OF PERFORMING ORGANIZATION: Student, HQDA, MILPERCEN	6b OFFICE SYMBOL (If applicable): DAPC-OPA-E
	7a NAME OF MONITORING ORGANIZATION: HQDA, MILPERCEN, ATTN: DAPC-OPA-E
6c ADDRESS (City, State, and ZIP Code): 200 Stovall Street, Alexandria, Virginia 22332	7b ADDRESS (City, State, and ZIP Code): 200 Stovall Street, Alexandria, Virginia 22332
8a NAME OF FUNDING / SPONSORING ORGANIZATION	8b OFFICE SYMBOL (If applicable)
	9 PROCUREMENT INSTRUMENT IDENTIFICATION NUMBER
8c ADDRESS (City, State, and ZIP Code)	10 SOURCE OF FUNDING NUMBERS: PROGRAM ELEMENT NO / PROJECT NO / TASK NO / WORK UNIT ACCESSION NO

11 TITLE (Include Security Classification)

TRANSPORT PROPERTIES OF PLASMAS IN MICROWAVE ELECTROTHERMAL THRUSTERS

12 PERSONAL AUTHOR(S)
Scott Stanley Haraburda, Captain, U.S. Army

13a TYPE OF REPORT	13b TIME COVERED	14 DATE OF REPORT (Year, Month, Day)	15 PAGE COUNT
FINAL-M.S. Thesis	FROM _____ TO _____	90 02 09	

16 SUPPLEMENTARY NOTATION
Approved for public release; distribution unlimited.

17 COSATI CODES			18 SUBJECT TERMS (Continue on reverse if necessary and identify by block number)
FIELD	GROUP	SUB-GROUP	M.S. Thesis, Michigan State University, NASA grant research, electric propulsion.

19 ABSTRACT (Continue on reverse if necessary and identify by block number)

The microwave electrothermal thruster is a potential propulsion system for spacecraft applications such as platform station keeping. It is a thruster which allows no contact between the electrodes and the propellant. For this thruster, the electromagnetic energy is transferred to the electrons in the plasma region of the propellant using the TM011 and TM012 modes of a microwave cavity system. The collisional processes by the electrons with the propellant causes transfer of the energy. Work was done to study these processes using several diagnostic techniques - calorimetry, photography, and spectroscopy. Experimental results of these techniques for nitrogen and helium gases are included. These diagnostic techniques are important in understanding plasma phenomena and designing practical plasma rocket thrusters. In addition, a broad theoretical background is included to provide a fundamental description of the plasma phenomena.

20 DISTRIBUTION / AVAILABILITY OF ABSTRACT	21 ABSTRACT SECURITY CLASSIFICATION
X UNCLASSIFIED/UNLIMITED ☐ SAME AS RPT ☐ DTIC USERS	
22a NAME OF RESPONSIBLE INDIVIDUAL	22b TELEPHONE (Include Area Code) / 22c OFFICE SYMBOL

DD FORM 1473, 84 MAR — 83 APR edition may be used until exhausted. All other editions are obsolete.

SECURITY CLASSIFICATION OF THIS PAGE

ABSTRACT

TRANSPORT PROPERTIES OF PLASMAS IN MICROWAVE ELECTROTHERMAL THRUSTERS

By

Scott Stanley Haraburda

The microwave electrothermal thruster is a potential propulsion system for spacecraft applications such as platform station keeping. It is a thruster which allows no contact between the electrodes and the propellant. For this thruster, the electromagnetic energy is transferred to the electrons in the plasma region of the propellant using the TM_{011} and TM_{012} modes of a microwave cavity system. The collisional processes by the electrons with the propellant causes transfer of the energy. Work was done to study these processes using several diagnostic techniques - calorimetry, photography, and spectroscopy. Experimental results of these techniques for nitrogen and helium gases are included. These diagnostic techniques are important in the understanding of plasma phenomena and the design of practical plasma rocket thrusters. In addition, a broad theoretical background is included to provide a fundamental description of the plasma phenomena.

This thesis is dedicated to my wife, Katherine Mae (Ten Have), and to my daughters, Beverly Louise, Jessica Allyson, and Christine Frances, who have and will endure the inconsistent and inhospitable environment associated with being part of a military family (a result of my voluntarily chosen profession).

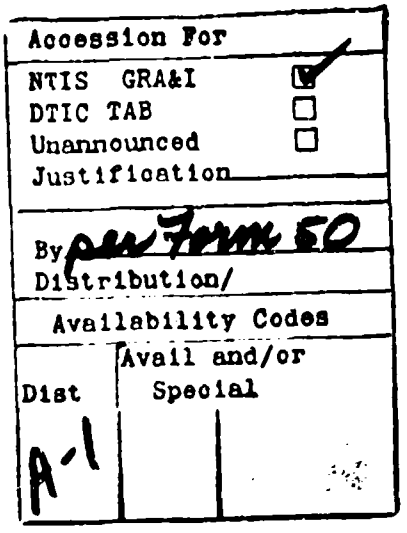

ACKNOWLEDGMENTS

The author gratefully acknowledges the encouragement and assistance received from Dr. Martin C. Hawley throughout this research. Additional thanks is given to: Jeff Hopwood for his help with experiments presented in this thesis, Marilyn Deady for her assistance in the laboratory, and the chemical engineering faculty for their guidance and instruction in understanding engineering concepts. Appreciation is given to the chemical engineering secretaries for their caring assistance in satisfying the university bureaucratic requirements (I thought it appropriate to mention them as they seem to enjoy reading these pages of one's thesis).

This research was supported in part by fully funded schooling from the United States Army under the provisions of Army Regulation 621-1 and by grants from the National Aeronautics and Space Administration - Lewis Research Center.

TABLE OF CONTENTS

LIST OF TABLES

LIST OF FIGURES

NOMENCLATURE

a	-	elliptical major axis length
A	-	neutral molecule
A^+	-	ionized molecule
A^*	-	excited molecule
A_m	-	m^{th} order constant
$\overline{A}$	-	arbitrary vector
A_{nm}	-	transition probability
b	-	elliptical minor axis length
B^+	-	ionized molecule
B^*	-	excited molecule
$\overline{B}$	-	magnetic induction (vector)
B_m	-	m^{th} order constant
$\overline{C}$	-	arbitrary vector
C_1	-	arbitrary constant
C_2	-	arbitrary constant
$\langle C \rangle$	-	average number of molecular collisions
C_m	-	m^{th} order constant
C_p	-	generic heat capacity
$C_{p,a}$	-	heat capacity of air
$C_{p,w}$	-	heat capacity of water
CRAF	-	Comet Rendezvous Asteroid Flyby
D	-	separate variable
$\overline{D}$	-	electric induction (vector)
D_m	-	m^{th} order constant
e	-	electron charge
e^-	-	electron
E	-	electrical energy
$\overline{E}$	-	electric field (vector)
E_a	-	energy absorbed by air
E_g	-	energy absorbed by gas (propellant)

E_m - m^{th} order constant
E_n - energy of electron state
E_r - radial component of $\bar{E}$
E_{rad} - energy lost by radiation
E_s - energy from microwave source
E_w - energy absorbed by microwave wall
E_x - x component of $\bar{E}$
E_y - y component of $\bar{E}$
E_z - axial component of $\bar{E}$
E_θ - angular component of $\bar{E}$
EWSK - East-West StationKeeping
$f(t)$ - time dependant function
$f(\alpha)$ - variable dependant function
F - force
F_a - flow rate of air
F_g - flow rate of gas
F_i - flow rate of energy into element
F_o - flow rate of energy out of element
F_w - flow rate of water
FES - flow of excited species
FNS - flow of neutral species
g - gravitational acceleration of earth
$g(\alpha)$ - variable dependant function
g_n - degeneracy term of transition (statistical weight)
h - Planck's constant
$\bar{H}$ - magnetic field
H_r - radial component of $\bar{H}$
H_x - x component of $\bar{H}$
H_y - y component of $\bar{H}$
H_z - axial component of $\bar{H}$
H_θ - angular component of $\bar{H}$
HCC - heat conduction / convection

I_m - measured relative emission line intensity

I_{sp} - specific impulse

INC - incremental step size in computer program

j - complex number $\left(= \sqrt{-1}\right)$

$\overline{J}$ - current density (vector)

J_m - m^{th} order Bessel function

J_0 - zero order Bessel function

k - Boltzmann constant

k_c - phasor constant

k_e - electromagnetic constant

k_z - $\frac{\partial}{\partial z}$ in phasor notation

K_i - Runge Kutta formula

L_p - microwave probe length

L_s - microwave short length

m - mass of small object; m^{th} order value

M - mass of large object

$\overline{M}$ - magnetization density (vector)

M_f - mass of spacecraft

M_0 - mass of spacecraft plus propellant

M_L - momentum loss per molecular collision

$\langle M_L \rangle$ - average momentum loss

MW - molecular weight

n_e - electron density

n_n - molecular density in neutral state

n_x - molecular density in excited state

N - gas density; normalized electron density

N_n - n^{th} order Bessel function; density of excited species

NASA - National Aeronautics and Space Administration

NSSK - North-South StationKeeping

$\overline{P}$ - polarization density (vector)

P_{cnd} - conduction power

P_{cnv} - convection power

P_e - electric field power

P_{el} - elastic collision power
P_{exc} - excitation power
P_i - incident microwave power
P_{ion} - ionization power
P_{mn} - n^{th} root of J_0
P_r - reflective microwave power
P_{rad} - radiation power
P_{rec} - electron recombination power
P_{rok} - rocket thruster power
P_{sel} - superelastic collision power
q - total charge of object
Q - partition function
Q_m - momentum cross section
r - radius within cylinder / sphere
r_e - generation rate of electrons
r_{en} - generation rate of energy
$\hat{r}$ - radial vector component
R - radius function of variable
R_0 - radius of cylinder
R_λ - spectral response function
Re[f] - real component of function
Rad - flow of radiation
RF - radio frequency
t - time
T - time function of variable
T_a - air temperature
T_e - electron temperature
T_{elc} - electronic temperature
T_0 - initial temperature
T_w - water temperature
TM_{mnp} - transverse magnetic mode
U - arbitrary variable
V - scalar velocity of object

V_a - tangential velocity of orbit

V_e - scalar electron velocity

V_g - gravitational velocity of orbit

V_p - scalar velocity of propellant

$\langle V_r \rangle$ - relative velocity of gas

$w(x)$ - weight function of integral

$\hat{x}$ - x-axis vector component

$\hat{y}$ - y-axis vector component

z - axial position in cylinder

$\hat{z}$ - axial vector component

Z - axial function of variable

$\frac{d\Omega}{4\pi}$ - solid angle

$\%E_a$ - percent energy absorbed by air coolant

$\%E_g$ - percent energy absorbed by plasma gas

$\%E_w$ - percent energy absorbed by water coolant

α - arbitrary variable

α_n - n^{th} term variable

β - arbitrary variable

β_n - n^{th} term variable

β_p - propagation constant

χ_e - electric susceptibility

χ_m - magnetic susceptibility

ε - absolute permittivity

ε_i - ionization coefficient

ε_n - laboratory collision energy

ε_0 - permittivity of free space

ε_{rel} - relative error in numerical analysis

ε_x - excitation coefficient

ε_{xi} - excited ionization coefficient

γ - electron recombination coefficient

γ_{col} - collisional e^- recombination coefficient

γ_{dis} - dissociative e^- recombination coefficient

γ_{rad} - radiative e^- recombination coefficient

γ_{rel} - fractional multiple in variable step program

$\varkappa_e$ - dielectric constant

$\varkappa_m$ - relative permeability

λ - wavelength

λ_{nm} - wavelength of transition

μ - absolute permeability

μ_m - reduced mass

μ_0 - permeability of free space

ν - wave number

ν_e - collision frequency

ν_i - ionization frequency

ν_{nm} - frequency of transition

ψ_1 - first scalar value

ψ_2 - second scalar value

ρ - charge density

θ - deflection angle of collision; cylinder angle

$\hat{\theta}$ - angular vector component

σ - electical conductivity

σ_d - differential cross section for de-excitation

σ_i - differential cross section for ionization

σ_x - differential cross section for excitation

σ_{xi} - differential cross section for excited ionization

σ_s - differential cross section for scattering

$\langle \sigma_s v_e \rangle$ - excitation rate

$\bar{v}$ - velocity of media (vector)

ω - frequency of waveform

ξ - collision frequency (recombination)

CHAPTER I

INTRODUCTION

1.1 Fourth State of Matter.

Solids, liquids, and gases are the well known three states of matter. "Solids" represent the state in which the relative motion of molecules is restricted and tends to retain a definite fixed position relative to each other, which results in a crystalline structure[1]. "Liquids" represent the state in which molecules are relatively free to change their positions about one another, while restricted by cohesive forces such that they maintain a relatively fixed volume[1]. And, "gases" represent the state in which molecules are virtually unrestricted by cohesive forces, resulting in neither definite shape nor volume[1].

A little over a hundred years ago, it was believed that another state of matter was observed. This state was characterized by an enclosed electrically neutral collection of ions, electrons, neutral atoms and molecules. It was further characterized by relatively large intermolecular distances and large internal energy in the particles[1]. The characteristics of this newly discovered matter do not fit any of the known three states of matter provided that gas does not represent a state of a collection of neutrals, ions, and electrons. Thus, it is clear that matter exists in more than three states. Commonly referred to as the "fourth state of matter," this new state is called the plasma state.

Plasmas exist in many forms. These forms range from the hot classical plasma found in the magnetospheres of

pulsars to the cold, dense degenerate quantum electron plasma of a white dwarf[2]. Usually, plasmas are characterized by a high degree of electrical conductivity[3].

A typical gas acts as a good electrical insulator. If one were to produce a plasma out of a normal gas, one would have a useful electrical component - a good conductor. With this potential usefulness, plasmas have been artificially produced in the laboratory. Some of the ways in which a plasma may be produced are shock, spark discharge, arc discharge, nuclear reaction, chemical reaction (of high specific energy), and bombardment by electromagnetic fields[3].

1.2 Plasma Applications.

Plasmas can be used for many applications. Some of these include production of nuclear fuels, research and diagnostics of medicine, research in agriculture, and environmental tracking of pollutants[2]. Compared to conventional metal combinations, the use of plasma thermocouples allows us to extract more thermoelectric power from nuclear reactors[3].

For military purposes, plasmas can be used for filtration systems in a toxic chemical environment[23]. Also, plasmas provide useful emission sources for producing emission spectra for chemical analysis. Additionally, plasmas provide a novel and useful role in jet propulsion for space flight[2].

1.3 Rocket Propulsion.

There are three major types of rocket thrusters: chemical, nuclear, and electrical.

Chemical rocket thrusters are the most commonly used type of thruster. Through chemical reactions (combustion), energy of a liquid propellant is transformed into internal energy in the form of hot, high pressure gas. These gases expand through a nozzle and form a propulsive jet[4].

Nuclear rocket thrusters require that a working fluid be present. Energy is transferred to the working fluid through temperature increases caused by the nuclear energy. This working fluid can perform one of two different functions. First, it can expand through a nozzle (similar to chemical propulsion) and act as a propulsive jet. Second, it can be converted to electrical energy for power in an electrical propulsion process. Unfortunately, the practical and political difficulties involved in using nuclear rocket propulsion are likely to hinder its development to widespread use[4].

Electrical rocket thrusters differ substantially from the other two in that the thruster must include some type of power plant to produce the electrical power for the thrust unit. This type of propulsion is useful for steering spacecraft already in space. However, electrical thrusters are not useful where gravity has a significant counteraction[5].

1.4 Microwave Induction.

Microwave induced plasmas are very efficient for uses in jet propulsion. Production of these plasmas involves using plasma columns the size of conventional resonance cavities. These cavities are stable, reproducible, and quiescent. These plasmas develop as a result of surface wave propagation and are characterized by ion immobility. The major physical processes governing the discharge are: (a) discharge conditions (such as the nature of the gas),

(b) gas pressure, (c) dimensions and material of the vessel, (d) frequency of the electromagnetic field, and (e) the power transferred to the plasma[7].

For microwave plasma electrothermal rocket thrusters, pressures of about one atmosphere and temperatures of about 1500 degrees Kelvin are being investigated. In the electromagnetic environment, free electrons are accelerated about the heavier and neutral molecules. These electrons collide with other elements or molecules of the gas to cause them to ionize as previously bound electrons are stripped off. In essence, kinetic energy is transferred from the accelerated electrons to the gas.

Figure 1.1 illustrates the various discharge properties within a microwave system. The cold propellant receives microwave energy resulting in the production of a plasma. This plasma gives off radiation and heat energy. The excited species flows away from the plasma while the cold species flows towards it. Finally, the plasma excited propellant is recombined downstream of the plasma with increased kinetic energy. This thermalized propellant exits through a nozzle as propulsion thrust.

1.3 Research Direction.

The research in this thesis is divided into three sections. The first section covers a theoretical background in the microscopic analysis of plasma physics. Additionally, a brief discussion is provided for potential plasma electric propulsion.

The next section covers an experimental study of a microwave induced plasma in a cylindrical cavity. The macroscopic power distribution, plasma dimensions, and electron temperatures are determined from measurements taken

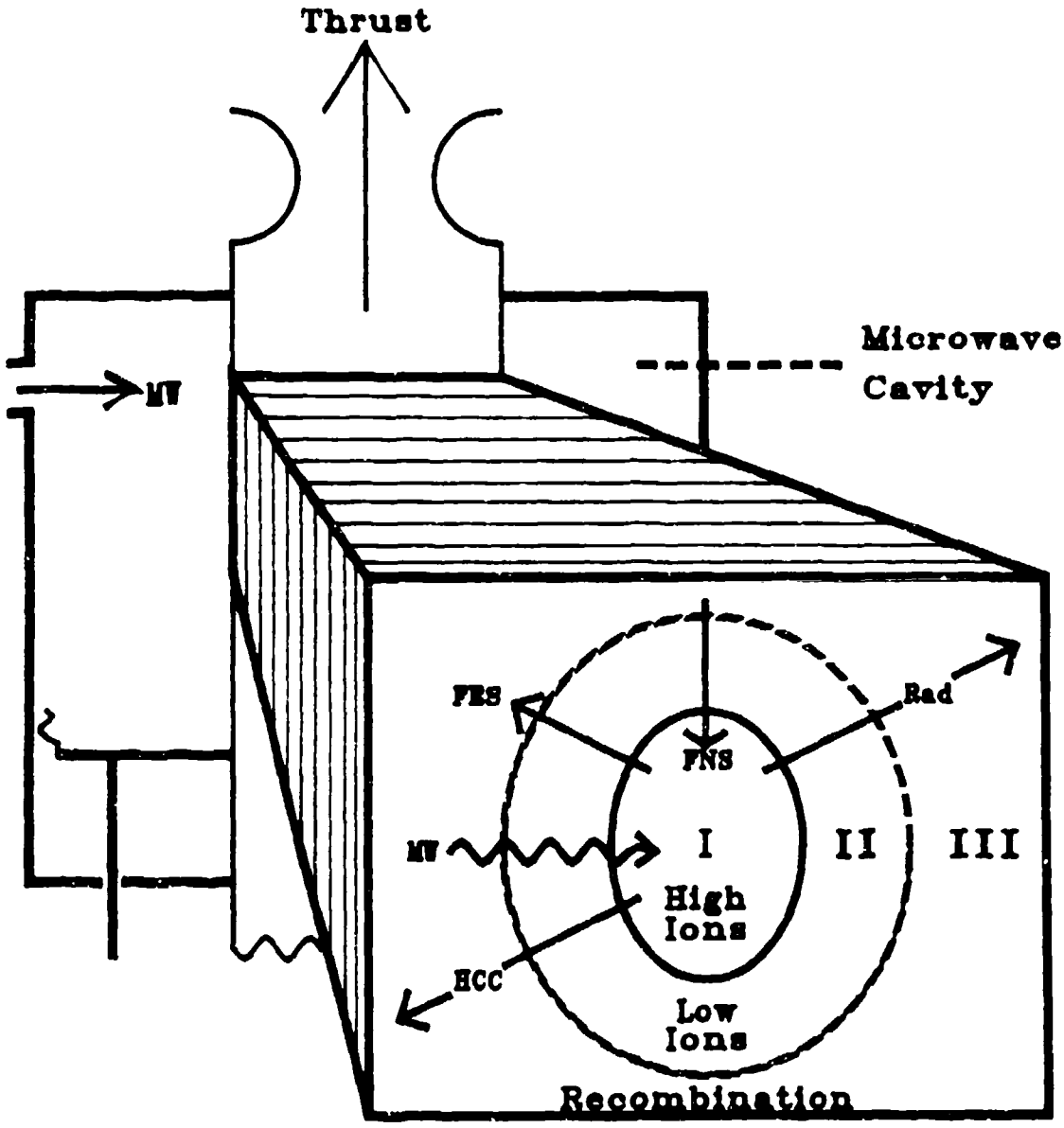

Figure 1.1 Microwave Plasma Discharge Properties

of helium and nitrogen plasmas. The pressure range is between 200-1000 torr with gas flow rates from 0-2000 SCCM. The input power varies between 200-275 watts.

The last section contains a computer analysis of the electron diffusion within the plasma area. A computer program was written to calculate the normalized electron density using the equations derived in the theoretical section. The computer simulation was used to calculate the electron gradient within the plasma discharge region. The major assumptions for this model are constant temperature and equal ion & electron densities.

CHAPTER II

THEORY

2.1 Introduction.

Modeling transport properties of the plasma region in the microwave electrothermal thruster is a dynamic process. The first section of this chapter covers rocket propulsion physics and identifies important concepts. The next section deals with the complexities involved in attempting to characterize the plasma region of the proposed thruster system. The latter section covers the theory involved in the experimental system.

2.2 Rocket Propulsion Physics.

Two different aspects, thrust and geo-centric trajectory (orbit), will be discussed. Not much detail will be given; but, several terms will be defined.

2.2.1 Thrust.

Thrust is defined as the force required to maintain velocity of expelling propellents as mass changes with respect to time[25].

$$F = V_p \frac{dm}{dt} \qquad 2.1$$

The instantaneous acceleration of a particular object is defined as the force required to change its velocity with respect to time[25].

$$F = M \frac{dV}{dt} \qquad 2.2$$

When dealing with rocket systems, those forces must be equal. When doing this, one must note that the change in mass of the propellent is the negative change in mass of the rocket.

$$dm = - dM \qquad 2.3$$

Additionally, the propellant velocity can be rewritten as[16]:

$$V_p = g\ I_{sp} \qquad 2.4$$

where I_{sp} is the specific impulse in units of time. The resulting differential equation is:

$$\frac{dm}{M} = \frac{dV}{g\ I_{sp}} \qquad 2.5$$

With M_f defined as the payload, propulsion system, and power and M_0 as M_f plus propellant, the resulting solution to the differential equation is:

$$\frac{M_f}{M_0} = \exp\left[\frac{-\Delta V}{g\ I_{sp}}\right] \qquad 2.6$$

The specific impulse is an important element required for the velocity of the rocket, as seen from equation 2.6. This specific impulse can be expressed in several ways[34].

$$I_{sp} = \frac{F}{m\ g} = \frac{Vp}{g} \qquad 2.7$$

For a final temperature of zero and isentropic expansion, the specific impulse can be calculated for pure monatomic or diatomic gas[18].

$$I_{sp} = 20.9 \sqrt{\frac{To}{MW}} \qquad \text{(monatomic)} \qquad 2.8$$

$$I_{sp} = 24.9 \sqrt{\frac{To}{MW}} \qquad \text{(diatomic)} \qquad 2.9$$

Another important aspect of specific impulse is for calculating the power requirements of the rocket thruster. Using the thrust term for force, the power needed can be calculated from the following equation:

$$P_{rok} = \frac{1}{2} F I_{sp} \qquad 2.10$$

To minimize power requirements, the appropriate propulsion should be used for its corresponding mission. For missions such as planetary lift-off, high thrust is required. For long duration orbital or interplanetary travel, high specific impulse is required. As mentioned before, chemical propulsion provides high thurst while electric propulsion provides high specific impulse.

2.2.2 Orbit.

Most applications for electric rocket systems involve platform station keeping as an orbit about a planet. Each orbit requires a different velocity. That velocity (Va) should be tangential to the orbit curvature and should have a magnitude close to the velocity resulting from the gravitational force of the planet (Vg). In other words for the specific case of a circular orbit pattern, the centrifugal force must equal gravitational acceleration. As seen in Figure 2.1, the object could orbit in either an

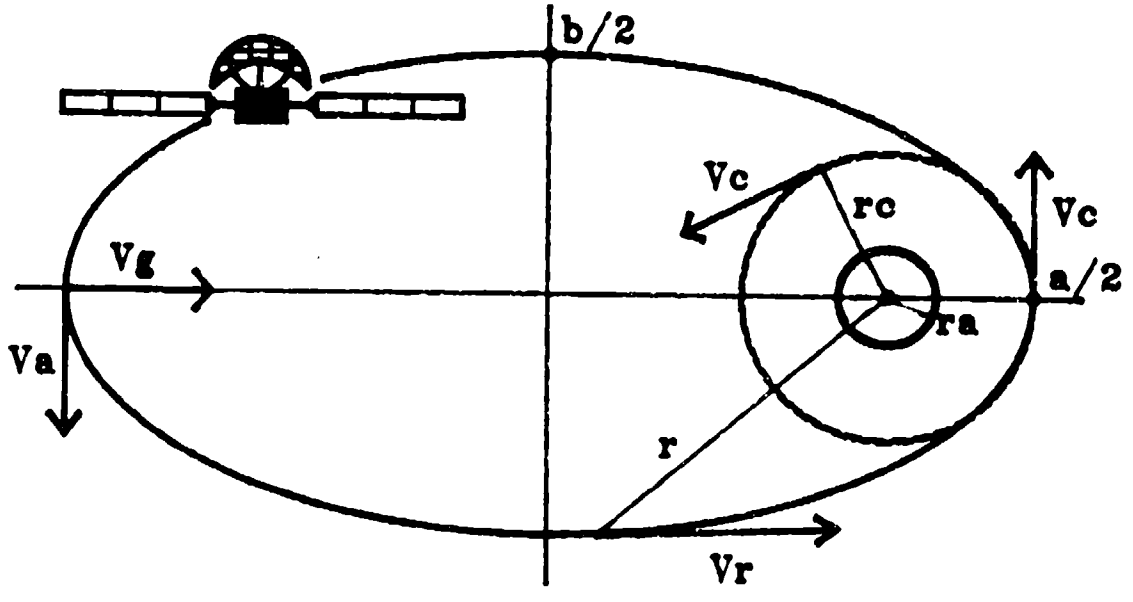

Figure 2.1 Geo-Centric Trajectory

elliptical or circular pattern. Using the nomenclature of that figure, the velocity equation needed by the rocket is:

$$v_r = \sqrt{R_e^2 \, g \left(\frac{2}{r} - \frac{1}{a} \right)} \qquad 2.11$$

The circular orbit is a special case when a = r.

2.3 Plasma Physics.

The plasma state is considered the "fourth" state of matter. As an anisotropic media in an electromagnetic environment, it is a complex region. Many types of species and reactions exist within the plasma region. An attempt is made to characterize those reactions using elementary plasma physics equations. Additionally, an elementary description of electromagnetics is provided.

Figure 1.1 depicts some of the discharge actions within a plasma. This figure schematically shows the plasma region within a microwave cavity. The center of the region (I) is highly ionized. The next region (II) is less ionized. The outer region (III) is the recombination region for excited molecules. Excited species (FES) flow outward, while neutral species (FNS) flow inward. The ions are initially propagated by incoming microwave power (MW). Finally, some energy is dissipated along the walls of the cylinder through heat by conduction / convection (HCC) and through radiation (Rad).

2.3.1 Reactions.

Reactions in this media can be viewed differently than a typical chemical reaction. For these reactions, the propagating mechanism is collision, with the reaction rate being a collision rate. The collisions can be divided into four general categories (see Figure 2.2). These four

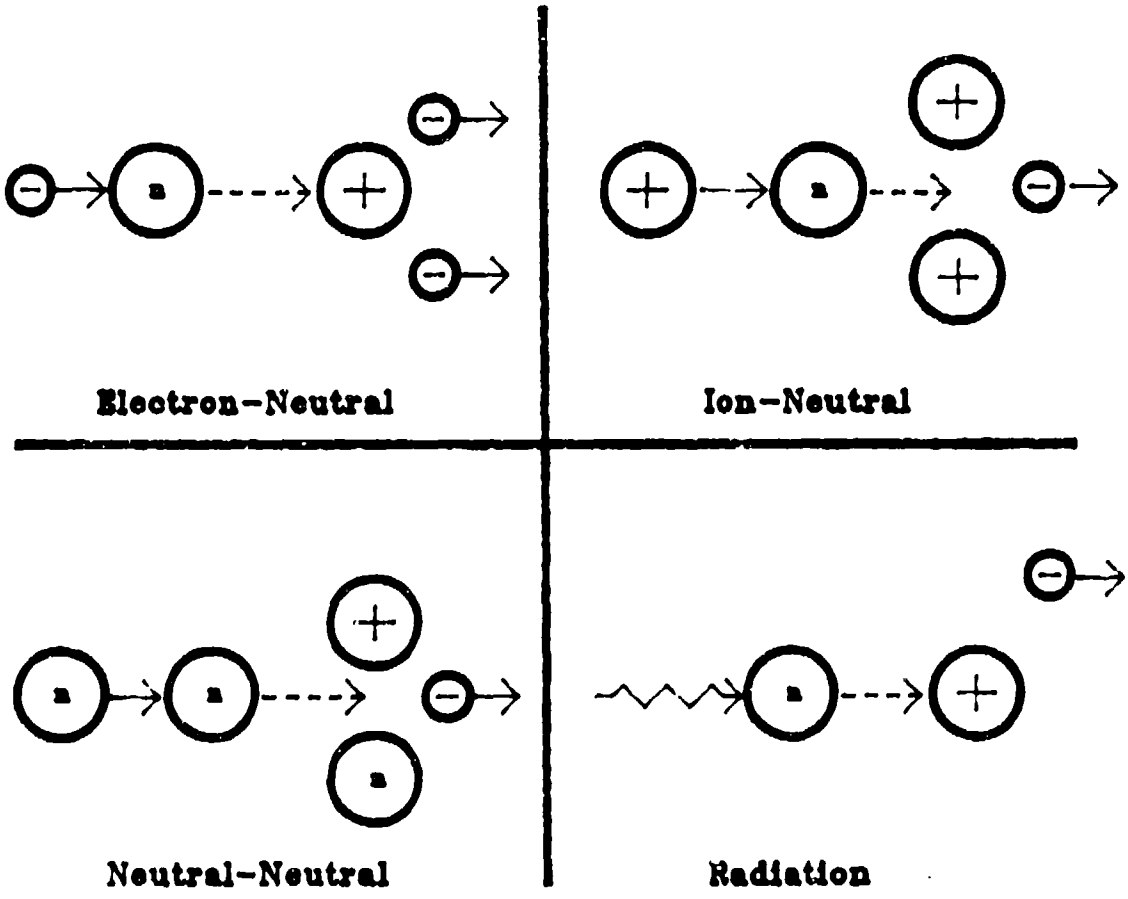

Figure 2.2 Collision Types

collision types contain the following basic reaction mechanisms[26]. Disassociation and recombination reactions for polyatomic molecules are specific cases for excitation and de-excitation reactions.

Electron - Neutral/Ion

$A + e^- \longrightarrow A^* + e^-$	electron excitation	2.12
$A^* + e^- \longrightarrow A + e^-$	electron de-excitation	2.13
$A + e^- \longrightarrow A^+ + 2e^-$	electron ionization	2.14
$A^+ + e^- \longrightarrow A + h\nu$	radiative recombination	2.15

Ion - Neutral

$A^+ + B \longrightarrow A + B^+$	electron transfer	2.16
$A^+ + A \longrightarrow 2A^+ + e^-$	ion ionization	2.17

Neutral - Neutral

$A + A \longrightarrow A^* + A$	neutral excitation	2.18
$A + A \longrightarrow A^+ + A + e^-$	neutral ionization	2.19
$A^* + B \longrightarrow A + B^*$	excitation transfer	2.20

Radiation

$A + h\nu \longrightarrow A^*$	radiative excitation	2.21
$A^* \longrightarrow A + h\nu$	radiative de-excitation	2.22
$A^* + h\nu \longrightarrow A^+ + e^-$	radiative ionization	2.23

2.3.2 Electromagnetic Field.

As implied by its name, an electromagnetic field is composed of an electric field ($\bar{E}$) and a magnetic field ($\bar{H}$). These vector fields satisfy four classic equations, known as Maxwell's equations (listed below)[30].

$$\nabla \cdot \bar{D} = \rho \qquad 2.24$$

$$\nabla \times \bar{E} = -\frac{\partial \bar{B}}{\partial t} \qquad 2.25$$

$$\nabla \times \bar{H} = \bar{J} + \frac{\partial \bar{D}}{\partial t} = \frac{\partial(\varepsilon \bar{E})}{\partial t} \qquad 2.26$$

$$\nabla \cdot \bar{B} = 0 \qquad 2.27$$

The electric induction ($\bar{D}$) is a function of $\bar{E}$, the polarization density ($\bar{P}$), and the permittivity of free space, ε_0.

$$\bar{D} = \varepsilon \bar{E} + \bar{P}_0 \qquad 2.28$$

The polarization density can be dropped from this term if we know the electric susceptibility (χ_e). The dielectric constant ($\varkappa_e$) is one plus χ_e. Therefore, the electric induction can be rewritten as follows:

$$\bar{D} = \varepsilon_0(1+\chi_e)\bar{E} = \varepsilon_0 \varkappa_e \bar{E} = \varepsilon \bar{E} \qquad 2.29$$

The magnetic induction ($\bar{B}$) is a function of $\bar{H}$, the magnetization density ($\bar{M}$), and the permeability of free space, μ_0.

$$\bar{B} = \mu_0(\bar{H} + \bar{M}) \qquad 2.30$$

Once again, the magnetization density can be dropped from this term if we know the magnetization susceptibility (χ_m). The relative permeability ($\varkappa_m$) is one plus χ_m. Therefore, the magnetic induction can be written as follows:

$$\bar{B} = \mu_0(\chi_m+1)\bar{H} = \mu_0\varkappa_m\bar{H} = \mu\bar{H} \qquad 2.31$$

The current density ($\bar{J}$) is a scalar multiple of $\bar{E}$ plus the velocity ($\bar{\upsilon}$) of the media crossed with $\bar{B}$. That scalar function is the electrical conductivity (σ).

$$\bar{J} = \sigma\bar{E} + \bar{\upsilon} \times \bar{B} = n_e\bar{\upsilon} \qquad 2.32$$

The total charge (q) of the media is the total volume integral of the charge density (ρ). For the plasma state, the q should be zero because the postive charges should equal the negative ones.

2.3.3 Conservation of Particles.

The conservation of mass must be upheld. Matter can neither be created nor destroyed. For this case, the conservation of particles can be defined as the accumulation of electrons with respect to time equal to the negative divergence of the current density plus the generation of electrons[27].

$$\frac{\partial n_e}{\partial t} = -\nabla \cdot \bar{J} + r_e \qquad 2.33$$

$$\frac{\partial n_e}{\partial t} = -\nabla \cdot (n_e\bar{\upsilon}) + r_e \qquad 2.34$$

The electron generation is composed of ionization minus deionization processes. That net generation term can be written as[28]:

$$r_e = \nu_i n_e - \alpha\, n_e n_i \qquad 2.35$$

For low pressures (roughly less than 100 torr), this generation term is commonly neglected. The resulting equation with all deionization occuring on the surface walls is:

$$\frac{\partial n_e}{\partial t} = -\nabla \cdot (n_e \bar{v}) \qquad 2.36$$

The electron density can be expressed as a function of position and time. The plasmas in this experiment were propogated in a cylindrical cavity. Using separation of variables (radial, axial, and time), the electron density can be expressed as[27]:

$$n_e = R(r)\, Z(z)\, T(t) \qquad 2.37$$

For this calculation, the electron density is assumed to be at steady state. The T(t) term drops out. Assuming only diffusional decay and no $\bar{E}$, the $n_e\bar{v}$ term was expressed as the negative scalar diffusion coefficient (D) times the gradient of the electron density. Then, equation 2.36 reduces to[27]:

$$-\nabla \cdot (n_e \bar{v}) = -\nabla \cdot (-D\nabla n_e) = D\nabla^2 n_e = 0 \qquad 2.38$$

In cylindrical coordinates (see Figure 2.3), this equation is[27]:

$$\frac{\partial^2 n_e}{\partial r^2} + \frac{\partial n_e}{r\,\partial r} + \frac{\partial^2 n_e}{r^2\,\partial\theta^2} + \frac{\partial^2 n_e}{\partial z^2} = 0 \qquad 2.39$$

Assuming radial symmetry, the electron density is not dependent upon angle. Thus, the partial of n_e with respect

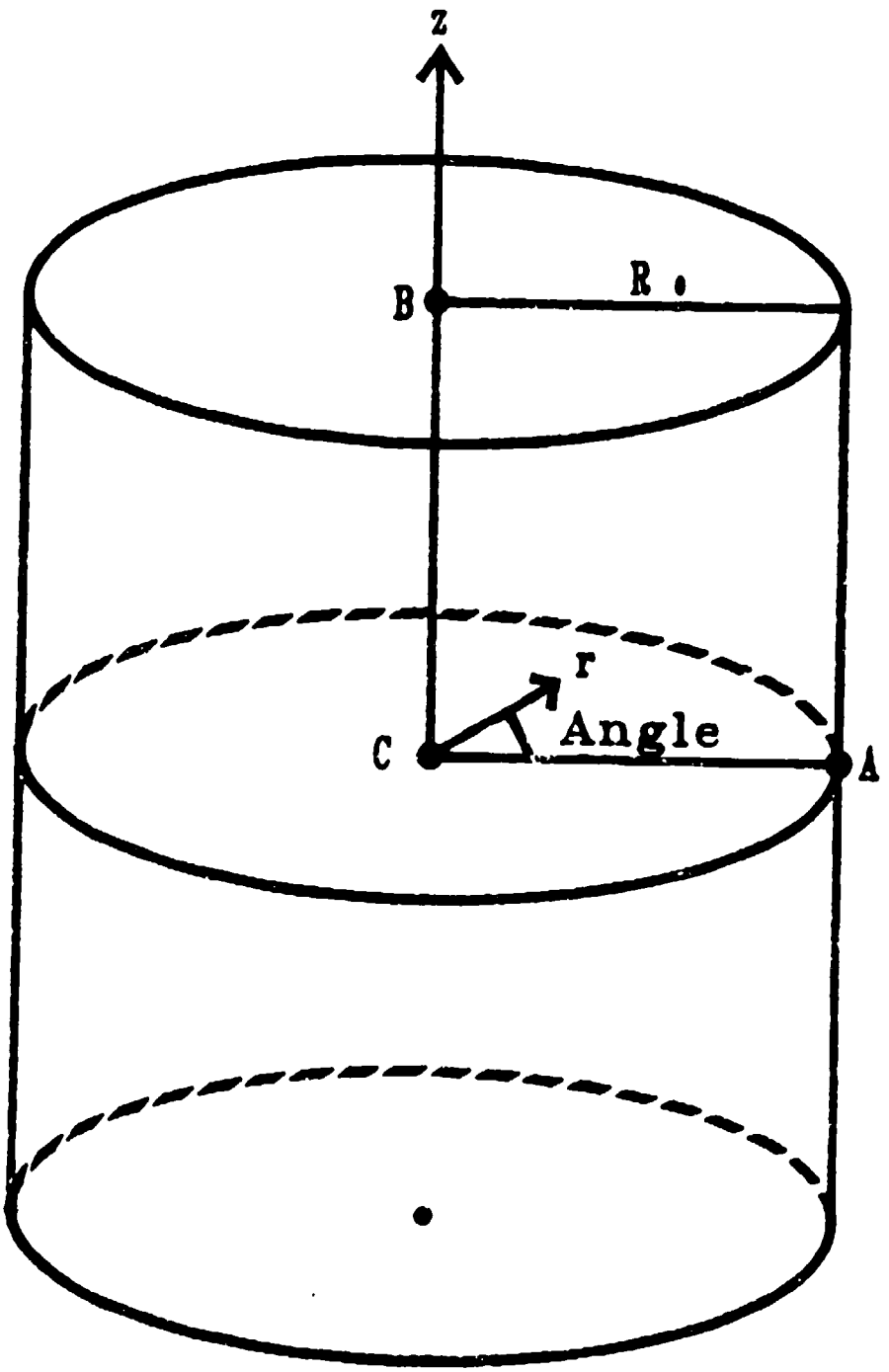

Figure 2.3 Cylindrical Cavity Coordinates

to the angle is zero. Using the separation of variables, equation 2.39 becomes[27]:

$$\frac{1}{R}\left(\frac{d^2R}{dr^2}+\frac{dR}{r\,dr}\right)+\frac{d^2Z}{Z\,dz^2}=0 \qquad 2.40$$

A solution to this equation can be found by rewriting equation 2.40 as[27]:

$$\beta^2+\alpha^2=0 \qquad 2.41$$

$$\frac{1}{R}\left(\frac{d^2R}{dr^2}+\frac{dR}{r\,dr}\right)=-\alpha^2 \qquad 2.42$$

$$\frac{d^2Z}{Z\,dz^2}=-\beta^2 \qquad 2.43$$

Equation 2.42 can be solved by using substitution of variables[27].

$$r=\frac{U}{\alpha} \qquad 2.44$$

Substituting equation 2.44 into 2.42 results in a zero order Bessel equation[27].

$$U^2\frac{d^2R}{dU^2}+U\frac{dR}{dU}+U^2R=0 \qquad 2.45$$

Using the boundary condition that the electron density is zero at r equal to the radius of the cavity, the α_n terms are the zeroes to the zero order Bessel function (J_0) of the first kind. Thus, one can write the solution to this equation as[27]:

$$R(r) = \sum_{n=1}^{\infty} B_n J_0(U_n) = \sum_{n=1}^{\infty} B_n J_0(\alpha_n r) \qquad 2.46$$

The solution to equation 2.43 is easier to find[27].

$$Z(z) = \sum_{n=1}^{\infty} C_n \, \mathrm{Cos}(\beta_n z) \qquad 2.47$$

Using the boundary condition that the electron density is zero at $z = \pm 1$ [27].

$$\beta_n = n \frac{\pi}{2} \qquad 2.48$$

Therefore, the final solution to this symmetric steady state plasma at low pressures is trivial. The result is a function of a zero order Bessel function for radial position and a cosine function for axial position[27].

$$n_e = n_{e0} \sum_{n=1}^{\infty} B_n C_n \, J_0\left(\frac{\alpha_n r}{R_0}\right) \mathrm{Cos}\left(\frac{n \pi z}{2}\right) \qquad 2.49$$

The constants $B_n C_n$ can be approximated to be normalized to that of the electron density at the center (point C), with the n_{e0} being defined as that electron density. These terms can be found by using the properties of orthogonality. Bessel functions and cosine functions are series of orthogonal terms. Thus, these terms can be calculated as:

$$B_n = \frac{2}{\alpha_n \, J_1(\alpha_n)} \qquad 2.50$$

$$C_n = \frac{4 \sin\left(\frac{n\pi}{2}\right)}{n\pi} \qquad 2.51$$

Those terms can be tabulated and are provided in Table 2.1.

Table 2.1 B_n and C_n Values of Simple Electron Density Function

n	B_n	C_n
1	1.602	1.273
2	-1.065	0.000
3	0.851	-0.424
4	-0.730	0.000

2.3.4 Conservation of Momentum.

As seen from the simple model provided by the conservation of particles, an accurate model of the plasma region can not be accomplished without accounting for electron generation. This generation involves collision physics. Equations involving conservation of momentum are needed to model the generation term in equations 2.34 and 2.35.

Classical scattering can be used to describe the momentum loss per collision, along with the average number of collisions expected within a certain region (see Figure 2.4). The average momentum loss per collision can be expressed by the following[27]:

$$M_L = \mu_m \nu_e (1 - \cos\theta) \qquad 2.52$$

The average number of collision expected between the deflection angle of collision (θ) and $\theta + d\theta$ is[27]:

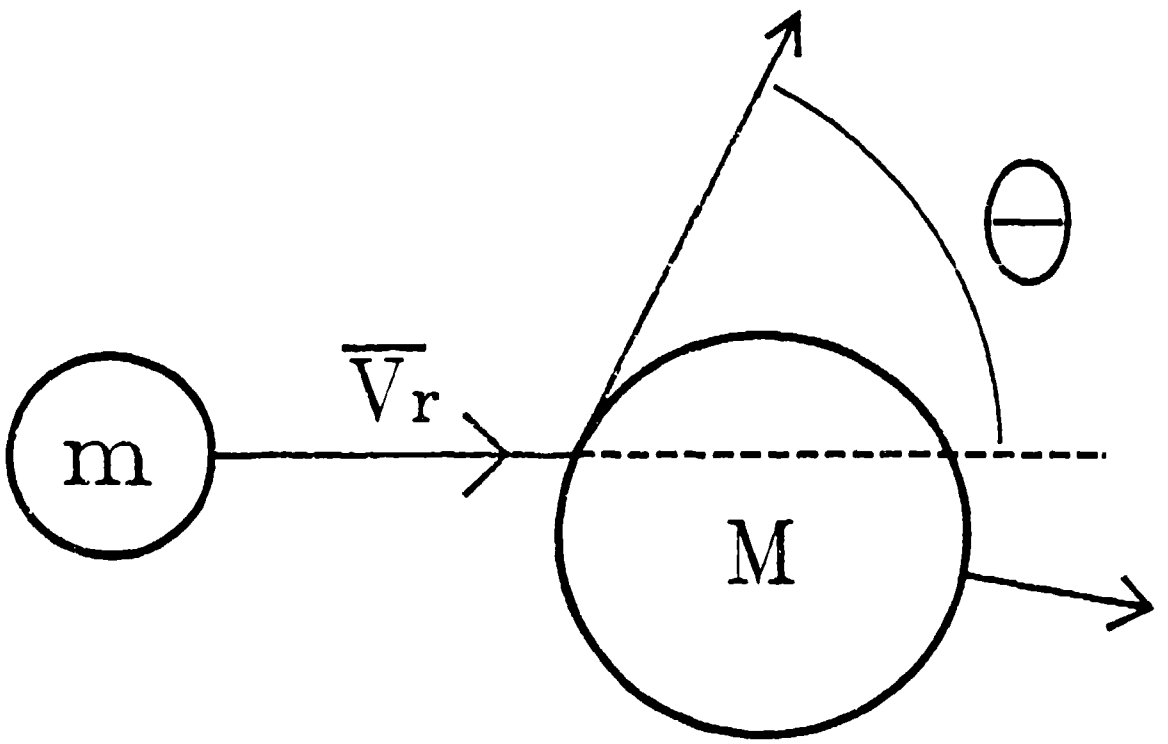

Figure 2.4 Classical Scattering Diagram

$$\langle C \rangle = N \bar{V}_r 2 \pi \sigma_s \sin\theta \, d\theta \qquad 2.53$$

The average momentum loss can be found by integrating the momentum loss times the average collision over all of θ. To simplify the expression, a momentum cross section term (Q_m) is defined as[28]:

$$Q_m = 2 \pi \int_0^{\pi} (1 - \cos \theta) \sin \theta \, \sigma \, d\theta \qquad 2.54$$

Using this cross section term, the average momentum loss can be expressed by the following equation[28]:

$$\langle M \rangle = \mu_m \nu_e N \bar{V}_r Q_m \qquad 2.55$$

The scattering differential cross section can be expressed considering only coulomb collisions. For this type of collision, the cross section can be calculated from the differential element[28]:

$$\sigma_s = \frac{d\sigma}{d\Omega} = \left(\frac{e_1 \, e_2}{8 \pi \varepsilon_0 \, m \, V_e^2 \sin^2 \left(\frac{\theta}{2} \right)} \right) \qquad 2.56$$

The collision frequency (υ_1) can now be defined[28].

$$\upsilon_1 = \frac{\langle M_1 \rangle}{\mu \nu_e} = N \langle \sigma V_e \rangle \qquad 2.57$$

The excitation rate $\langle \sigma V_e \rangle$ can be broken down into specific excitation or de-excitation terms. The following equation should hold true[28]:

$$\langle \sigma_{1,0} V_e \rangle = \frac{n_0}{n_1} \langle \sigma_{0,1} V_e \rangle \qquad 2.58$$

Experimentally, the Q_m cross section term can be found from ion beam scattering using the following expression[27]:

$$Q_m \approx 2 (a_1 - a_2 \ln \varepsilon_n)^2 = 2 Q_{ex} \qquad 2.59$$

The Q_{ex} is the total cross section for charge exchange. The a_2 term is calculated from the linearity of $Q_{ex}^{1/2}$ versus the log of ε_n where ε_n is the laboratory collision energy. A complete explanation of the theory and experimental procedure of ion beam scattering may be found in Mason and McDonald's book[27].

Deionization is needed to complete the conservation of momentum. Electron recombination is the process of deionization. This recombination is highly dependant upon the electron temperature (T_e). For simplicity, only approximations will be given for three primary types of recombinations (radiative, dissociative, and collisional)[27]. These values are approximated from experimental data of gases in various environments.

$$\gamma_{rad} = T_e^{-0.7} \qquad 2.60$$

$$\gamma_{dis} = T_e^{-0.5} \qquad 2.61$$

$$\gamma_{col} = T_e^{-4.5} \qquad 2.62$$

2.3.5 Conservation of Energy.

Another important aspect of modeling the plasma region is developing an accurate model showing the temperature gradient within the plasma. The conservation of energy equation can be used for this model. This energy equation can be written on a differential element of the plasma at the microscopic level. The accumulation of energy ($\partial E/\partial t$) is equal to the flow of energy in (F_i) minus the flow of

energy out (F_o) plus the generation of energy (r_{en}) within the differential element[9].

$$\frac{\partial E}{\partial t} = F_i - F_0 + r_{en} \qquad 2.63$$

This energy can be expressed in terms of power at the microscopic level. The flow terms and the generation term can be sub-divided by the following power terms[28]:

$$F_i - F_0 = P_{rad} + P_{cnd} + P_{cnv} \qquad 2.64$$

$$r_{en} = P_e + P_{rec} + P_{sel} - P_{el} - P_{exc} - P_{ion} \qquad 2.65$$

The radiation, conduction, and convection terms are functions of temperature, heat capacity, and boundary conditions (such as cavity wall temperature and material type)[9]. The electron recombination term may be neglected for low pressures. The electric field power can be written as[28]:

$$P_e = \sigma E^2 \qquad 2.66$$

with the conductivity coefficient written as[28]:

$$\sigma = \frac{n_e e^2}{m (\xi + j\omega)} \qquad 2.67$$

The excitation and ionization terms are functions of the density of the species and of their excitation / ionization rates. These two terms can be written for the electron as[28]:

$$P_{exc} = n_e n_n \varepsilon_x \langle \sigma_x v_e \rangle \qquad 2.68$$

$$P_{ion} = n_e n_n \varepsilon_i \langle \sigma_i v_e \rangle + n_e n_x \varepsilon_{xi} \langle \sigma_{xi} v_e \rangle \qquad 2.69$$

Finally, the collision terms provide both generation and degeneration of energy. The generation type involves superelastic (or de-excitation) collisions and can be express as[28]:

$$P_{sel} = n_e\, n_x\, \varepsilon_x\, \langle \sigma_d \upsilon_e \rangle \qquad 2.70$$

The degeneration term involves elastic collisions of electrons and neutral species which can be expressed as[28]:

$$P_{el} = n_e\, n_n \left(\frac{2m}{M}\right) \langle \sigma_s \upsilon_e \rangle \qquad 2.71$$

2.4 Discharge Properties.

2.4.1 Energy Distribution

The measurement of the energy distribution for this research involved a macroscopic frame of reference. The macroscopic energy balance only covers energy entering and leaving the entire system. The system is defined as the microwave resonance cavity (see Figure 2.4). An energy balance written around this system can be written as[9]:

$$E_s = E_g + E_a + E_w + E_r \qquad 2.72$$

E_s is the energy entering the system from the microwave power source and is represented by the following expression:

$$E_s = P_i - P_r \qquad 2.73$$

E_a is the energy absorbed by the air cooling and is measured by the air flow rate (F_a) and its temperature rise (ΔT_a) using the following equation (assuming the heat capacity, $C_{p,a}$, is constant over the temperature range)[9]:

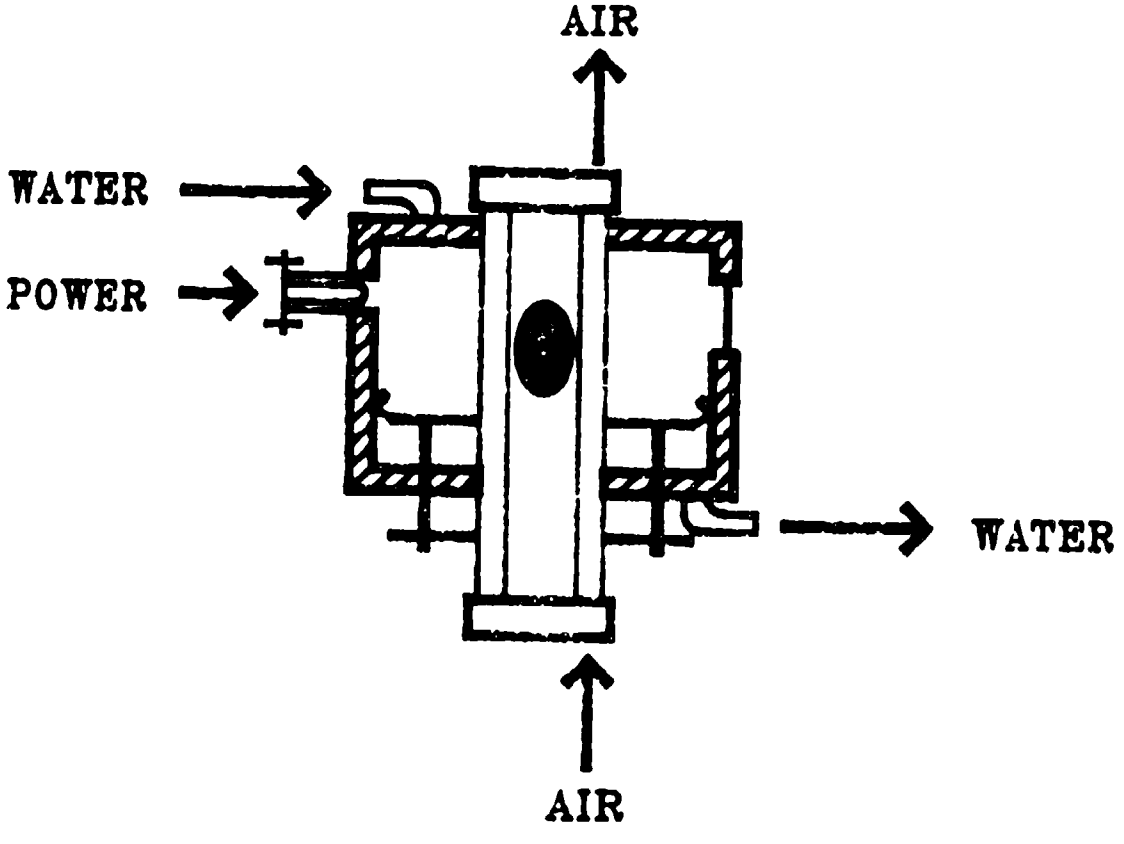

Figure 2.5 Calorimetry System

$$E_a = C_{p,a} F_a \Delta T_a \qquad 2.74$$

E_w is the energy absorbed by the water cooling and is measured by the water flow rate (F_w) and its temperature rise (ΔT_w) using an equation similar to 2.74. E_r is the energy escaping the system as emission radiation. Because the system is almost entirely enclosed, this radiation is neglected. Rearranging the above equations yields the following:

$$E_g = P_i - P_r - C_{p,a} F_a \Delta T_a - C_{p,w} F_w \Delta T_w \qquad 2.75$$

For this research, the above energy expressions are reported in percentages, as opposed to absolute values. The following equations indicate how these values are computed:

$$\%E_a = \frac{E_a}{E_s} \times 100\% \qquad 2.76$$

$$\%E_w = \frac{E_w}{E_s} \times 100\% \qquad 2.77$$

$$\%E_g = \frac{E_g}{E_s} \times 100\% \qquad 2.78$$

As determined from reading (measurement) errors and statistical deviations, the following absolute error range estimates are provided: 2% for both air and water energy, 3% for power source energy, and a composite of 7% for gas energy. These percentages are given with respect to the microwave source energy.

2.4.2 Electromagnetic Resonator Modes in Microwave Cavity

The experiments for this thesis use a cylindrical cavity resonator. A transverse magnetic (TM_{mnp}) mode is

used. To understand the electromagnetic field in the cavity, one must analyze the three cylindrical components of the electric ($\bar{E}$) and magnetic ($\bar{H}$) fields. For a circular TM_{mnp} mode, the axial (z) component of the magnetic field (H_z) is zero.

A solution to Maxwell's equations will be calculated using phasors to characterize the time dependance of the wave fields. Before solving Maxwell's equations for the waveform, it may be clearer to define a few constants (terms).

$$k_e = \omega \sqrt{\mu\epsilon} \qquad 2.79$$

$$k_z = \frac{\partial}{\partial t} = j\omega \qquad \text{(phasor constant)} \qquad 2.80$$

$$k_c = \sqrt{k_e^2 + k_z^2} \qquad 2.81$$

$$\beta_p = \sqrt{k_c^2 - \left(\frac{P_{mn}}{R_0}\right)^2} \qquad 2.82$$

Using Maxwell's equations (number 2.27 and 2.28) and equation 2.31, one could calculate the electric and magnetic fields in the cavity. First, one must calculate the waveguide equations before considering the resonator. Using the boundary condition that H_z is zero, the radial (r) and angular (θ) components of the electric and magnetic fields are calculated as follows (in phasor and cylindrical coordinates)[33]:

$$\frac{\partial E_z}{r\,\partial\theta} - k_z E_\theta = -j\omega\mu H_r \qquad 2.83$$

$$k_z E_r - \frac{\partial E_z}{\partial r} = -j\omega\mu H_\theta \qquad 2.84$$

$$-k_z H_\theta = j \omega \epsilon E_r \qquad 2.85$$

$$k_z H_r = j \omega \epsilon E_\theta \qquad 2.86$$

These four equations can be simplified by separating the unknown field components and rewriting them as functions of one variable (E_z). The following are the simplified equations[33]:

$$E_r = \frac{k_z \partial E_z}{k_c^2 \partial r} \qquad 2.87$$

$$E_\theta = \frac{k_z \partial E_z}{k_c^2 r \partial \theta} \qquad 2.88$$

$$H_r = \frac{j \omega \epsilon \partial E_z}{k_c^2 r \partial \theta} \qquad 2.89$$

$$H_\theta = -\frac{j \omega \epsilon \partial E_z}{k_c^2 \partial r} \qquad 2.90$$

The solution to the above equations could easily be calculated if we knew E_z. Using the Laplacian operation (∇^2) and separation of variables (radial and axial functions) on E_z, we can derive a general solution. This derivation is similar to that done in section 2.3.3. The following is the general solution to $\nabla^2 E_z = 0$ [33].

$$E_z = \left[C_m J_m(k_c r) + D_m N_m(k_c r)\right]\left[A_m \sin(m\theta) + B_m \cos(m\theta)\right]\exp(k_z z) \qquad 2.91$$

For finite values at the origin (r=0), one obtains a reduced solution for E_z [33].

$$E_z = B_m C_m J_m(k_c r) \cos(m\theta) \exp(k_z z) \qquad 2.92$$

$$E_z = E_m J_m(k_c r) \cos(m\theta) \exp(\mp j \beta_p z) \qquad 2.93$$

Therefore, the remaining five components of this waveform are:

$$E_r = \frac{j\beta_p R_0^2 E_1}{P_{mn}^2}\left[\frac{m}{r}J_m\left(\frac{P_{mn}r}{R_0}\right) - \frac{P_{mn}}{R_0}J_{m+1}\left(\frac{P_{mn}r}{R_0}\right)\right]\cos(m\theta)\exp(j\beta_p z) \quad 2.94$$

$$E_\theta = \frac{-j\beta_p R_0^2 m E_1 J_m\left(\frac{P_{mn}r}{R_0}\right)}{P_{mn}^2 R_0}\sin(m\theta)\exp(j\beta_p z) \quad 2.95$$

$$H_r = \frac{-j\omega\varepsilon R_0^2 m E_1 J_m\left(\frac{P_{mn}r}{R_0}\right)}{P_{mn}^2 R_0}\sin(m\theta)\exp(j\beta_p z) \quad 2.96$$

$$H_\theta = \frac{-j\omega\varepsilon R_0^2 E_1}{P_{mn}^2}\left[\frac{m}{r}J_m\left(\frac{P_{mn}r}{R_0}\right) - \frac{P_{mn}}{R_0}J_{m+1}\left(\frac{P_{mn}r}{R_0}\right)\right]\cos(m\theta)\exp(j\beta_p z) \quad 2.97$$

$$H_z = 0 \quad 2.98$$

A table showing the m^{th} zero of $J_m(P_{mn})$ follows. The waveform is characterized by this zero and is written as TM_{mn}.

Table 2.2 m^{th} Zero of $J_n(P_{mn})$

	n			
m	0	1	2	3
1	2.405	3.832	5.136	6.380
2	5.520	7.016	8.417	9.761
3	8.654	10.173	11.620	13.015
4	11.792	13.323	14.796	16.200

For a resonator, one must consider boundary conditions for E_z at the base and height of the cavity. For $z=0$ and $z=L_s$ (L_s equals the height of the cavity - otherwise known as the microwave short length), the following is true:

$$E_z = 0 \qquad 2.99$$

For the radius at the edge of the cavity ($r=R_0$), the electric field reaches a maximum value.

$$\frac{\partial E_z}{\partial r} = 0 \qquad 2.100$$

The exponential term of E_z (see equation 2.93) may be transformed to a sine function of z if we take the following value for the propagation constant:

$$\beta_p = \frac{p\,\pi}{L_s} \qquad 2.101$$

The E_z term then reduces to:

$$E_z = E_m J_m(k_c r) \cos(n\theta) \sin\left(\frac{p\,\pi\,z}{L_s}\right) \qquad 2.102$$

Thus, the solution to this equation defines a TM_{mnp} mode. Additionally, the frequency of the microwave must be known to calculate k_c (see equations 2.79 through 2.82). The frequency (ω) is 2.45 GHz. This frequency also characterizes the electric and magnetic field components. For this experiment, TM_{011} and TM_{012} modes were used (see Figure 2.5 for wave patterns of those modes).

2.4.3 Spectroscopic Analysis.

Free electrons are an integral part of a plasma[39]. Thus, ionization and deionization processes within a plasma occur frequently and may be thought of as the plasma's

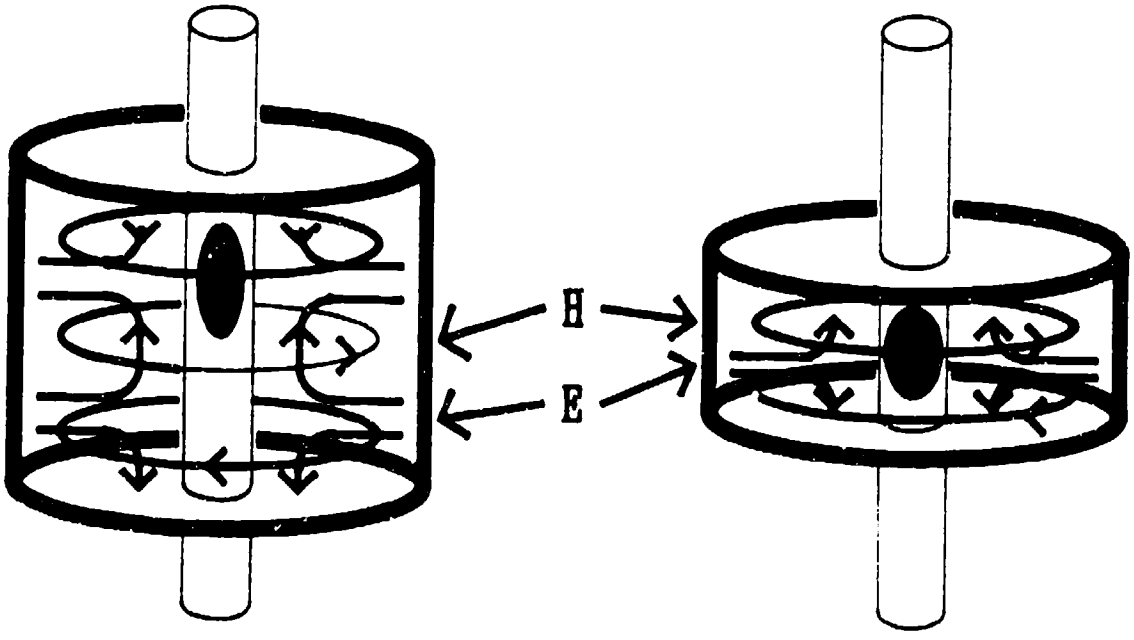

TM_{012} TM_{011}

Figure 2.6 Experimental TM Modes

sustainment (or driving force). As such, the electron temperature can be seen as one of the few properties characterizing the state of a plasma. One way to measure the electron temperature is through spectroscopy.

There are two distinct methods for conducting spectroscopic measurements, absorption and emission. For this research, emission spectroscopy is used. The spectrometer detects the spectral lines emitted by the gas as the atom decays from the excited state to the ground state. In the plasma, the atoms are excited from electromagnetic radiation and from collisions of species[38].

The intensity of the spectral line is determined by two factors, the Boltzmann distribution and the transmission moment (with Einstein coefficients). The Boltzmann distribution law characterizes the population of various excited levels (N_n) using the following equation (with the degeneracy term, g_n, added)[38]:

$$N_n = g_n N \exp\left(\frac{-E_n}{k T}\right) \qquad 2.103$$

The transition moments are determined through the interactions of the species with the emitted radiation. Using the relative emission line intensities for spectroscopic measurements, an emission line intensity going through the spectrometer can be given by[8]:

$$I_m = \frac{N h g_n A_{nm} R_\lambda \nu_{nm} d\Omega}{Q 4\pi} \exp\left(\frac{-E_n}{k T}\right) \qquad 2.104$$

For ground state transitions when Q becomes independent of temperatures, this equation can be reduced to provide an easier equation to calculate the electronic temperature.

$$\ln\left(\frac{I_m \lambda_{nm}}{R_\lambda g_n A_{nm}}\right) = \text{constant} - \frac{E_n}{k T_{elc}} \qquad 2.105$$

For this thesis, local thermal equilibrium is assumed. Although this assumption may not provide accurate results, it does allow for a quick "ball-park" calculation of the electron temperature. This assumption allows us to assume that the electron temperature is approximately equal to the electronic (excitation) temperature.

$$T_e \approx T_{elc} \qquad 2.106$$

Errors are involved in this techinique to measure the electronic temperature. Although we can easily measure the relative population of an excited species, the absolute value is not accurately obtained. This comes from the procedure of measuring relative emision line. An absolute emision line can not be measured in this spectroscopy experiment. Additionally, emission spectroscopy does not provide information about the ground state species, which happens to be the most populated state. According to an analysis by Chapman, we can expect errors in excess of 50% because of these limitations[8].

A better way of measuring the electron temperature is measuring line width species such as hydrogen which undergoes a linear Stark broadening and which does not assume local thermal equilibrium.

CHAPTER III

ELECTRIC PROPULSION

3.1 Characteristics.

Electrical propulsion systems use charged particles accelerated by an electric field as a working fluid. These systems are capable of creating greater specific impulses than chemical or nuclear propulsion systems. Likewise, this capability further supports their suitability for steering rockets in space. There are three basic types of electric rocket thrusters: electrothermal, electrostatic, and electromagnetic[4].

Electrothermal thrusters use electric energy to power an arc or resistance heater to heat a conventional working fluid. Ions or colloidal particles make up the working fluid in an electrostatic system and are accelerated by an electrostatic field. Finally, a travelling magnetic and electric field system accelerates a plasma in an electromagnetic system.

3.2 Propellants.

As mentioned in chapter two, specific impulse is an important parameter for propulsion systems. A higher specific impulse means lower propellant flow rate to produce a given thrust (see equations 2.1 and 2.4). In comparison, chemical systems have specific impulses in the range of 250 - 450 seconds, while electric systems have the range of 300 - 5000* seconds[20].

On the negative side, electric propulsion systems are characterized by low thrust[20]. In other words, these systems do not possess the force needed to quickly overcome a strong gravitational counteraction. This requires longer operations to achieve the desired velocity change than chemical propulsion. For example, a mission may require several hours of operation per day for electric propulsion. An equivalent mission for chemical propulsion would require several minutes per week.

Why is propellant amount so important? The propellant is a major factor in the cost of a spacecraft mission. In one example, the propellant accounted for 43% of the mass in the Galileo mission. In another example, 76% of the mass in the Comet Rendezvous Asteroid Flyby (CRAF) mission was propellant.

3.3 Applications.

Currently, electrothermal propulsion performs North-South StationKeeping (NSSK) on many geosynchronous satellites[16,21]. American Telephone & Telegraph Company (AT&T) include electric propulsion options on their newest satellites - Telstar IV. This type of propulsion will be used on the Space Station Freedom as well as other man occupied platforms[16,21].

Figure 3.1 schematically illustrates a basic NSSK satellite. The solar panels (power source) define the North-South axis. For a NSSK, the rocket thrusters act in the direction of the solar panels. This thruster configuration is more efficient than East-West StationKeeping (EWSK). Typically, two pairs of rocket thrusters are used. These pairs are located at the north and south side of the satellite. Although only one

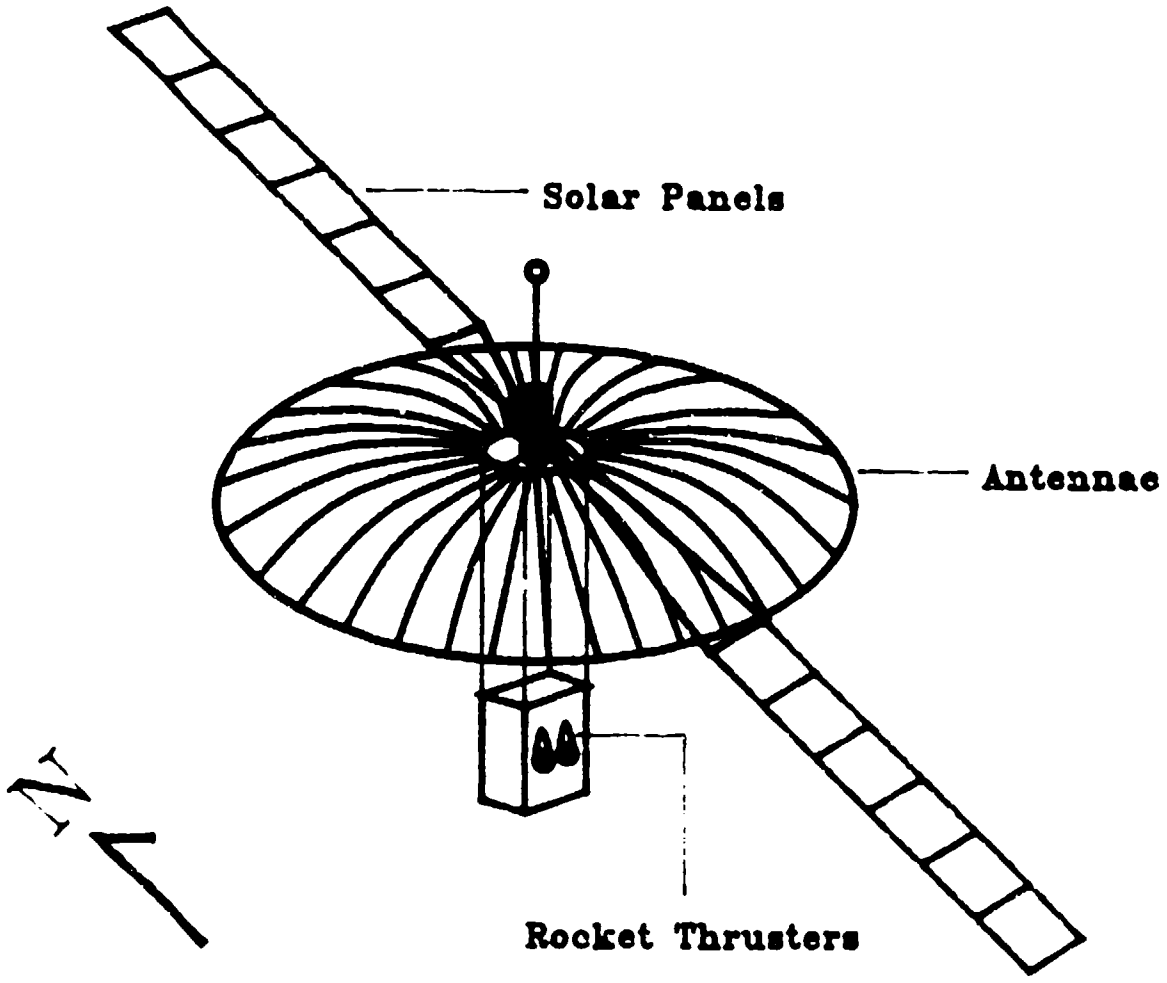

Figure 3.1 NSSK Satellite

thruster is needed for each side, two are used with one as a backup in case the other malfunctions.

Propellant contamination is also a concern for application purposes. Problems arise when communication must be transmitted through some portion of the thruster plume. The radio frequency (RF) signal may interact with charged species of that plume. This interaction is serious as the following may occur: reflection of the signal, attenuation and phase shift of the signal, or generation of noise in the signal.

3.4 Proposed System.

One type of electrothermal propulsion system uses a microwave induced plasma[6]. Although this system uses an electromagnetic environment, it is classified as an electrothermal because it uses a nozzle (not the electromagnetic field) to accelerate the propellant. Schematically shown in Figure 3.2 is a version of this system.

The power is beamed to the spacecraft from an outside source (such as a space station or planetary base) as microwave or millimeter wave power. This power is focused onto a resonant cavity to sustain a plasma in the working fluid via heating it. The hot gas would expand through a nozzle to produce thrust. Alternately in a self-contained situation, power from solar panels or from nuclear reaction could be used to run a microwave frequency oscillator to sustain the plasma.

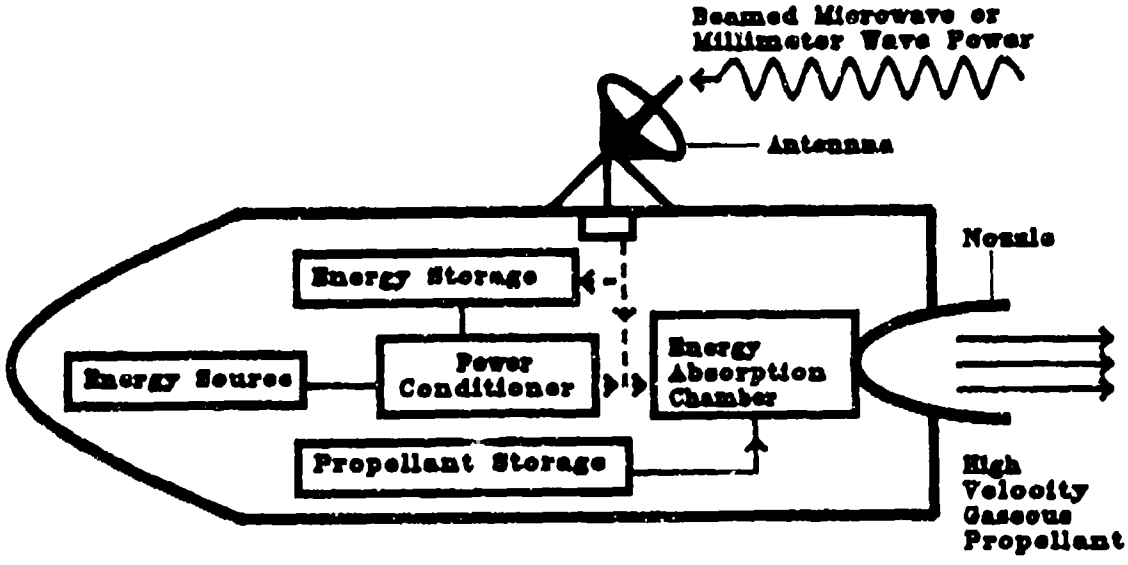

Figure 3.2 Electrothermal Propulsion System

CHAPTER IV

EXPERIMENTAL SYSTEM

4.1 Introduction.

The system used in this experiment was designed to conduct diagnostic measurements of three elements of plasma characteristics. At the macroscopic level, the power distribution and plasma dimensions were determined using thermocouples and visual photography respectively. And at the microscopic level, the electron temperature were measured using an optical emission spectrometer. See Figure 4.1 for the overall set-up.

4.2 Microwave Cavity.

An electromagnetic system was needed to generate a plasma. The microwave cavity body was made from a 17.8 cm inner diameter brass tube. As seen in Figure 4.2, the cavity contained a sliding short and a coupling probe (the two major mechanical moving parts of the cavity). The movement of this short allowed the cavity to have a length varying from 6 to 16 cm. The coupling probe acted as an antenna which transmitted the microwave power to the cavity. The sliding short and coupling probe were adjusted (or moved) to obtain the desired resonant mode. A resonant mode represents an eigenvalue of the solution to Maxwell's equations. Two separate resonance modes were used in these experiments: TM_{011} (L_s = 7.2 cm) and TM_{012} (L_s = 14.4 cm)[8].

Additional features of this cavity included: two copper screen windows located at 90 degree angles from the coupling probe (which allowed photographic and spectral

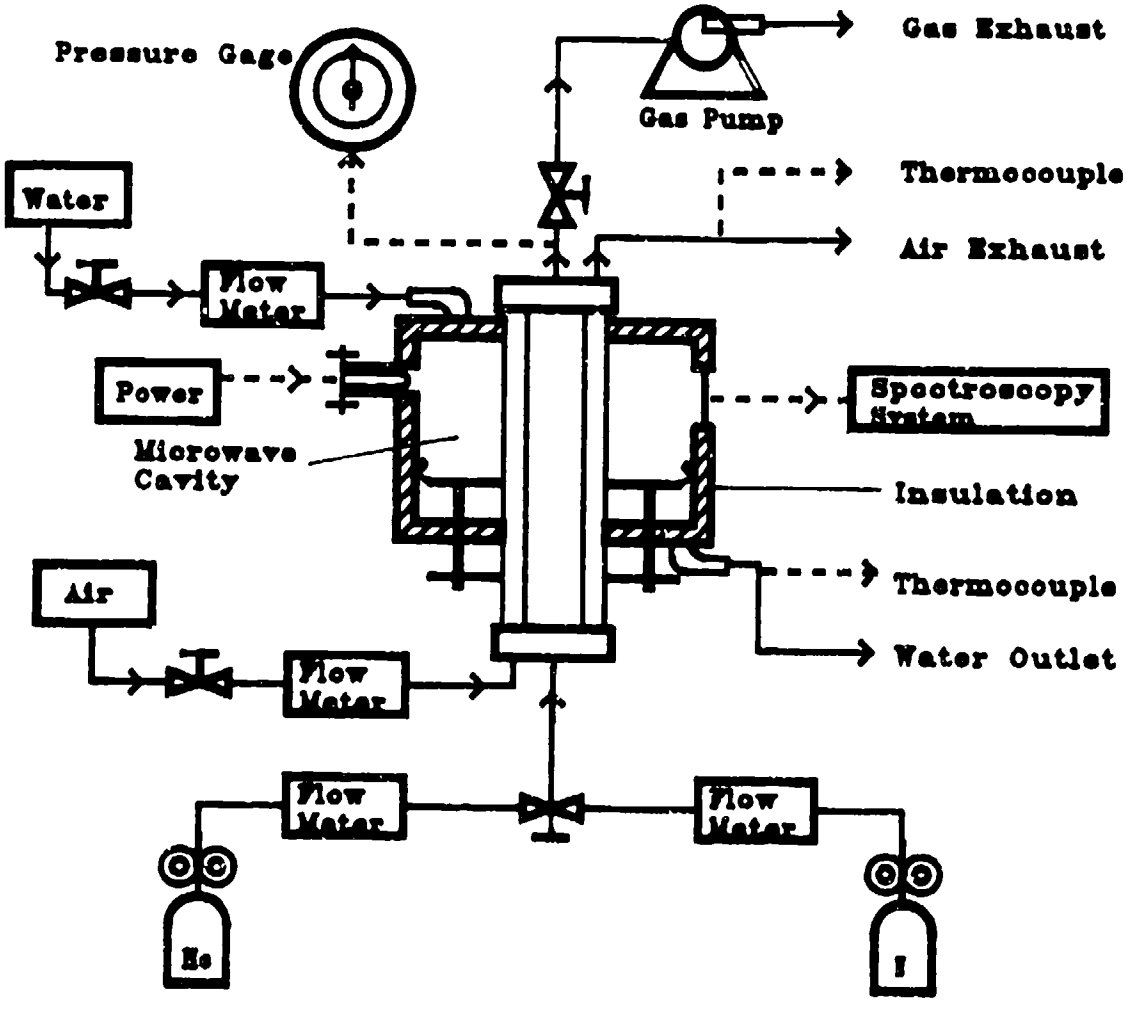

Figure 4.1 Experimental Set-up

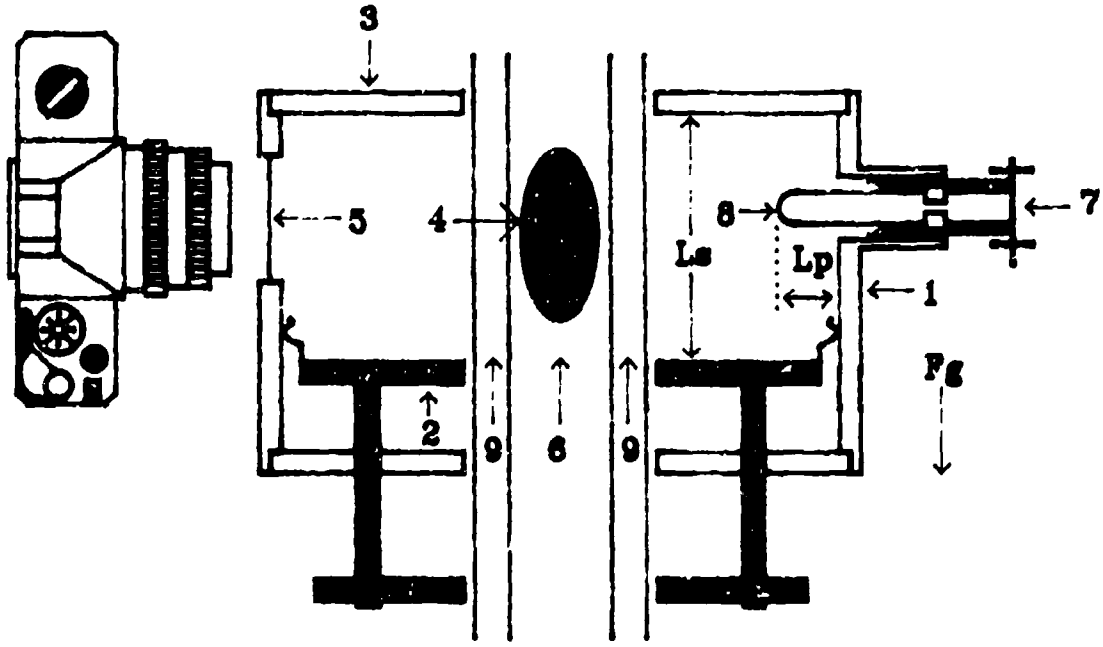

LEGEND

1.	Cavity Wall	7.	Microwave Power
2.	Sliding Short	8.	Coupling Probe
3.	Base Plate	9.	Air Cooling Chamber
4.	Plasma Discharge	Fg.	Gravity Force
5.	Viewing Window	Lp.	Probe Length
6.	Discharge Chamber	Ls.	Short Length

Figure 4.2 Microwave Cavity

measurements), and two circular holes (in both the base and top plates) to allow propellant and cooling air flows through the cavity.

4.3 Plasma Containment.

The plasma was generated in quartz tubes placed within the cavity (see Figure 4.3). The inner tube is 33 mm outer diameter and was used for the propellant flow. The outer tube was 50 mm outer diameter and was used for air cooling of the inner tube. Both tubes were about 2 1/2 feet long and was epoxied to aluminum collars. These collars fed the gas and air to and from the cavity. For additional protection, water cooling was done on the collar downstream of the cavity.

4.4 Flow System.

Flow of 99.99% pure nitrogen and helium was controlled using a back pressure regulator and a 3/4 inch valve in front of the vacuum pump. A Heise gauge with a range from 1-1600 torr was used to measure the pressure of the plasma chamber. Four sets of flow meters were used to measure the gas, water, and air flows. Thermocouples were used to measure the temperature of the air and water both entering and exiting the cavity.

4.5 Microwave Power.

A Micro-Now 420B1 (0-500 watt) microwave power oscillator was used to send up to 400 watts of power at a fixed frequency of 2.45 GHz to the cavity (see Figure 4.4). Although rated for 500 watts, energy was lost from the microwave cable, circulator, and bidirectional coaxial coupler.

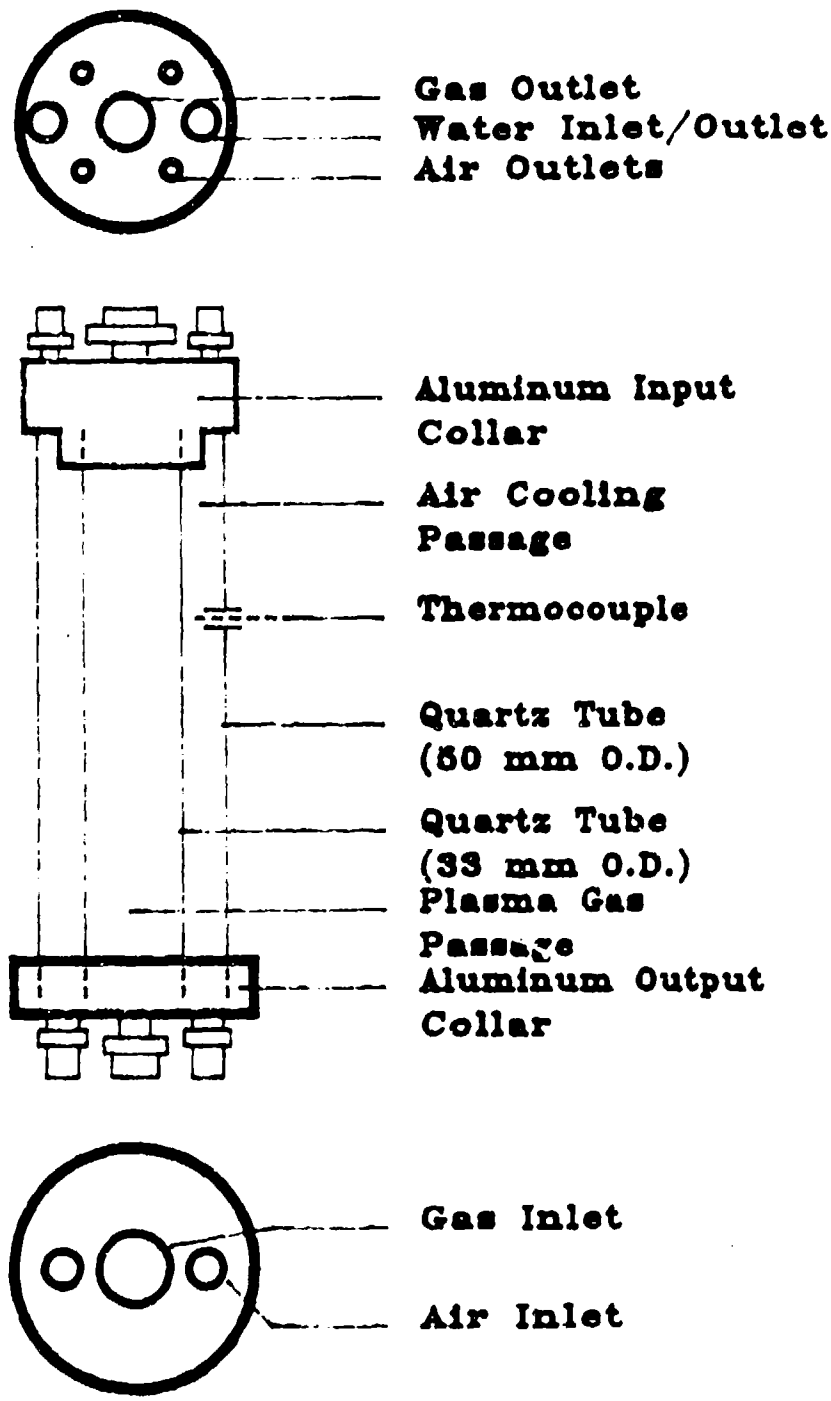

Figure 4.3 Plasma Containment Tubes

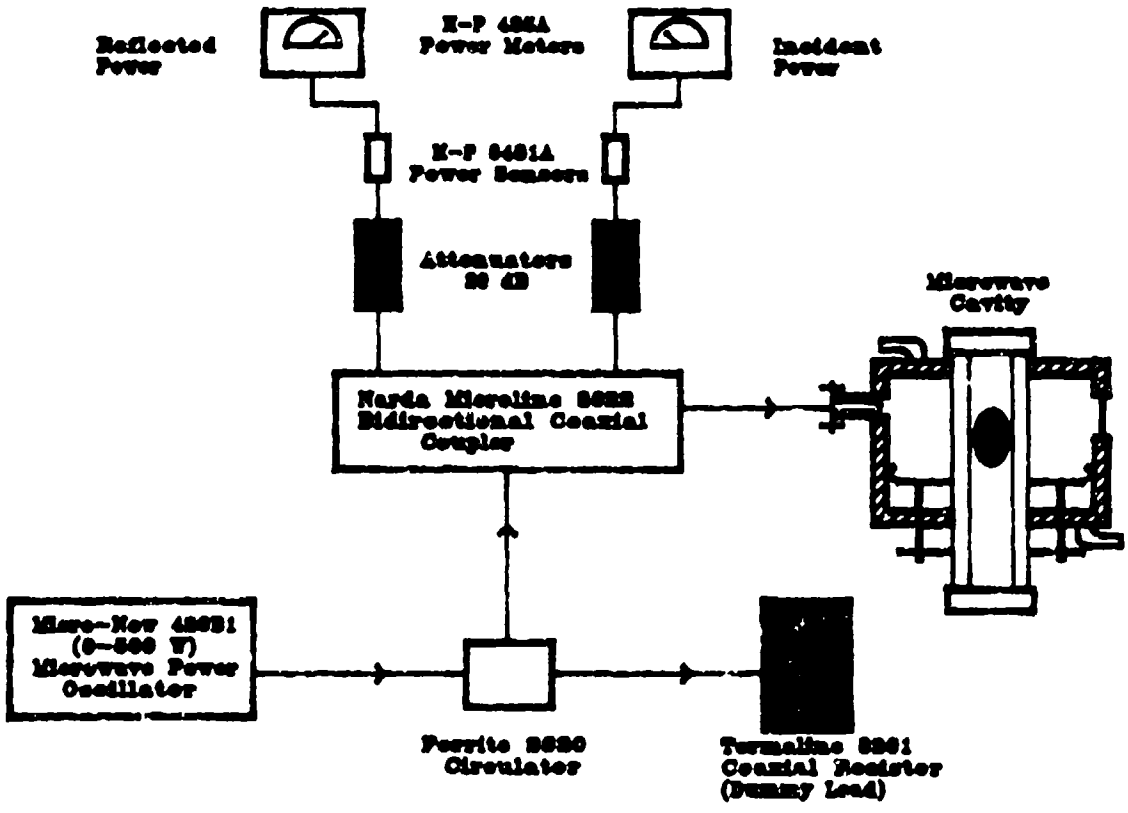

Figure 4.4 Microwave Power Source

Connected to the microwave oscillator was a Ferrite 2620 circulator. This circulator provided at least 20 dB of isolation to each the incident and reflected power sensors. The circulator protected the magnetron in the oscillator from reflected signals and increased the accuracy of the power measurements. The reflected power was absorbed by the Termaline 8201 coaxial resistor. The incident and reflected powers were measured using Hewlett-Packard 8481A power sensors and 435A power meters.

4.6 Temperature Probes.

Type T thermocouples (copper constantan) with braided glass insulation were placed at the inlet and outlet for the water and air cooling (see Figure 4.1). An Omega 400B Digicator was used to measure the temperature at these four locations.

4.7 Spectroscopy.

The radiation emitted by the plasma was measured using a McPherson Model 216.5 Half Meter Scanning Monochromator and photomultiplier detector. A high voltage of 900 volts was provided to the photomultiplier tube (PMT) using a Harrison (Hewlett-Packard) Model 6110A (DC) power supply. The output from the PMT was processed through a Keithly Model 616 digital electrometer. The processed output is sent to a Metrabyte data acquisition & control system and recorded on a Zenith 80286 personal computer (see Figure 4.5).

The monochromator was positioned about 100 cm from the plasma. The emission radiation was focussed on the monochromator using two 25 cm focal length glass lenses. This lens system concentrated the emission radiation on the entrance slit opening of the monochromator. To optimize the

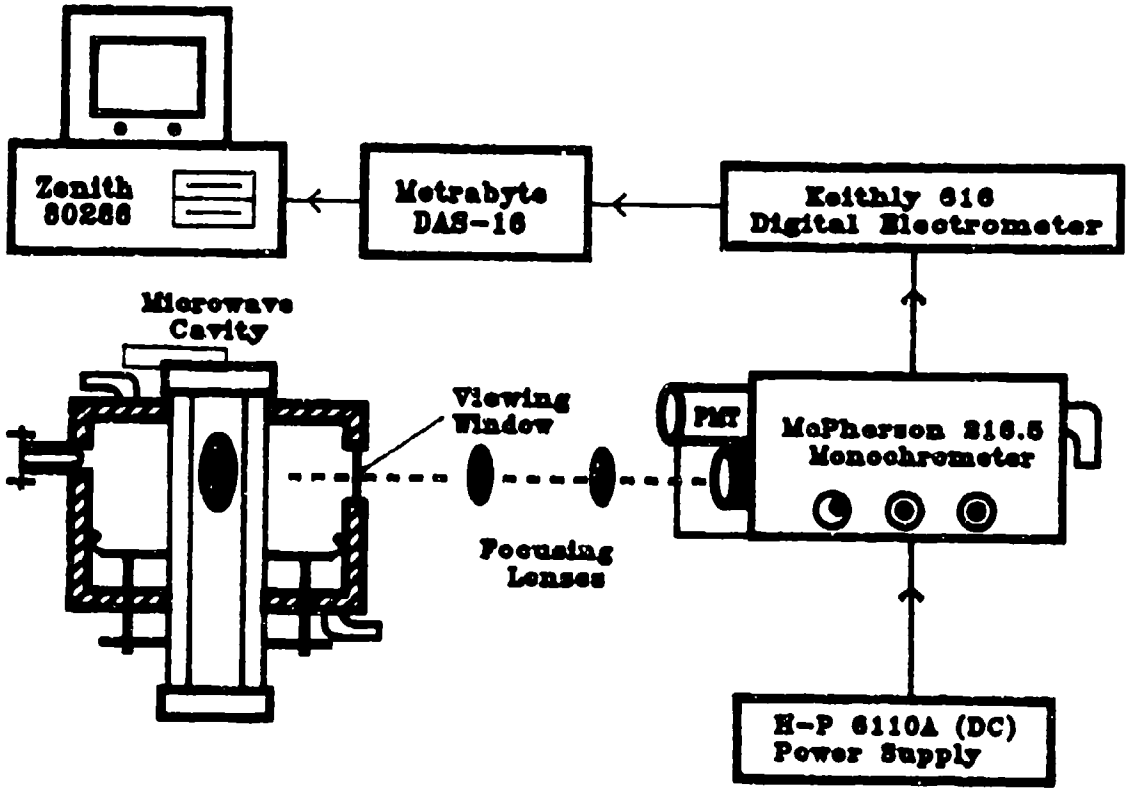

Figure 4.5 Spectroscopy System

intensity of the spectroscopic emissions, the slit widths for this experiment were set at 100 microns for the entrance slit and 50 microns for the exit slit. The atomic spectra was taken using the 1200 grooves per mm grating (plate) with a range of 1050 - 10000 Å. This groove setting allowed for a large range of wavelengths to be observed. The reciprocal linear dispersion was 16.6 Å per mm. The focal length of the spectrometer was one half meter.

CHAPTER V

ENERGY DISTRIBUTION

5.1 Pressure Dependence.

The energy distribution within the microwave cavity was analyzed over various pressures, ranging from 200 to 800 torr. Using the same microwave system, Hoekstra had conducted this experiment using the two separate modes (TM_{011} and TM_{012}) and the two pure gases (nitrogen and helium)[10]. In each of these experiments, the power used was about 250 watts with air cooling flow of 2 SCFM and water cooling flow of 5.75 ml/sec. Hoekstra's experiments involved gas flow in the direction of the gravitational force (F_g). An additional experiment was done reversing the flow of the gas. Using this new data and Hoekstra's results for the same experiment, an estimate is done to determine the gravitational effects on the other three Hoekstra pressure experiments.

Reverse of the gas flow showed a slight change for energy absorbed by the gas (see Figure 5.1). Nevertheless, a significant difference in the power distribution was observed. About 5% of the total energy, which was absorbed by the cavity wall, was redistributed to the air cooling. Thorough cleaning of the cavity before the new experiment may be the main cause of this difference. Dirt and oil deposits on the cavity walls would absorb a large amount of input energy. Thus, removing this dirt and oil would account for the large energy distribution change from the wall. This new energy distribution agrees with the work done by Chapman[8]. Figures 5.2 - 5.4 shows estimated energy

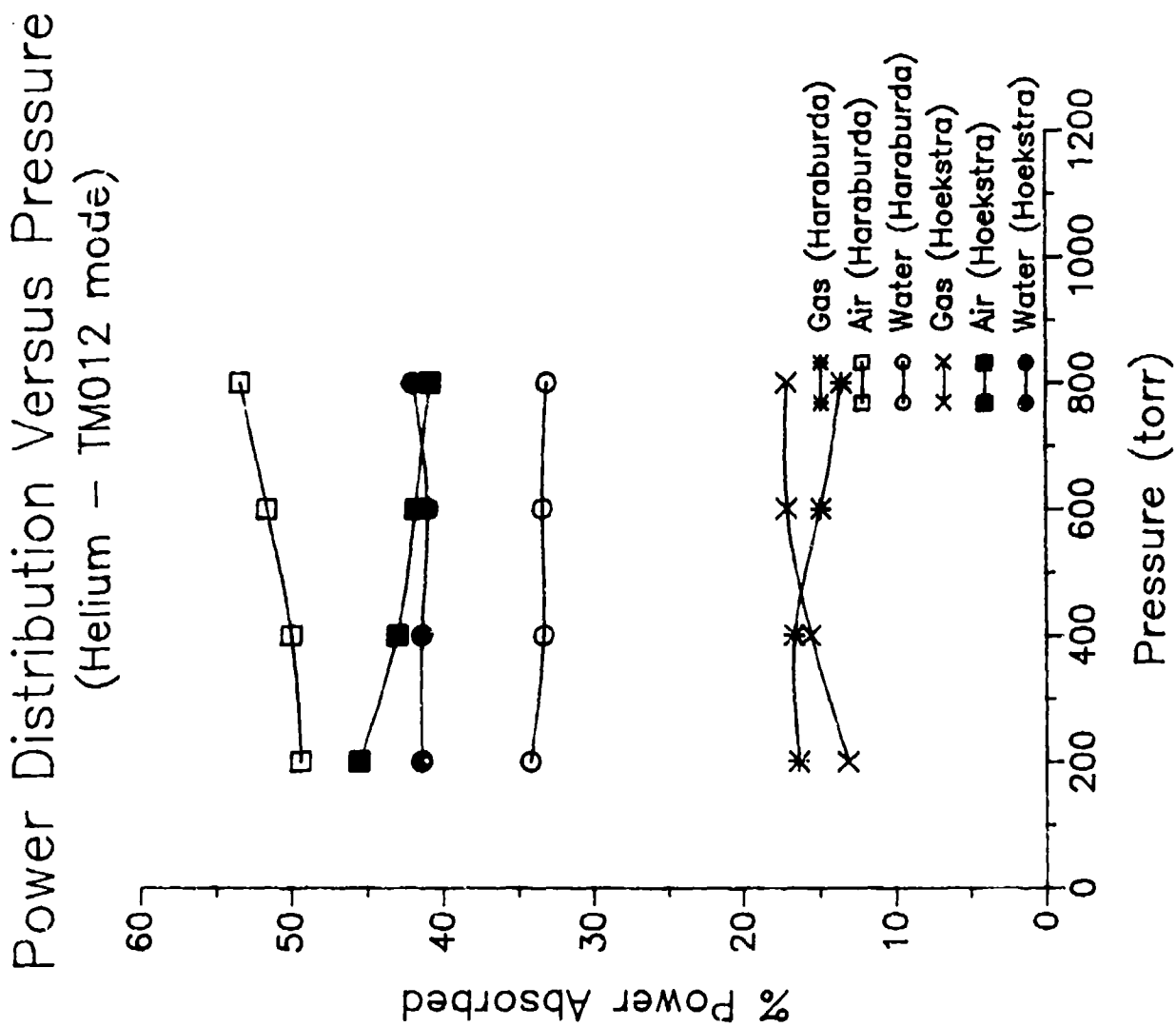

Figure 5.1 Calorimetry Graph I

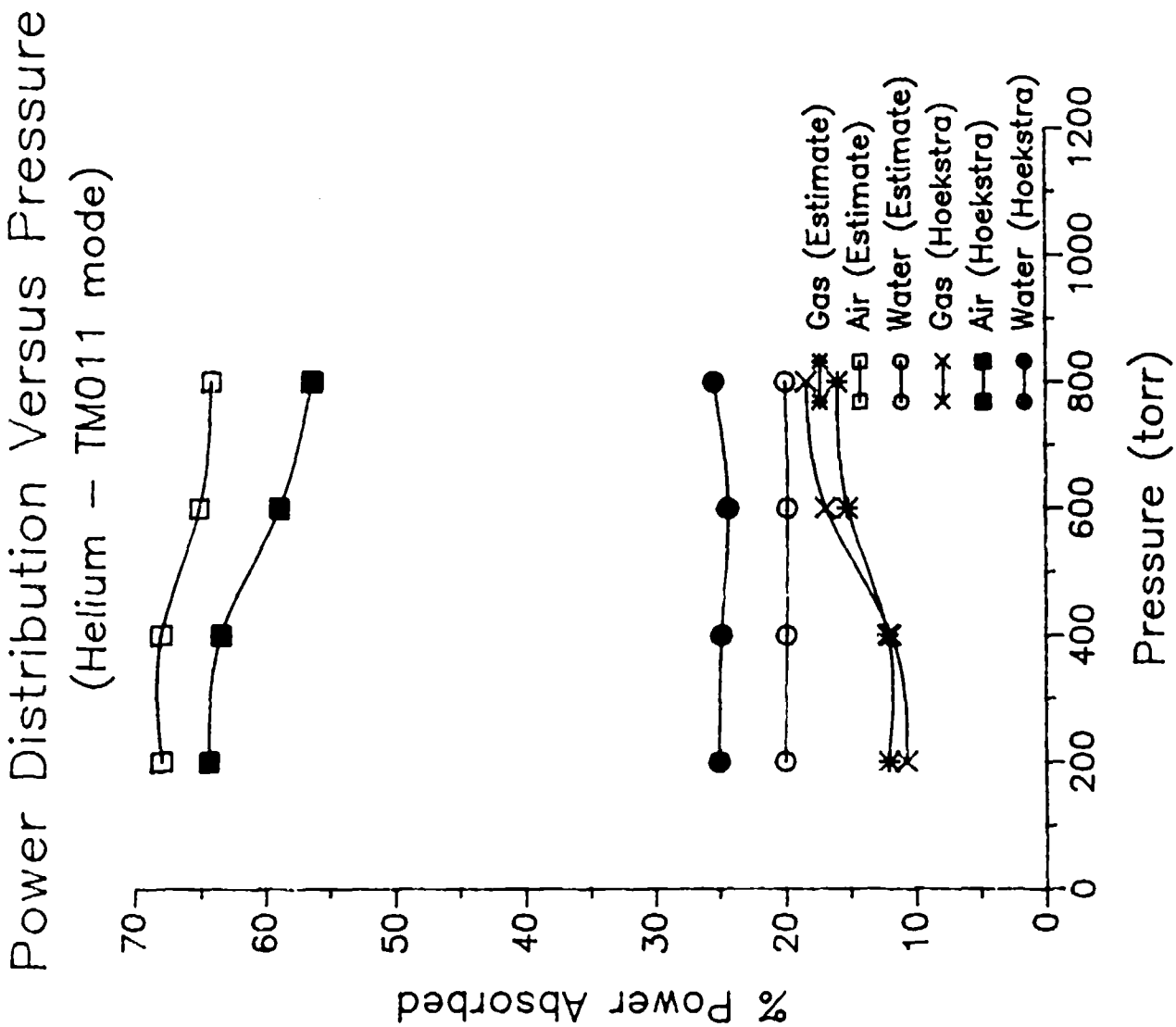

Figure 5.2 Calorimetry Graph II

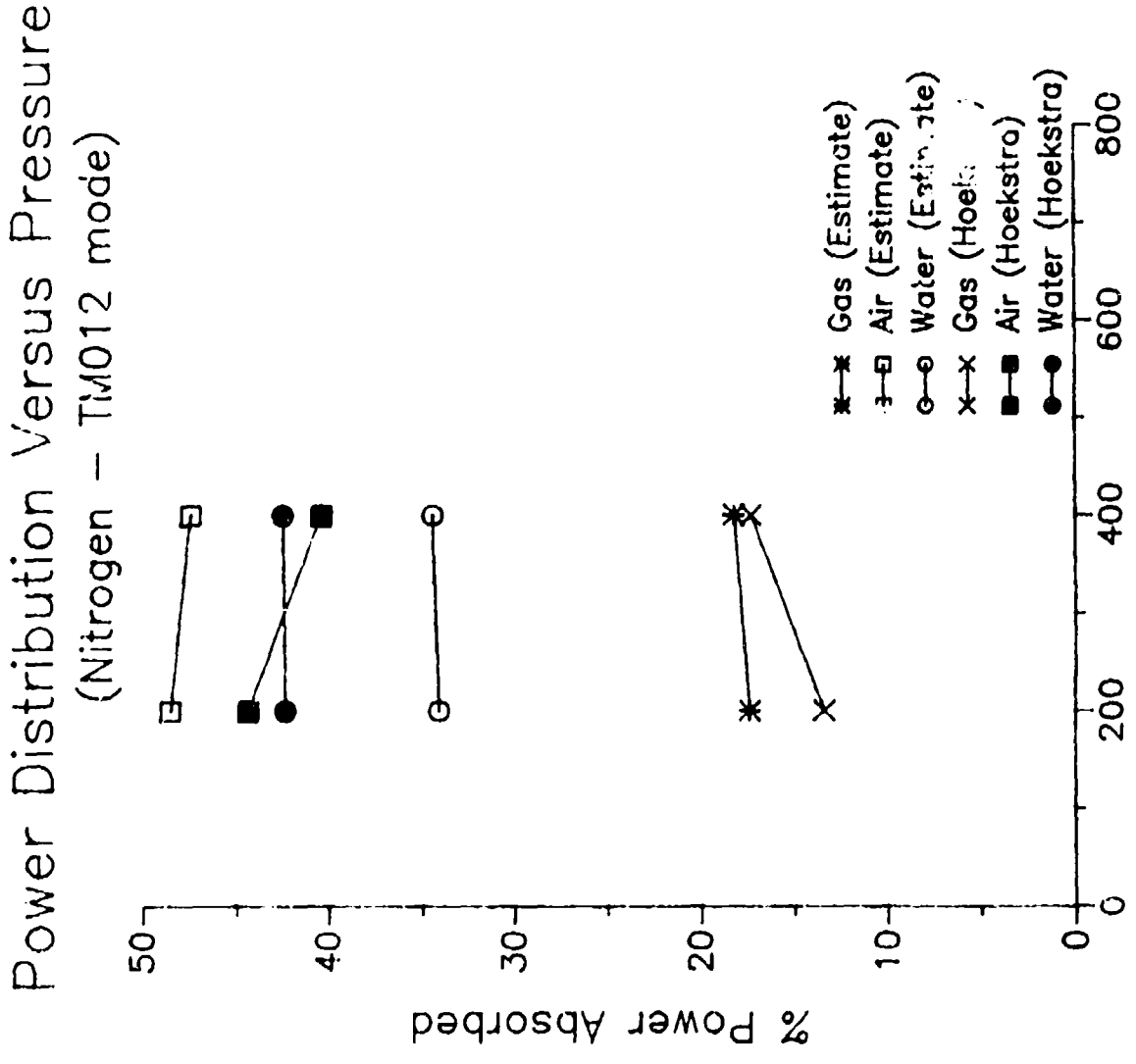

Figure 5.3 Calorimetry Graph III

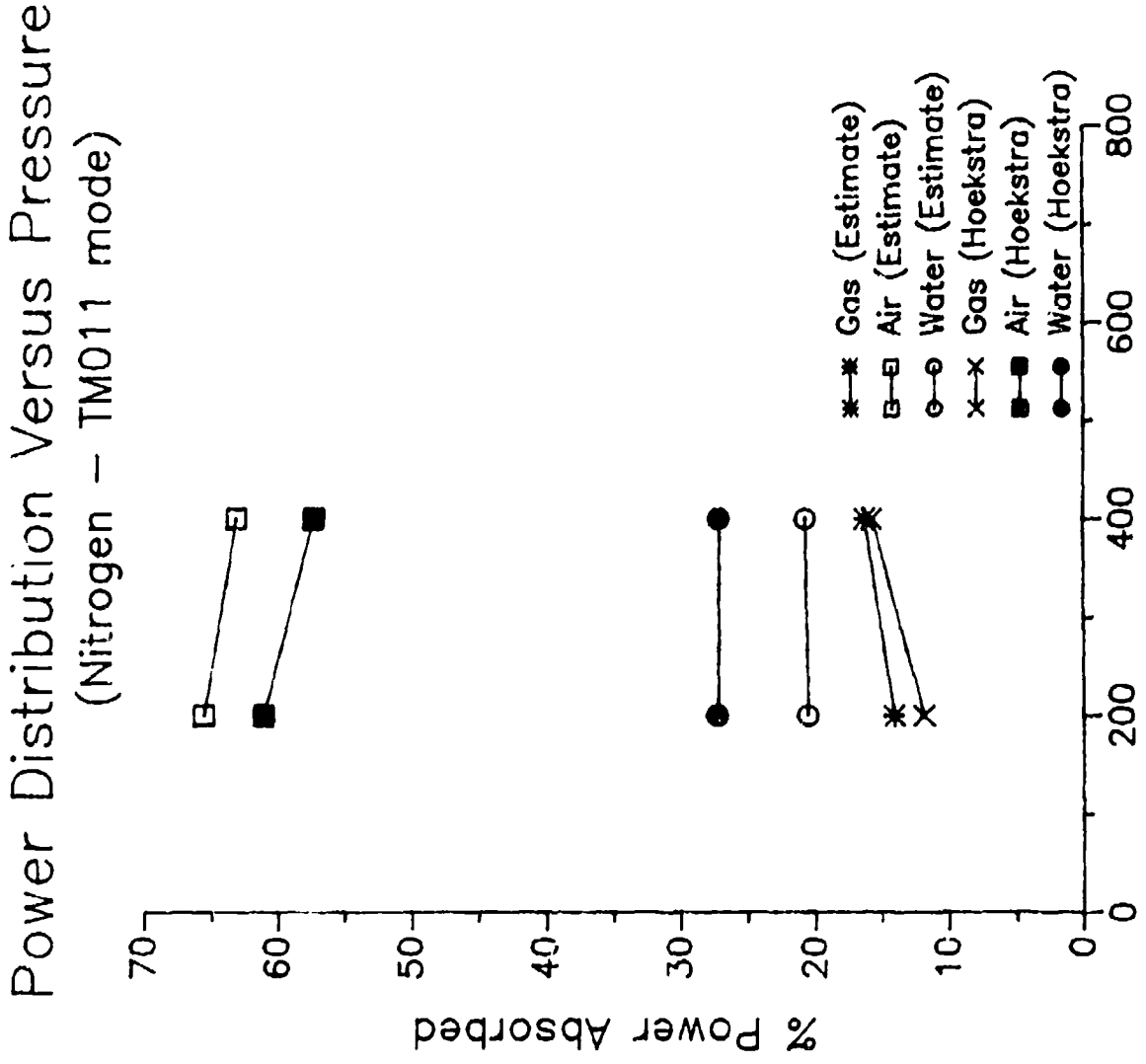

Figure 5.4 Calorimetry Graph IV

distribution values for the reversed gas flows compared to Hoekstra.

5.2 Flow Dependence.

The power absorption by the helium gas was calculated over a range of various flow rates at a constant pressure of 200 torr using an air cooling rate of 2 SCFM and water cooling rate of 5.75 ml/sec. This experiment was only conducted in the TM_{012} mode. Once again using Hoekstra's results, an estimate is made for each mode (see Figure 5.5). Hoekstra conducted a similar experiment in the TM_{011} mode.

With the exception of the power distribution (which may be caused by dirt on the cavity wall), the gravitational force had an insignificant effect on the plasma. The difference between the data for flows with and against gravity were within the range of experimental error. A difference caused by gravity may be observed by significantly reducing this error. Unfortunately, that difference can not be observed using the current experimental system.

5.3 Plasma Power Absorption.

The power initially absorbed by the plasma is the combination of the power absorbed by the gas and by the cooling air. For helium, power absorbed by the plasma was about 67% in the TM_{012} mode and about 80% in the TM_{011} mode. The remaining power was that power which is absorbed by the cavity walls through radiation and convection.

This plasma power absorption was the initial anticipated power we can expect to use for propulsion. As an example, Figure 5.6 shows the total power absorbed by the

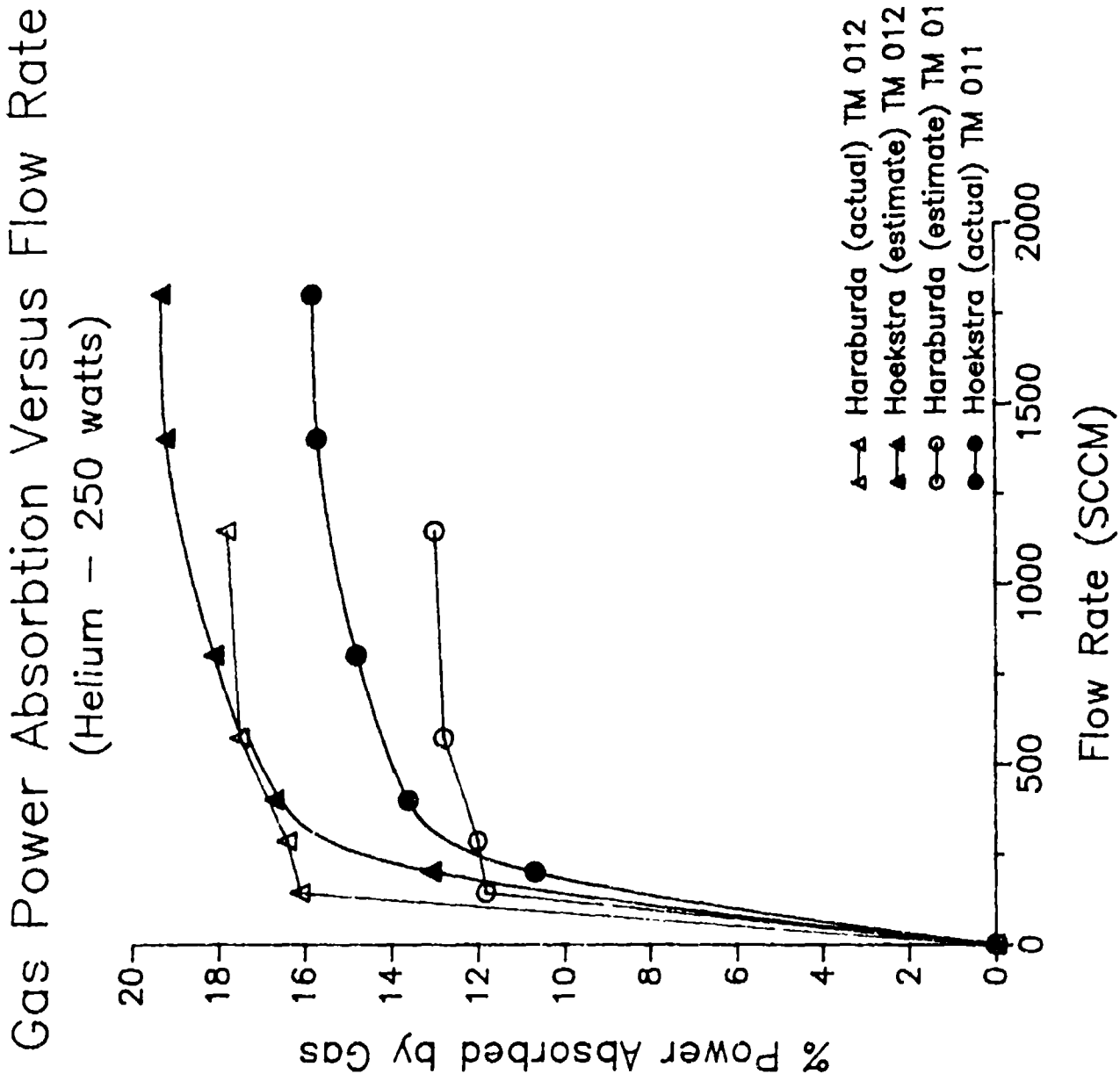

Figure 5.5 Calorimetry Graph V

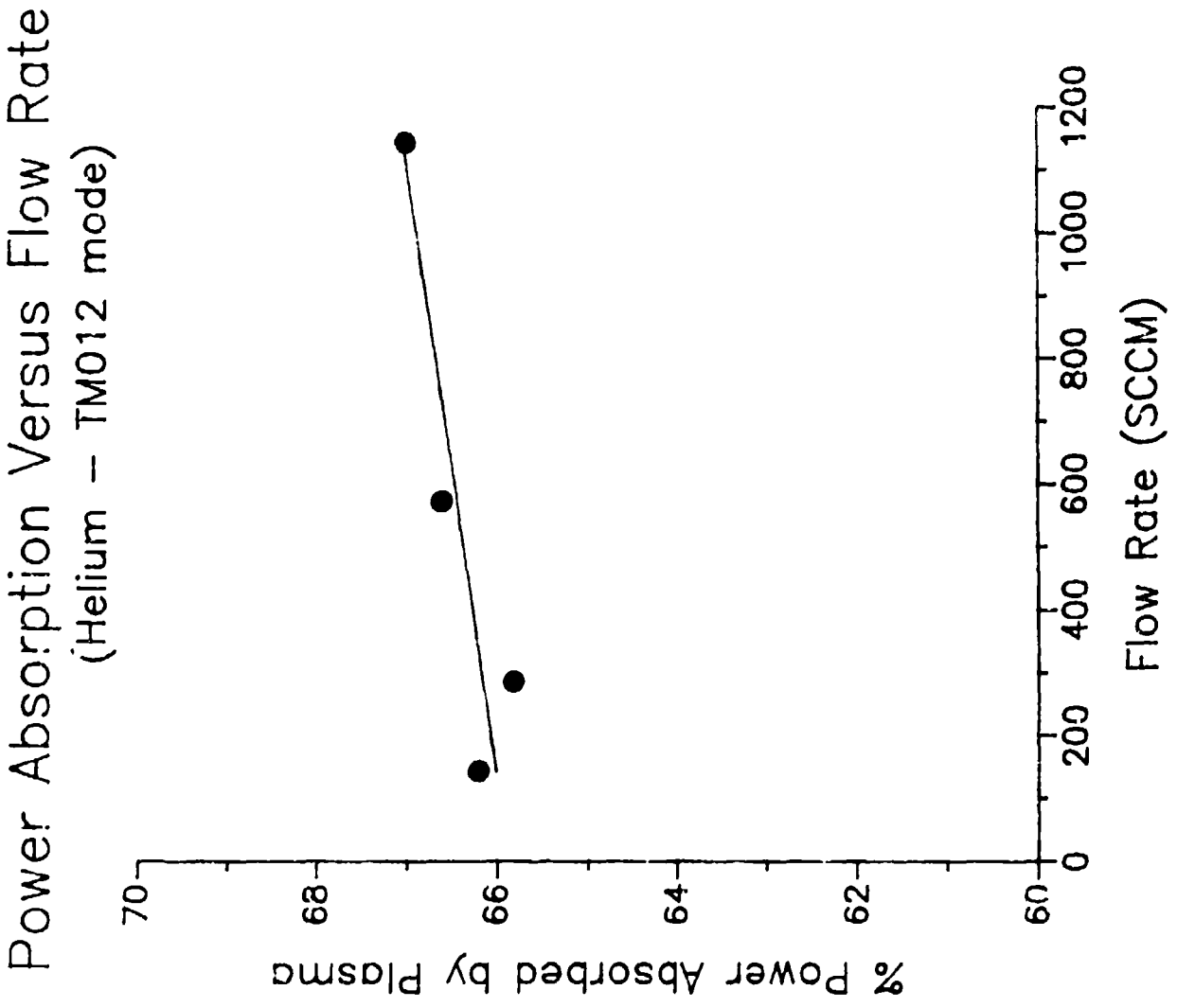

Figure 5.6 Calorimetry Graph VI

plasma for various flow rates, which was dramatically different than the power absorbed by the gas as shown in Figure 5.5. The power absorbed by the wall can be recovered by such methods as using heat exchangers. A heat exchanger can transfer energy to the propellant before it enters the cavity.

CHAPTER VI

PLASMA DIMENSIONS

6.1 Introduction.

An important element of microwave generated plasmas is its size and shape. Its size varies about pressure, flow, and power changes. These measurements can be used to model heat transfer and chemical processes within a plasma. Plasma dimensions were calculated from 35 mm color slide pictures. The projected images were measured and compared with a known grid pattern. This grid pattern is photographed and projected at the same distance as the plasma. Water cooling flow rate of 5.75 ml/sec and air cooling flow rates of 2 SCFM for helium gas and 3 SCFM for nitrogen gas were used.

A 35 mm camera, on a tripod, was position about 2 cm from the microwave cavity window (see Figure 4.2). Pictures were taken using a 50 mm lens, using Ektachrome 200 ISO color slide film. Several aperture and shutter speed settings were analyzed to determine the optimal settings. The following data were reported for aperture and shutter speed settings of f2.8 and 1/250s, respectively. Using only the TM_{012} mode, four sperate measurements were made for each plasma: height and width for strong and weak regions. Plasmas for both helium and nitrogen were observed to have two distinct regions - a more intense lighter color inner region surrounded by a diffuse darker outer region. Thus, it was appropriate to record two separate measurements, identifying the inner and outer regions as strong and weak ionization regions respectively.

6.2 Pressure and Flow Dependency.

Measurements were done on helium plasmas in the pressure range of 400 - 1000 torr using a power source of about 250 watts. Three gas flow rates (0, 572, and 1144 SCCM) were used for each pressure point (see Figures 6.1 - 6.3). Nitrogen was observed in the pressure region of 400 - 500 torr using the same power. Three gas flow rates (0, 102, 204 SCCM) were used for each pressure observation (see Figures 6.45 - 6.6). It was noticed that plasma size decreases with increases in pressure and increases slightly with increases in gas flow rate.

6.3 Power Dependency.

Measurements were done on helium plasmas at a constant pressure of 400 torr with no gas flow for both nitrogen and helium. The power was varied between 100 - 250 watts for helium (see Figures 6.7 - 6.8) and between 210 - 260 watts for nitrogen (see Figure 6.9). The primary observation was that small changes in power at these pressure ranges affected the plasma dimensions. Increases in power resulted in a larger plasma, as expected.

6.4 Plasma Color and Shape.

For both helium and nitrogen plasmas, the strong ionization regions displayed an intense white color. The color difference is observed in the weak ionization region. Helium displayed a purple color, while nitrogen displayed an orange color. Additionally, these two gases displayed a different shaped plasma. Both shapes can simply be represented by an oblate ellipsoid. The helium plasma differed slightly in the middle with a small indentation, resulting in a "dumbbell shaped" figure. Figure 6.10 shows

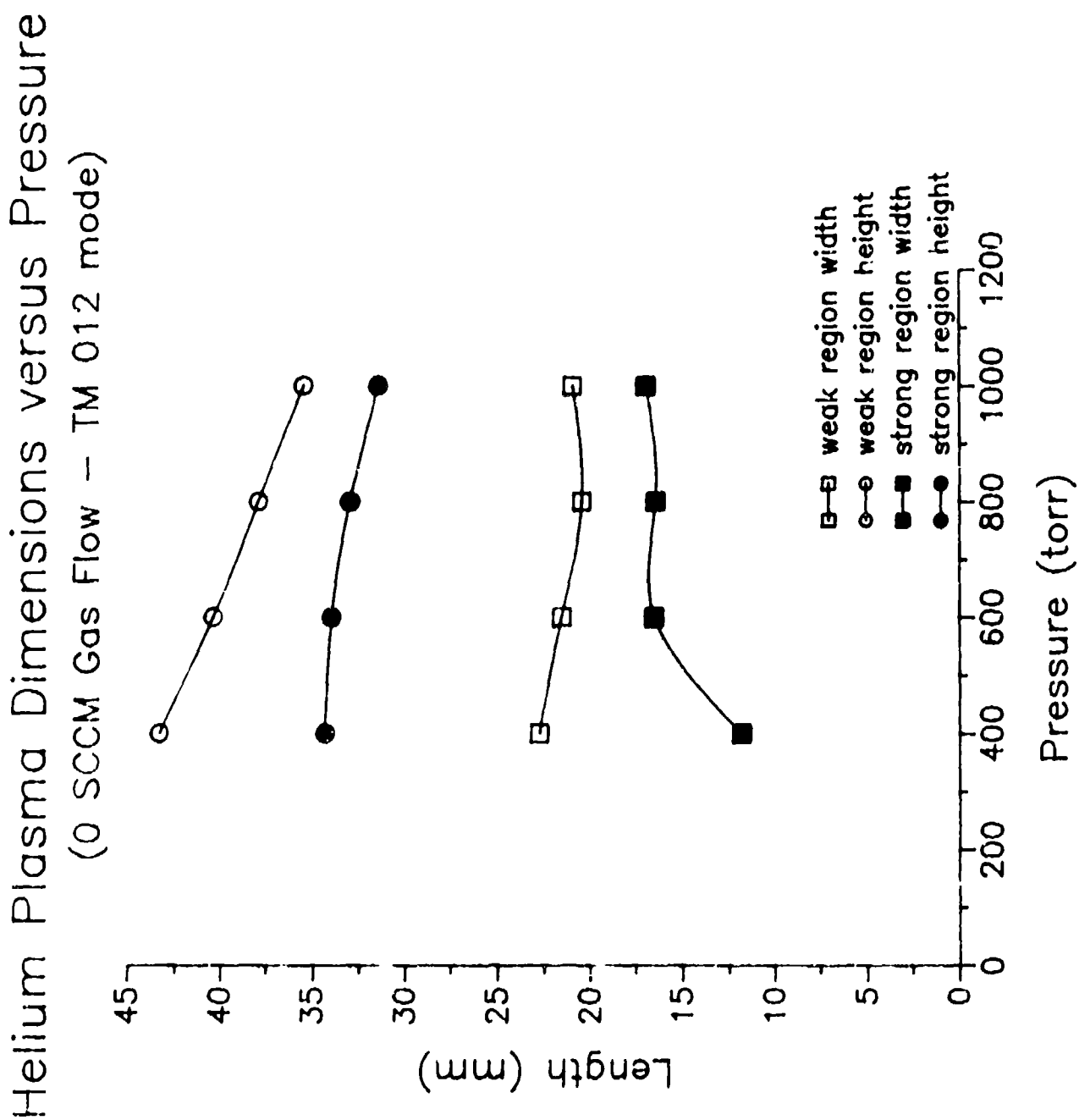

Figure 6.1 Plasma Dimensions Graph 1

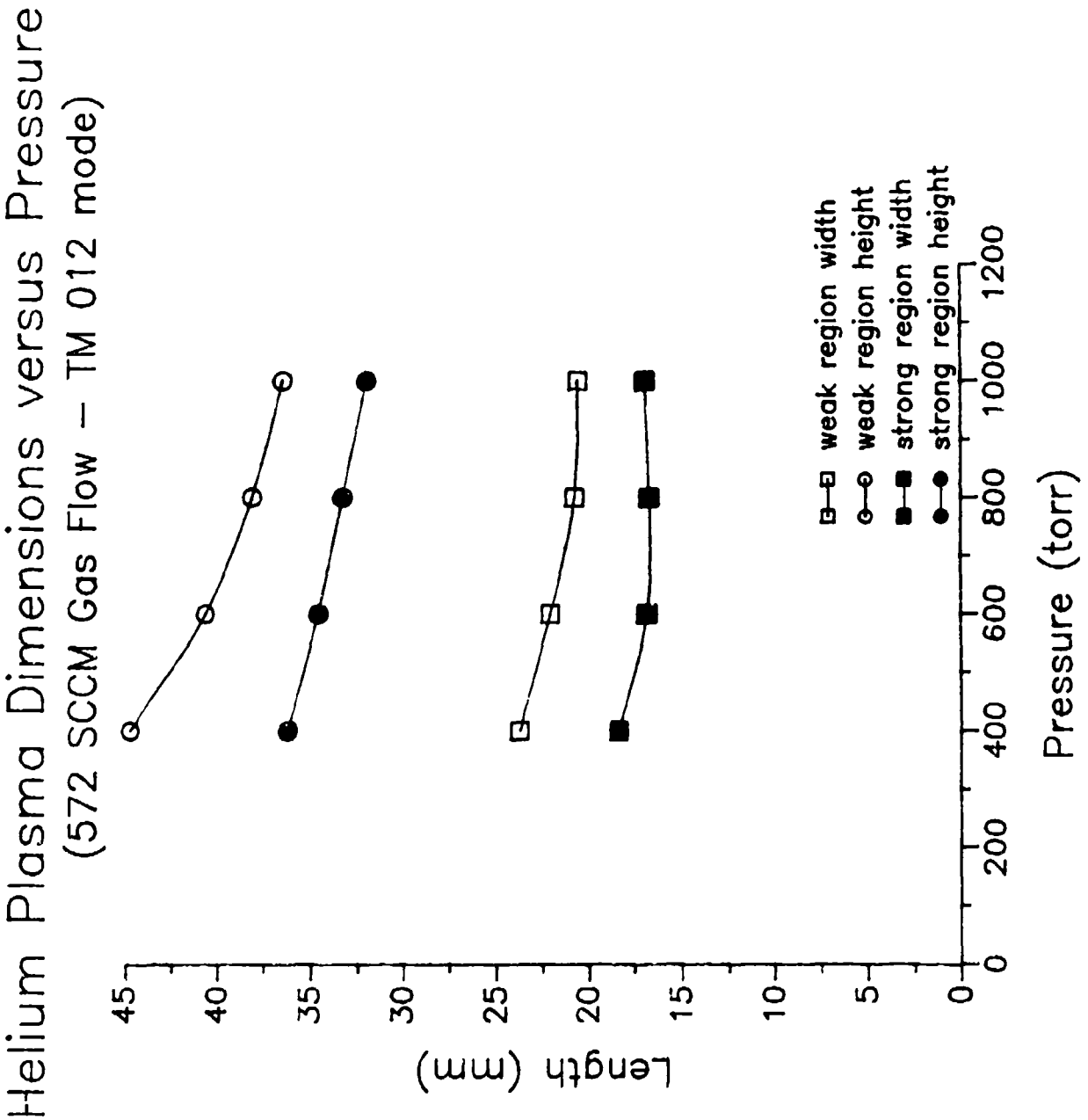

Figure 6.2 Plasma Dimensions Graph II

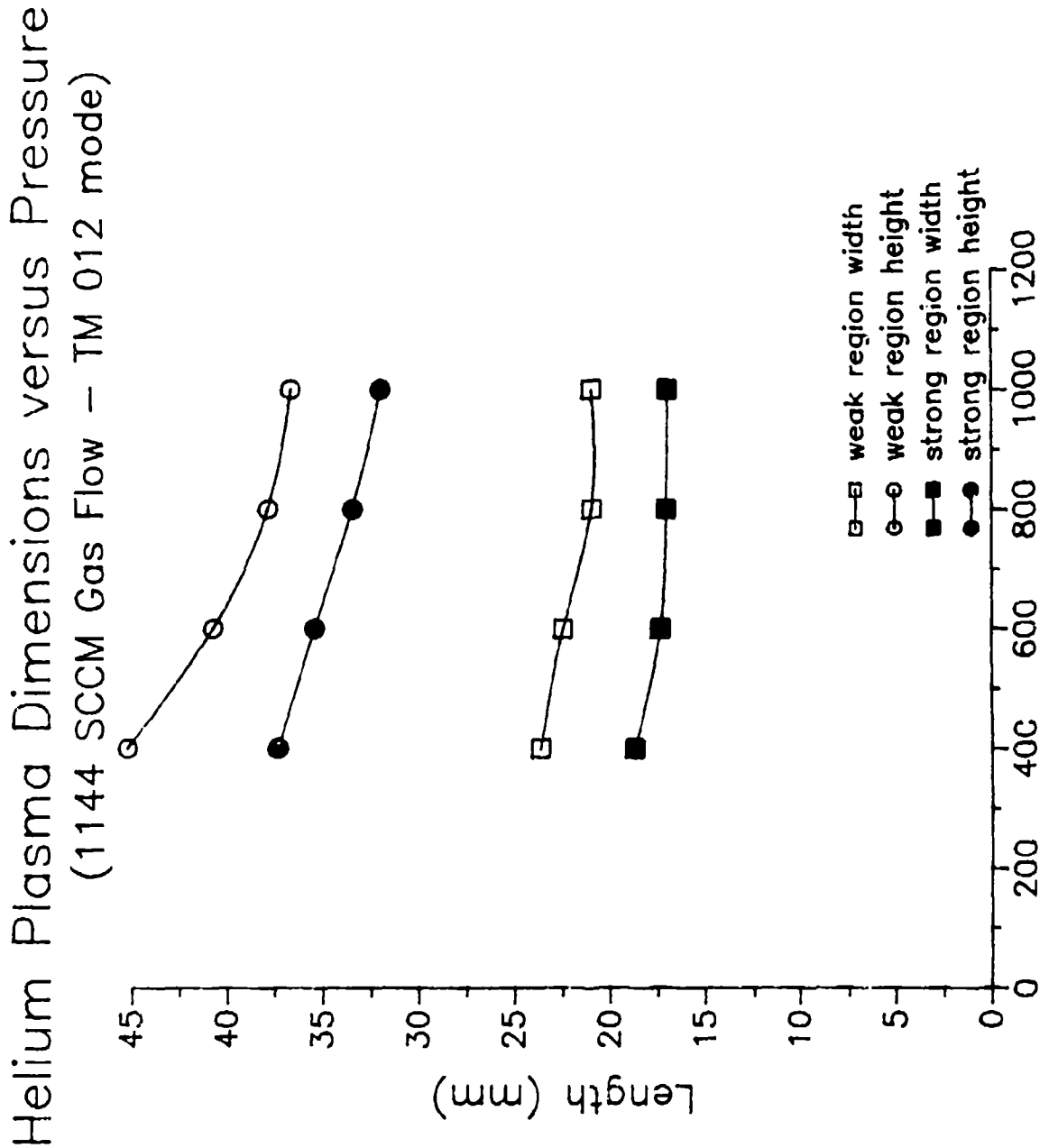

Figure 6.3 Plasma Dimensions Graph III

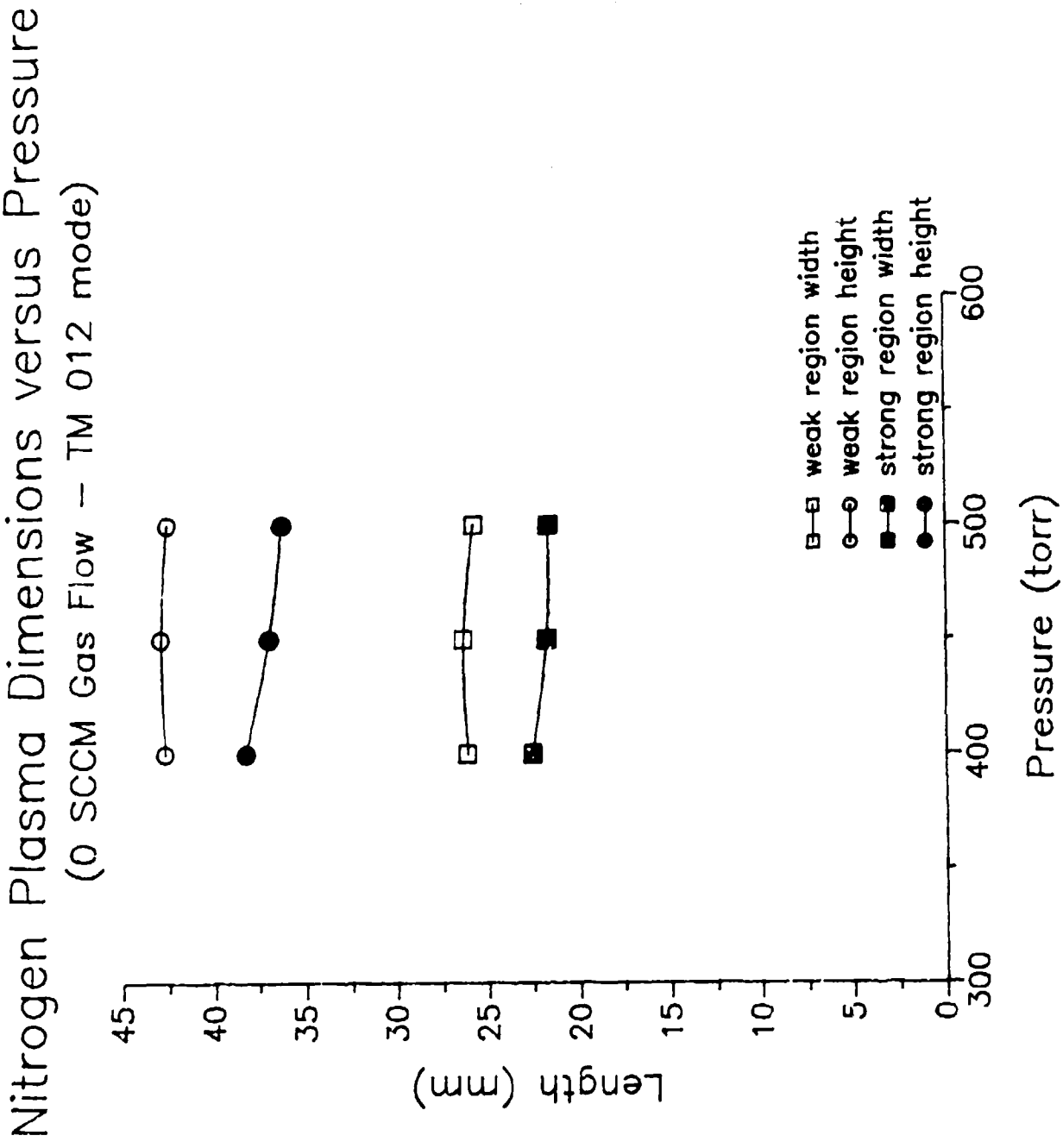

Figure 6.4 Plasma Dimensions Graph IV

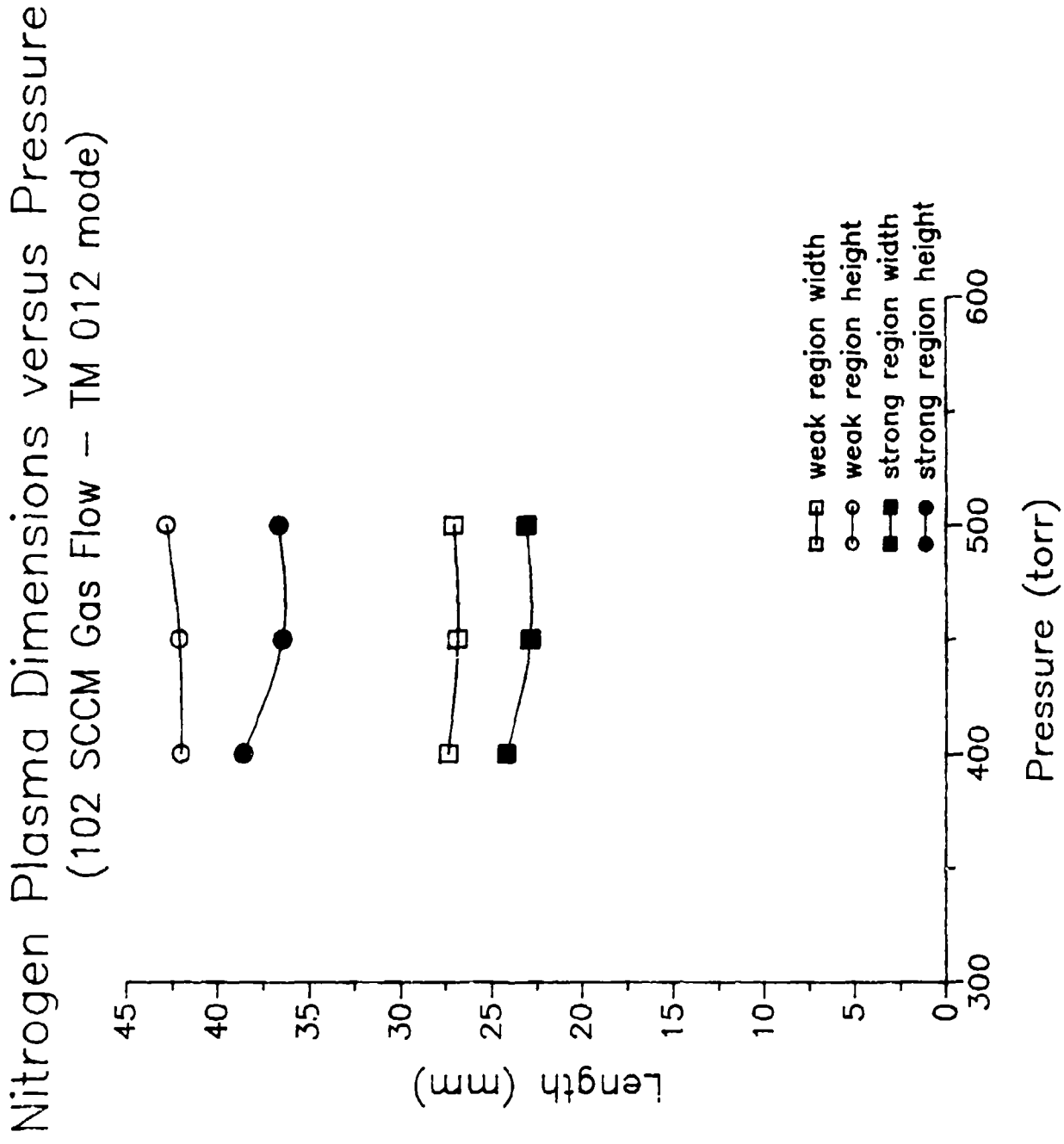

Figure 6.5 Plasma Dimensions Graph V

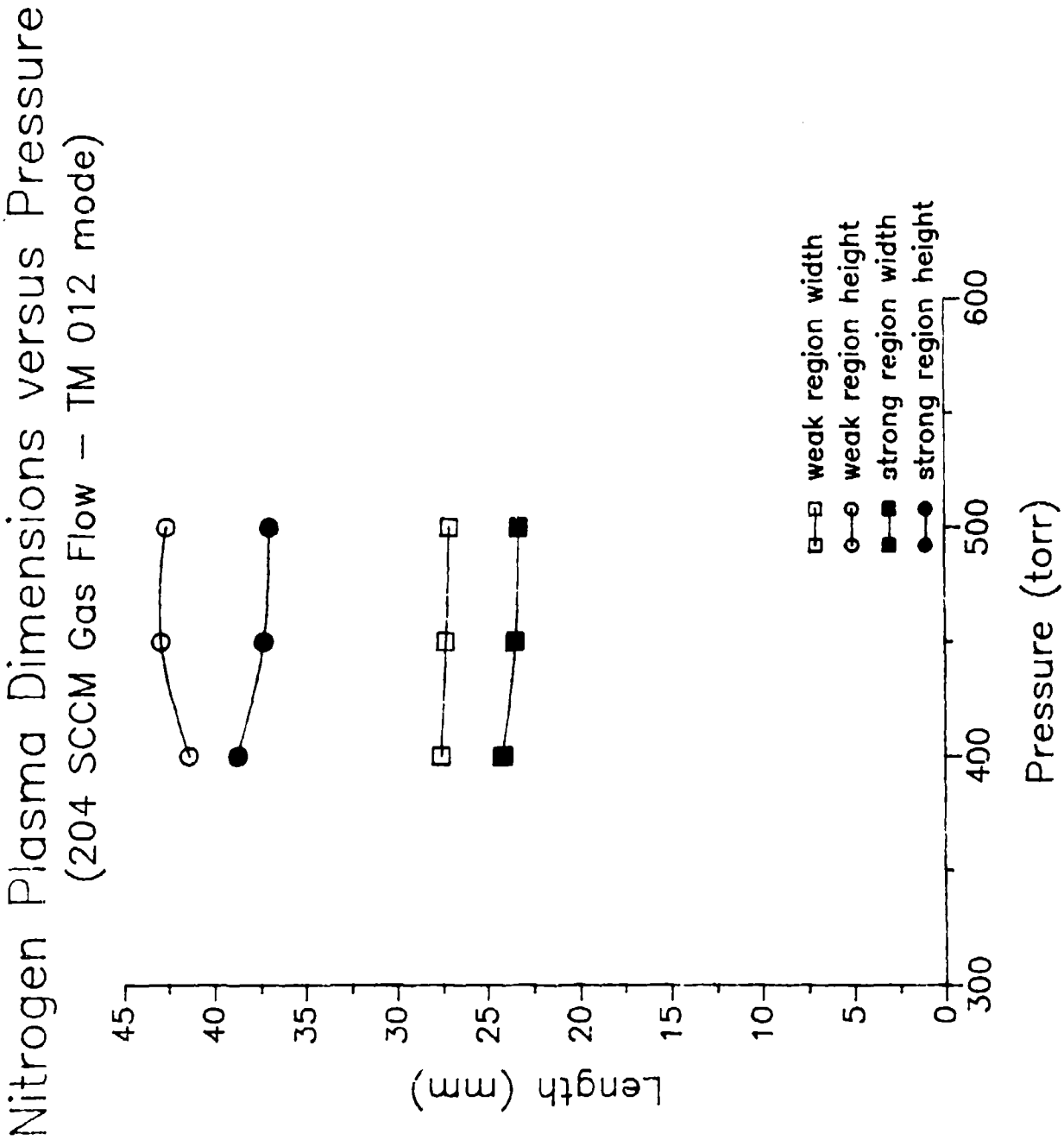

Figure 6.6 Plasma Dimensions Graph VI

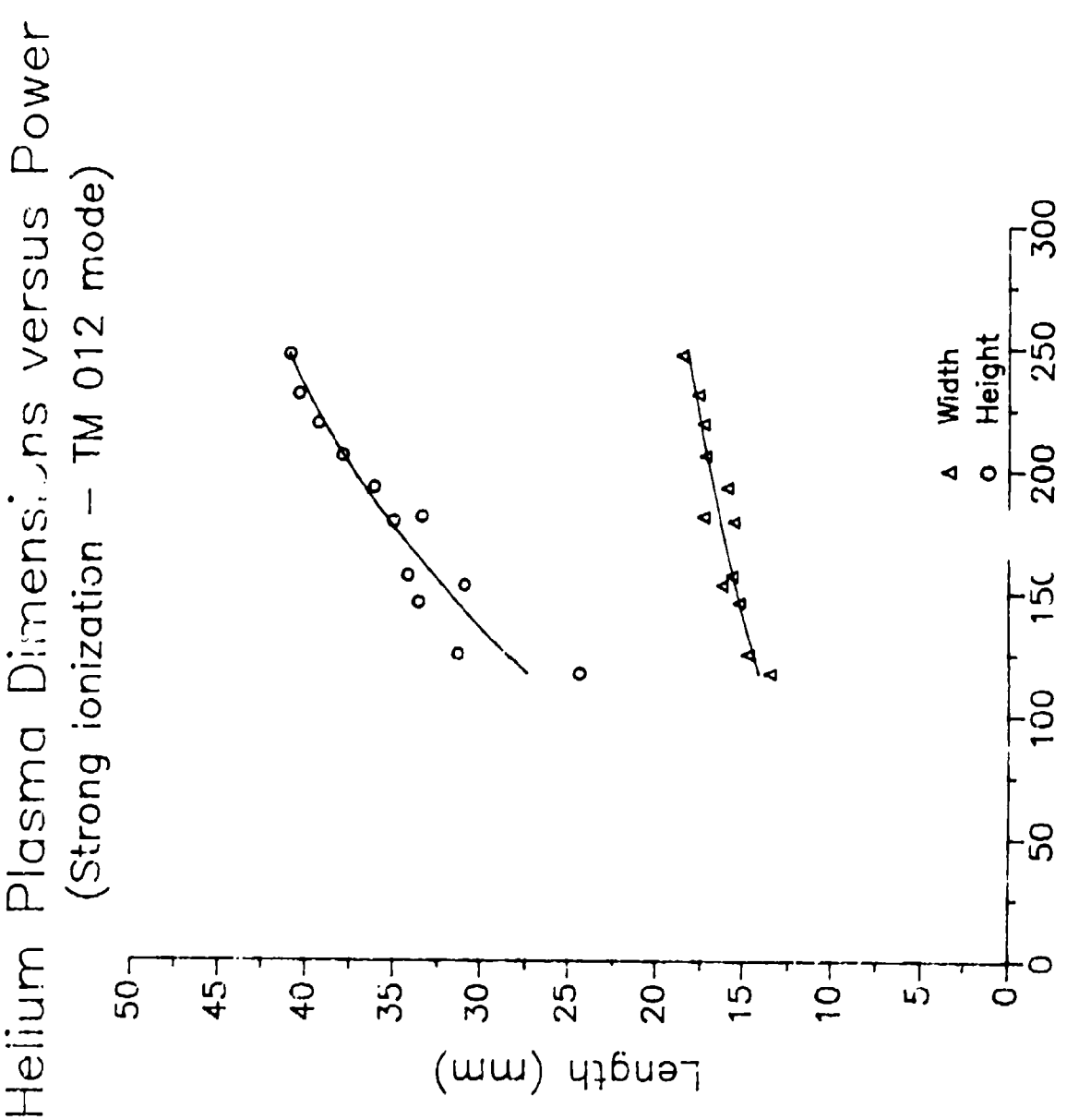

Figure 6.7 Plasma Dimensions Graph #1

..elium Plasma Dimensions versus Power

(Weak Ionization – TM 012 mode)

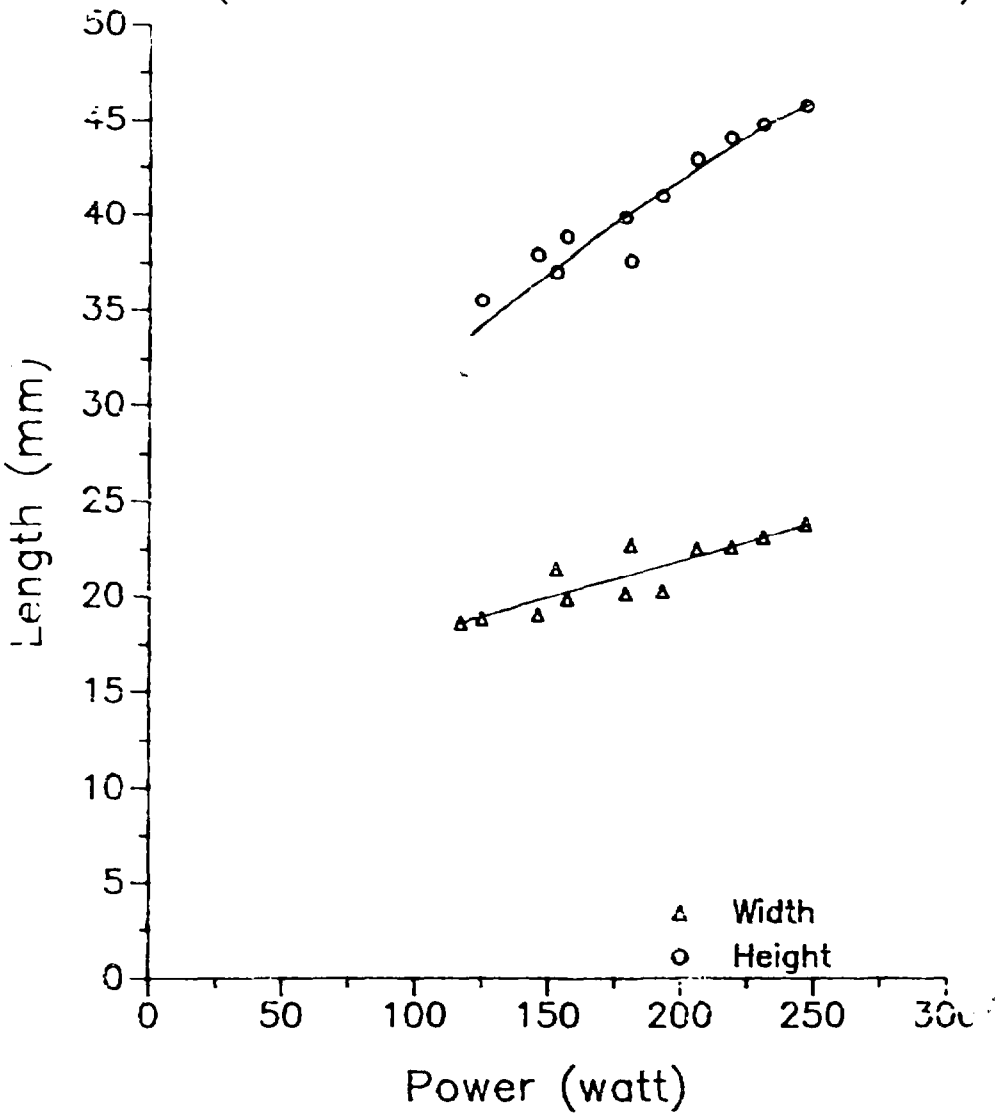

Figure 6. Plasma Dimensions Graph VIII

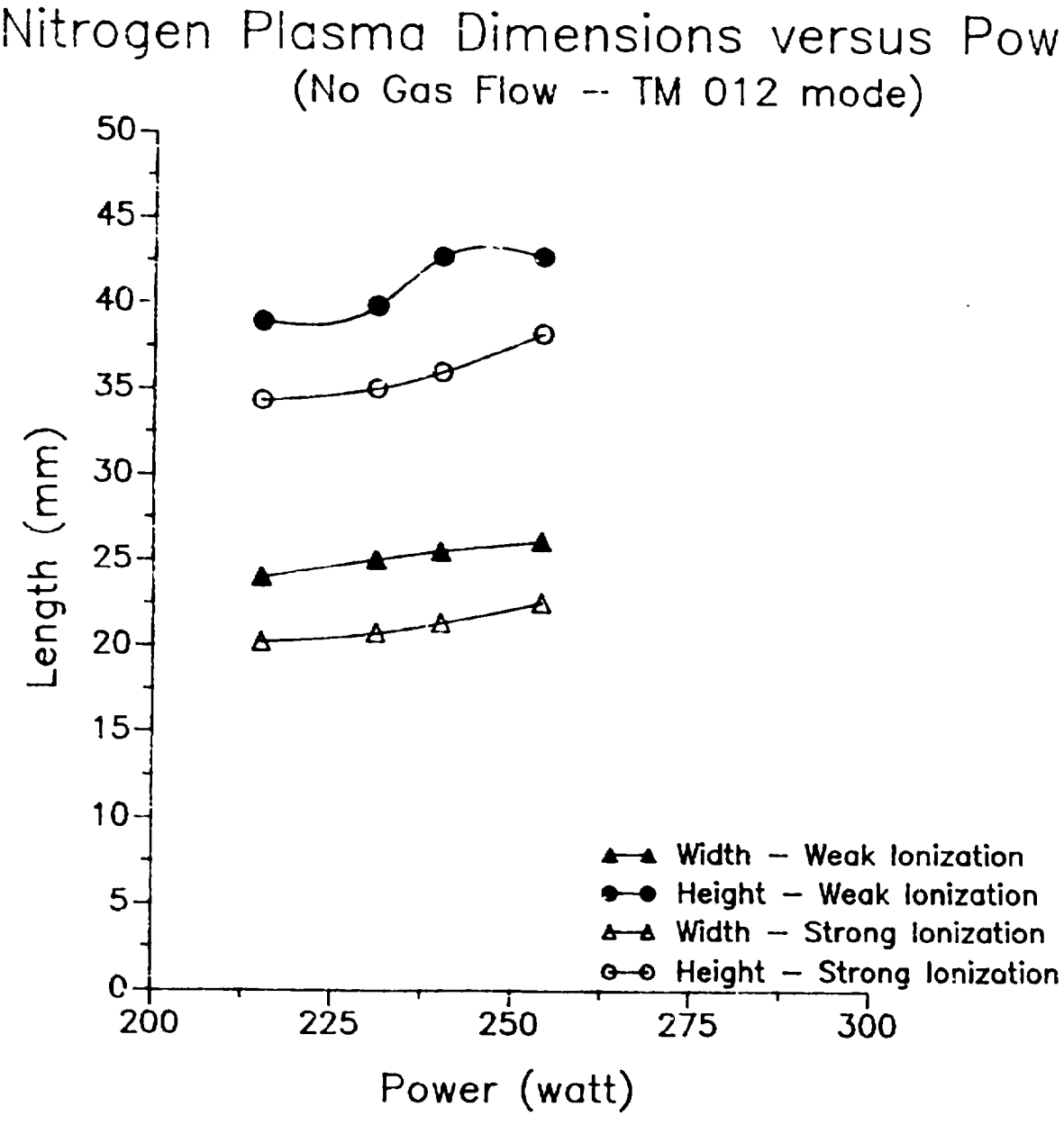

Figure 6.9 Plasma Dimensions Graph IX

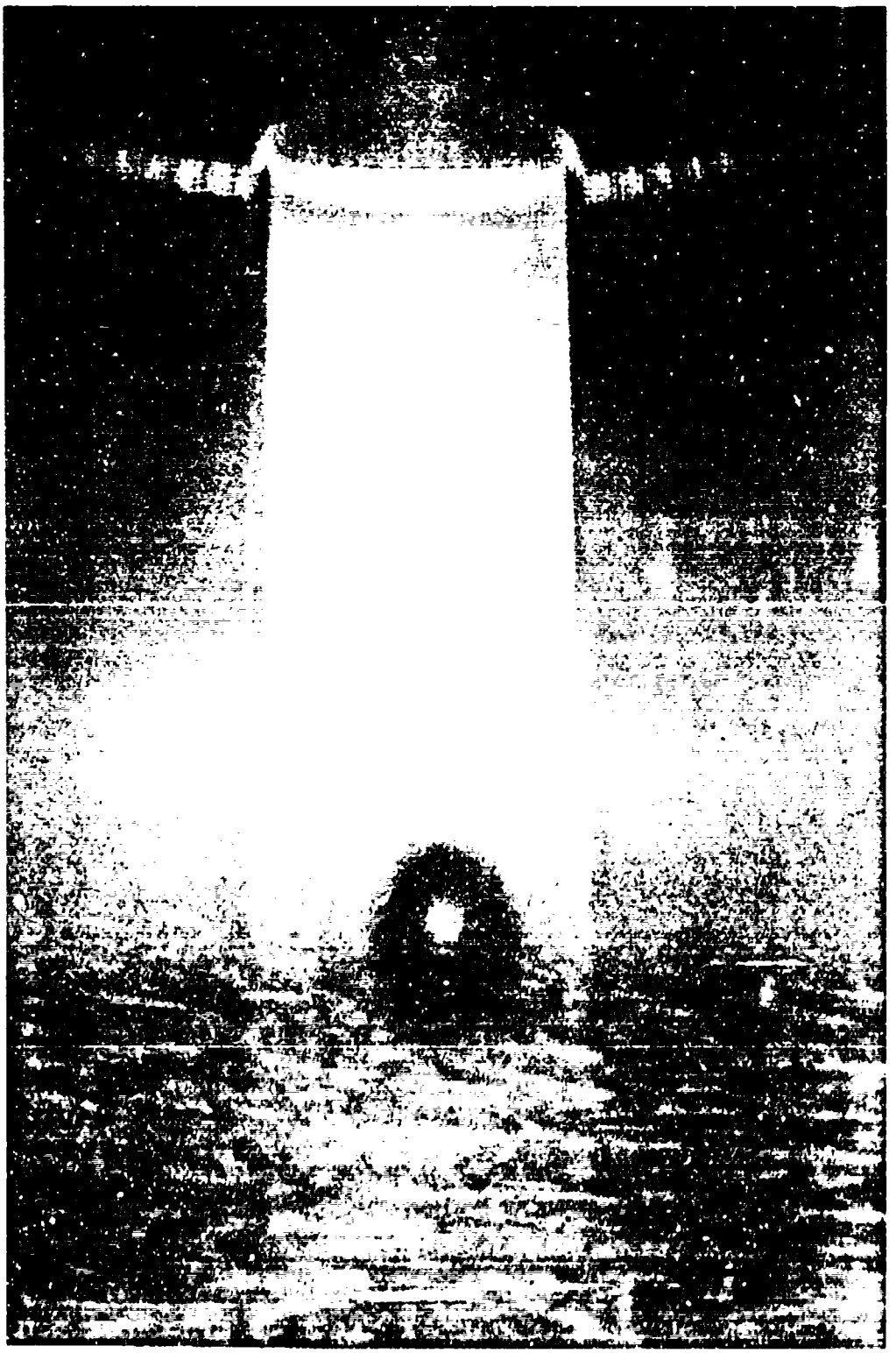

a photograph of a nitrogen plasma in a TM_{012} mode (courtesy of Maris Mantenieks of NASA - Lewis Research Center).

6.5 Plasma Volume.

The plasma volume was easily obtained assuming axial symmetry and neglecting the indentation of the dumbbell shape. The volume was calculated as though the plasma region behaved as an oblate ellipsoid. The simple equation for this calculation is:

$$\text{Volume} = \frac{4\pi}{3} \times \left(\frac{\text{Height}}{2}\right) \times \left(\frac{\text{Width}}{2}\right)^2 \qquad 6.1$$

The data from Figures 6.1 - 6.6 were calculated for this volume determination. This calculated volume data is provided in Table 6.1.

As seen from this data, the volume was dependant upon both pressure and flow rate. When pressure decreased or flow rate increased, the volume of the plasma increased.

6.6 Mechanical Observations.

A small mechanical measuring device was constructed by Hoekstra and modified by Haraburda to measure objects from a distance. As shown in Figures 6.11 and 6.12, an 8 x 7 inch object constructed of two steel plates with a fixed hole on one side and an adjustable iris on the other was a device designed to provide immediate feedback information concerning plasma dimensions. Using this device, one could obtain a reasonable measurement within minutes. On the other hand, a more accurate measurement could be obtained through photography within hours. Thus, this device could be used during an experiment to determine any irregularities in the dimension. This was helpful because the experimental

Table 6.1 Helium and Nitrogen Plasma Volumes

EXPERIMENT	Cavity Pressure (torr)	Strong Region (cm^3)	Weak Region (cm^3)
HELIUM (0 SCCM FLOW)	400	2.50	11.68
	600	4.83	9.75
	800	4.63	8.24
	1000	4.70	8.10
HELIUM (572 SCCM FLOW)	400	6.35	13.15
	600	5.10	10.29
	800	4.85	8.53
	1000	4.77	8.01
HELIUM (1144 SCCM FLOW)	400	6.76	13.18
	600	5.55	10.69
	800	5.05	8.45
	1000	4.77	8.37
NITROGEN (0 SCCM FLOW)	400	10.13	15.23
	450	9.10	15.54
	500	8.84	14.70
NITROGEN (102 SCCM FLOW)	400	11.74	16.39
	450	9.91	15.83
	500	10.14	16.34
NITROGEN (204 SCCM FLOW)	400	11.87	16.51
	450	10.79	16.74
	500	10.52	16.38

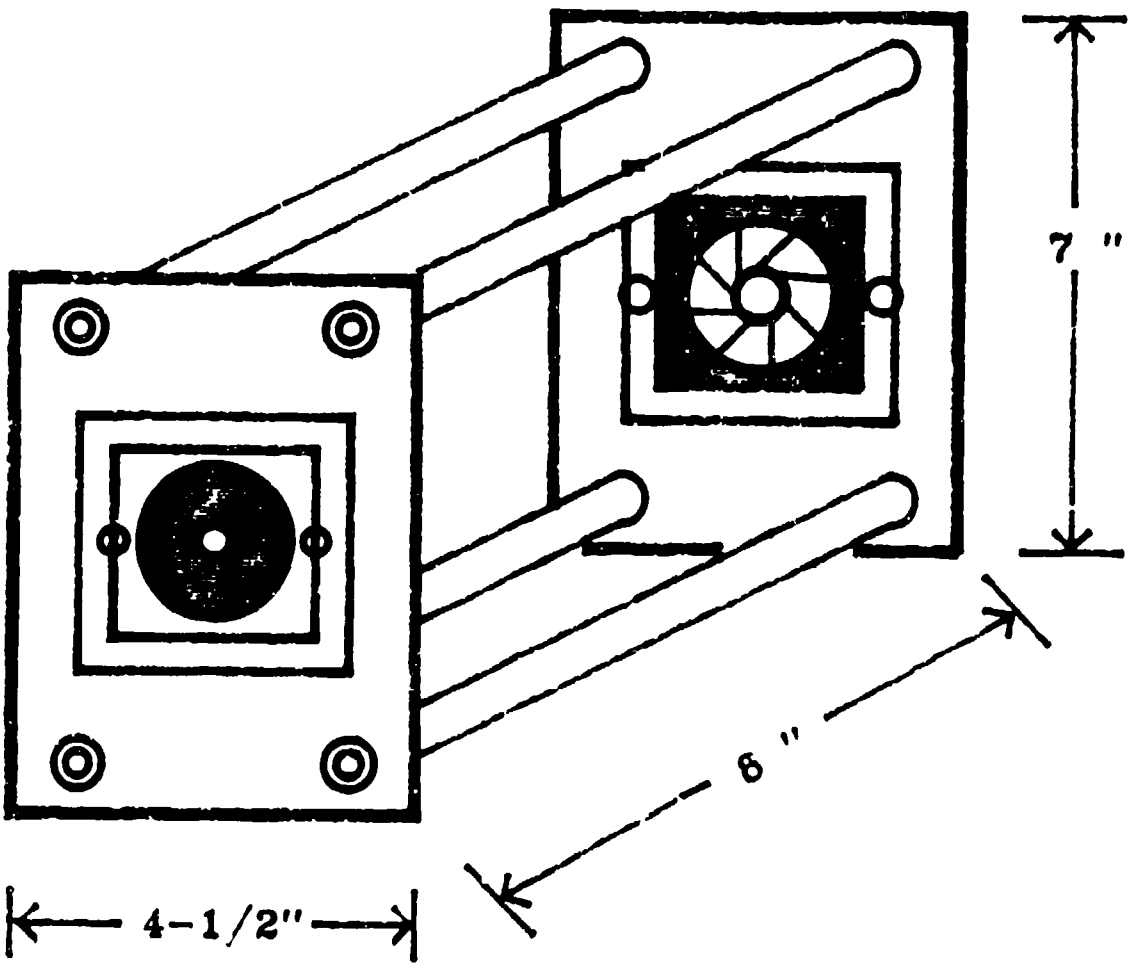

Figure 6.11 Mechanical Measuring Device - Side View

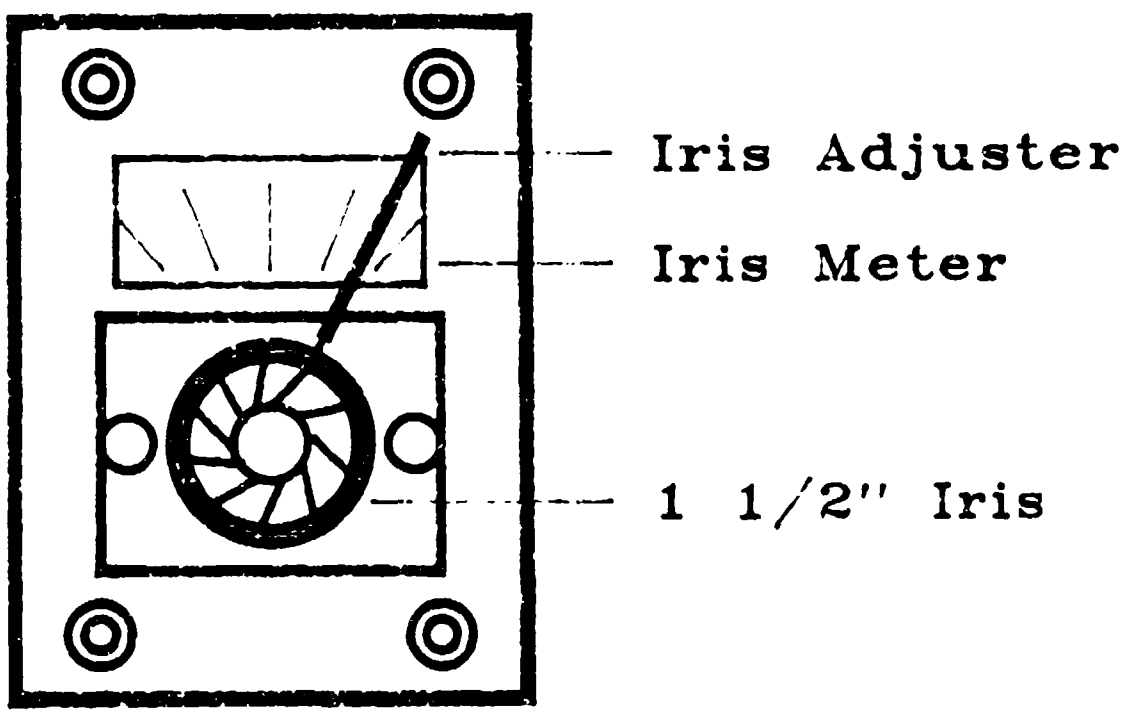

Figure 6.12 Mechanical Measuring Device - Rear View

run was normally terminated before the photographic measurement.

To use this device, the iris side is placed against the microwave viewing window. The person looks through the other hole at the plasma and adjusts the iris to contain the plasma, both its height and width. Using the scale provided, a plasma dimension can be obtained by multiplying the reading value by a calibrated number. This device has a measurement error of 10%.

CHAPTER VII

SPECTROSCOPY

7.1 Introduction.

The electron temperature was an important parameter characterizing the plasma. The spectroscopy experiment was used to calculate (or approximate a calculation of) that temperature. Chapter two described the theory behind this calculation and chapter four described the experimental system.

Before doing spectroscopic experiments, two things were done. First, a computer program was written (in Basic language) to use the data acquisition system. The adjustment coefficients in the program and the frequency (timing) of data acquisition were optimized such that the measurement errors were less than 0.5% from the digital electrometer.

Second, the spectrometer was calibrated using a Model 245C tungsten lamp (from Optronics Laboratories, Inc.) with known intensity readings. The known intensity readings were obtained from the 17 AUG 82 calibration of the lamp. A current of 6.500 ± 0.001 amps was supplied to the lamp. Instrumental readings were taken for the spectrometer over a wavelength range of 3000 Å through 9000 Å. The results of this calibration are provided in Table 7.1. Linear interpolation was used to calculate the spectral response function (R_λ) for specific wavelengths. The R_λ's in Table

7.1 were calculated using the following non-dimensionalized equations:

$$R_\lambda = \left(\frac{\text{Measured Intensity}}{\text{Known Intensity}}\right)_{\lambda=6300} \times \left(\frac{\text{Known Intensity}}{\text{Measured Intensity}}\right) \qquad 7.1$$

$$R_\lambda = 120 \left(\frac{\text{Known Intensity}}{\text{Measured Intensity}}\right) \qquad 7.2$$

To use equation 2.105, several coefficients must be provided. Because the electron temperature was calculated from the slope of the equation calculations, several wavelengths must be measured. From several scans of the spectrum, four strong and recognizeable transition regions (wavelengths) were observed. The data for those wavelengths are provided in table 7.2[1]. Although equation 2.105 requires those transitions to be ground state originating, not enough strong transition regions were observed to calculate an electron temperature. Therefore, equation 2.105 was used for non-ground state transitions.

Table 7.2 Electronic Transition Values for Helium

λ_{nm}	R_λ	g_n	A_{nm}	E_n
2945.11	0.087	9	0.0320	3.851E-18
3888.65	0.086	9	0.0948	3.687E-18
4471.48	0.220	15	0.2460	3.803E-18
8361.69	25.51	9	0.0033	3.878E-18

Table 7.1 Spectrophotometer Calibration (using 6.5 amp Tungsten Lamp)

λ	Known Intensity	Measured Intensity	R_λ	λ	Known Intensity	Measured Intensity	R_λ
3000	0.00358	3.06	0.141	6100	0.4692	63.33	0.890
3100	0.00547	2.77	0.238	6200	0.4914	62.54	0.942
3200	0.00735	2.84	0.311	6300	0.5136	61.66	1.000
3300	0.0139	4.14	0.316	6400	0.5358	49.67	1.295
3400	0.0145	9.86	0.177	6500	0.5580	34.26	1.956
3500	0.0180	21.04	0.103	6600	0.5796	21.78	3.195
3600	0.0234	35.97	0.078	6700	0.6012	13.70	5.268
3700	0.0288	52.37	0.066	6800	0.6228	9.40	7.958
3800	0.0374	61.66	0.073	6900	0.6444	6.48	11.93
3900	0.0461	62.64	0.088	7000	0.666	4.89	16.34
4000	0.0547	63.13	0.104	7100	0.683	3.89	21.08
4100	0.0680	63.62	0.128	7200	0.700	3.55	23.69
4200	0.0812	63.87	0.153	7300	0.717	3.35	25.68
4300	0.0945	63.87	0.178	7400	0.734	3.45	25.54
4400	0.1077	63.87	0.202	7500	0.751	3.47	25.95
4500	0.1210	64.11	0.227	7600	0.763	3.45	26.55
4600	0.1348	64.36	0.251	7700	0.775	3.74	24.85
4700	0.1586	64.11	0.297	7800	0.788	4.06	23.29
4800	0.1774	64.36	0.331	7900	0.7998	4.21	22.82
4900	0.1962	64.36	0.366	8000	0.812	4.04	24.15
5000	0.2150	64.36	0.401	8100	0.819	3.82	25.76
5100	0.2372	64.36	0.443	8200	0.825	3.87	25.62
5200	0.2594	64.36	0.484	8300	0.832	3.82	26.17
5300	0.2816	64.36	0.525	8400	0.839	4.01	25.10
5400	0.3038	64.11	0.569	8500	0.846	4.04	25.16
5500	0.3260	64.11	0.611	8600	0.852	4.43	23.10
5600	0.3502	64.11	0.656	8700	0.859	4.70	21.95
5700	0.3744	63.87	0.704	8800	0.866	5.14	20.23
5800	0.3986	63.87	0.749	8900	0.872	5.80	18.05
5900	0.4228	63.62	0.798	9000	0.879	6.41	16.46
6000	0.4470	63.38	0.847				

7.2 Experimental Results.

An experiment was done using helium in the TM_{012} mode with no gas flow at a power of 220 watts. The pressure range was 400 - 800 torr. For this experiment, the electron temperature was assumed to be that of the electronic temperature under the assumption that local thermal equilibrium occurs (see equation 2.106). The results are provided in Figure 7.1.

Because there was a shape and magnitude difference between my data and that of Hoekstra, I plotted the same data for a similar experiment from Mueller and Micci[32]. Although not shown, Chapman's results were important in that his results showed the electron temperature dependence upon pressure[8]. Additionally, it shows results using Hoekstra's technique of data acquisition and interpretation.

The volume electron temperature is expected to decrease as pressure increases. It takes less energy to maintain a smaller volume of plasma (which decreases with increasing pressure). However, the peak electron temperature is expected to increase with pressure increases. Chapman's results for very low pressure (0.5 - 10 torr) showed a decreasing temperature with an increasing pressure[8].

The magnitude difference can be explained because a different technique in data acquisition occurred. Hoekstra used the same technique Chapman did by measuring the peak heights on a chart recorder. Chapman's results had temperatures around 5,000°K. My data were calculated measuring the area under the peak using a data acquisition system with a computer.

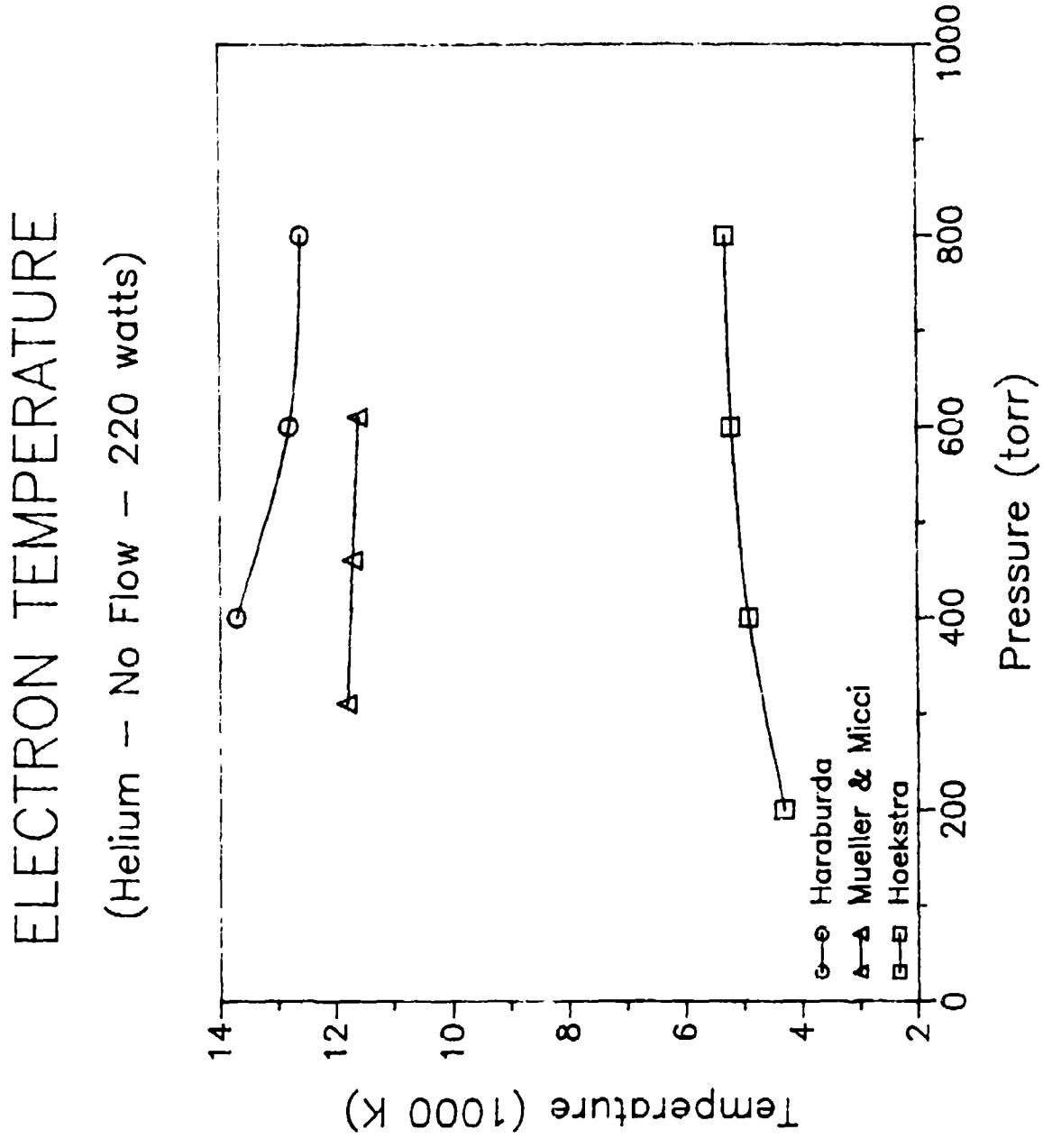

Figure 7.1 Electron Temperature of Helium

Therefore, the electron temperature is expected to be near 13,000°K for pressures near atmospheric. Additionally, the electron temperature is expected to decrease with increasing pressure.

CHAPTER VIII

COMPUTER MODEL OF ELECTRON DIFFUSION

8.1 Introduction.

An explanation of the diffusion of the electron in the plasma region was briefly covered in chapter two. An analytical solution was obtained by neglecting the generation term in the continuity equation. As previously mentioned, this is typically assumed for very low pressures. Unfortunately, this assumption is not valid for high pressures, such as atmospheric. As pressure increases, the density of the gas increases. This increased density results in an increase in the collision rates, such as recombination and ionization. The purpose of this chapter is to develop a numerical method to see the effects that electron recombination and electron ionization have upon the distribution gradient of the electron density within the plasma.

8.2 Development of Mathematical Model.

An assumption is made that the ion and electron densities are equal. As a result, equation 2.34 (continuity equation for electrons) can be re-written as (with N defined as the normalized electron density):

$$\frac{\partial^2 N}{\partial r^2} + \frac{\partial N}{r\,\partial r} + \frac{\partial^2 N}{\partial z^2} = \alpha N^2 - \nu_i N \qquad 8.1$$

This equation includes ambipolar diffusion. For no generation, this equation can be simplified by separating N into separate variables as mentioned in chapter. However, this method will not work for generation because of the non-linear recombination term on the right hand side. This thesis only considered the radial part of this equation. To calculate the electron density along the radial axis about the center plane (z=0) can be done by saying that:

$$\frac{\partial^2 N}{\partial z^2} = 0 \qquad 8.2$$

This is valid because the change of N is symmetric about the origin. The resulting equation is a second order differential equation:

$$\frac{d^2 N}{dr^2} = \frac{-\ dN}{r\ dr} + \alpha N^2 - \nu_1 N \qquad 8.3$$

This equation was re-written as a set of two first order differential equations by setting:

$$D = \frac{dN}{dr} \qquad 8.4$$

Therefore, the following set of first order differential equations were used to determine the electron density distribution in the radial direction along the center plane:

$$\frac{dN}{dr} = D \qquad 8.5$$

$$\frac{dD}{dr} = -\frac{D}{r} + \alpha N^2 - \nu_1 N \qquad 8.6$$

These equations were solved using the normalized density. The normalized density was the non-dimensional quantity with

N equal to one when the electron density is at its maximum value (or the center of the plasma).

For this simulation, the maximum density will be assumed to be $1x10^{12}$ electrons / cm^3. This density uas used because Chapman observed electron densities around this value[8]. Using this assumption, the recombination coefficient must be normalized. This coefficient is a function of temperature. For the assumed maximum electron density and for a temperature range of 250 - 64,000 °K, the recombination coefficient has a range of $1x10^{-13}$ - $1x10^{-6}$ recombinations cm^3 / sec [40].

The two boundary conditions required to solve this problem are:

$$N = 0 \qquad \text{at } r = R \tag{8.7}$$

$$N = 1 \qquad \text{at } r = 0 \tag{8.8}$$

8.3 Numerical Analysis.

A variable-step Runge Kutta method will be used to solve these two differential equations with the given boundary conditions. A fourth and fifth order evaluation with six evaluations per step will be done. These two evaluations will be done to estimate the relative error of each step. The following formulas for solving equation 8.5 will be used in the computer program[34]:

$$f(r_i, N_i) = \frac{dN_i}{dr} \tag{8.9}$$

$$K_1 = f(r_i, N_i) \tag{8.10}$$

$$K_2 = f\left(r_i + \frac{INC}{4},\ N_i + \frac{INC}{4} K_1\right) \qquad 8.11$$

$$K_3 = f\left(r_i + \frac{3}{8} INC,\ N_i + INC\left(\frac{3}{32} K_1 + \frac{9}{32} K_2\right)\right) \qquad 8.12$$

$$K_4 = f\left(r_i + \frac{12}{13} INC,\ N_i + INC\left(\frac{1932}{2197} K_1 - \frac{7200}{2197} K_2 + \frac{7296}{2197} K_3\right)\right) \qquad 8.13$$

$$K_5 = f\left(r_i + INC,\ N_i + INC\left(\frac{439}{216} K_1 - 8 K_2 + \frac{3680}{513} K_3 - \frac{845}{4104} K_4\right)\right) \qquad 8.14$$

$$K_6 = f\left(r_i + \frac{INC}{2}, N_i + INC\left(\frac{-8}{27}K_1 + 2K_2 - \frac{3544}{2565}K_3 + \frac{1859}{4104}K_4 - \frac{11}{40}K_5\right)\right) \qquad 8.15$$

$$N_{i+1} = N_i + INC\left(\frac{25}{216} K_1 + \frac{1408}{2565} K_3 + \frac{2197}{4104} K_4 - \frac{1}{5} K_5\right) \qquad 8.16$$

$$N_{i+1}^{(est)} = N_i + INC\left(\frac{16}{135} K_1 + \frac{6656}{12825} K_3 + \frac{28561}{56430} K_4 - \frac{9}{50} K_5 + \frac{2}{55} K_6\right) \qquad 8.17$$

The above formulas are the save for solving equation 8.6. Because those two equations (8.5 and 8.6) are coupled, they must be solved simultaneously. The relative error per unit step can be written as:

$$\left|N_{i+1}^{(est)} - N_{i+1}\right| \leq \varepsilon_{rel} \frac{INC}{(b - a)} \left|N_i\right| \qquad 8.18$$

The variable step in this program is the recalculation of the step size if the relative error is exceeded for that step. The gamma value (γ_{rel}) is the fraction of the old increment (INC) step size predicted to satisfy the error limitation. Because this method is a fourth order estimation, the fraction required will be the fourth root of the error equation (8.18) and will be defined as:

$$\gamma_{rel} = \left[\frac{\varepsilon_{rel}\ INC\ \left|N_i\right|}{\left|N_{i+1}^{(est)} - N_{i+1}\right| (b - a)}\right]^{0.25} \qquad 8.19$$

The new step size will be defined as:

$$INC^{(new)} = 0.8\ \gamma_{rel}\ INC^{(old)} \qquad 8.20$$

As needed, the program will recalculate the step size until the size is small enough to satisfy the error limitation. The program for this numerical analysis is located in appendix B.

The boundary conditions for this differential equation are not both initial value conditions. Because they contain an initial and final value, a "shooting method" approach was used for the numerical method. An estimation for the initial derivative of N at R=1 is predicted. This prediction is continually changed until the final boundary condition is obtained.

8.4 Computer Simulation.

Simulations were done using the above method (see appendix B). One simulation looked at the effects of recombination while the other looked at the effects of ionization. The step sizes for the simulations were reduced until the step size required for the no generation simulation resulted in a solution matching the analytical solution of equation 2.49.

In the first simulation, the ionization frequency was set to zero. Four runs of the program were done varying the dimensionless recombination coefficient from 0 to 1000 (or from 0 to 1×10^{-9} recombinations cm^3 / sec in dimensional form). For low recombination coefficients, the plasma electrons extend to the wall. As seen in Figure 8.1, higher values of recombination cause the plasma to contract. As

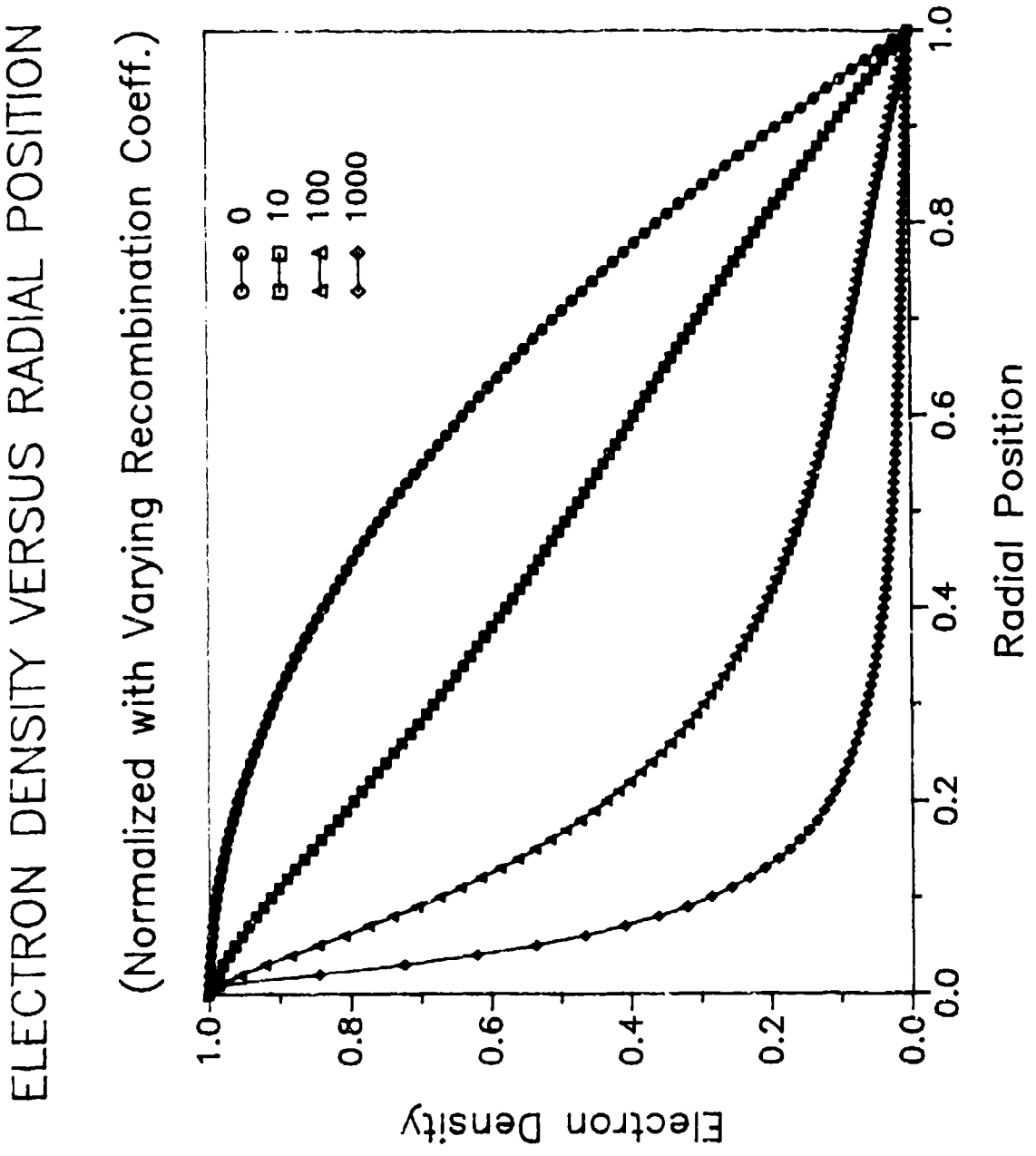

Figure 8.1 Radial Electron Density Gradient - Recombination Effects

observed in chapter six, the plasma width becomes smaller as pressure increases. This simulation illustrates why that happens. Additionally, the difference between strong and weak regions can be implied by the shape of those curves (in Figure 8.1). The curve clearly shows that the center of the plasma has the highest density of electrons. The outer region becomes less dense. Depending upon the cutoff density for each observed region, an electron density profile may be generated for plasma conditions observed in chapter six.

The second simulation held the dimensionless recombination at 1000 and varied the ionization frequency from 0 to 30 ionizations / sec. Because of the large amount of energy required to ionize a neutral atom, multiple collisions are required by the electrons for ionization to occur. Therefore, the ionization is expected to be small and almost negligible. As seen in Figure 8.2, the electron density near the wall becomes slightly larger when ionization occurs.

These simulations illustrate that an accurate model describing the electron distribution must include the generation term. These simulations do not provide a very accurate model as they used constant values for recombination and ionization. These values are a function of temperature and pressure, which in turn depends upon position. Nevertheless, the simulations do provide some insight into what the electron gradient is and why it is for various situations.

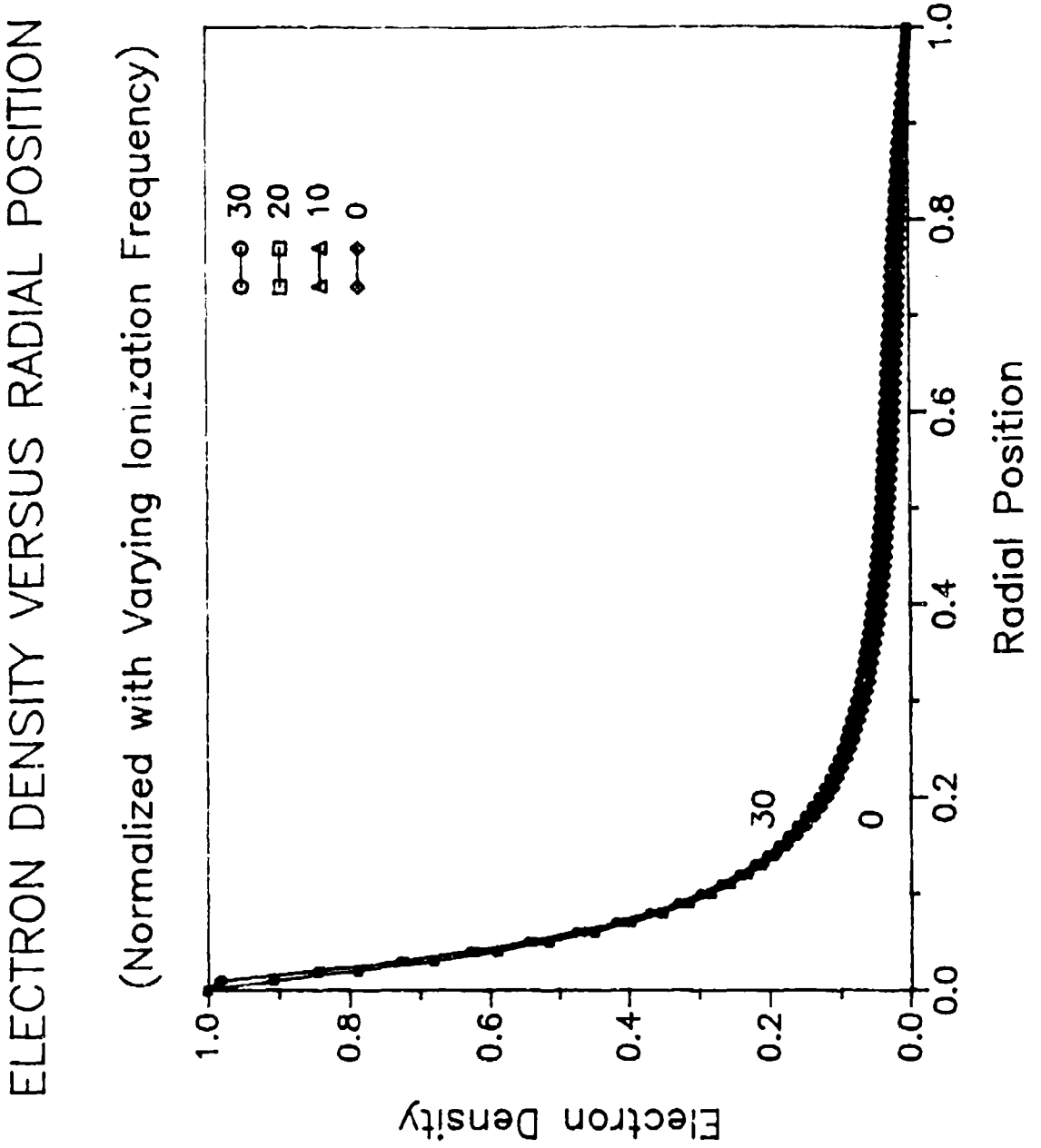

Figure 8.2 Radial Electron Density Gradient - Ionization Effects

CHAPTER IX

CONCLUSIONS

Several different conclusions can be drawn upon the work of this thesis. Potential use of this type of thruster is important. Also, the need for conducting a microscopic theoretical analysis for plasma phenomena is addressed. The three diagnostic techniques discussed provide needed information to characterize the macroscopic energy transfer within a microwave induced plasma. Finally, computer numerical models provide useful information concerning plasma transport phenomena.

Because the microwave-induced plasma electrothermal rocket system experimentally displays similar characteristics to other electrothermal rocket systems, it has shown its potential application for spacecraft propulsion. Electrothermal thrusters lack high thrust, but have high specific impulse which is very useful for platform station keeping.

Investigating the microscopic theory of plasma particles is very important. From the conservation of particles and momentum, the shape of the plasma can be predicted. From the conservation of energy, the gradients of important parameters can be predicted, such as temperature and pressure gradients. Therefore, modeling transport properties must include a microscopic theoretical analysis.

The energy distribution experiment provided us with the importance behind the condition of the containment wall. A dirty wall can absorb a large amount of power. Reversing the gas flow showed a negligible difference in the energy distribution. The power distribution appears to stabilize for flow rate beyond 500 SCCM. Finally, initial power absorption to the plasma is 67% in the TM_{012} mode and 80% in the TM_{011} mode.

The plasma dimensions experiment provided us with the effects that pressure, flow rate, and power have upon the volume and shape of the plasma. The volume is decreased as pressure increases, flow rate decreases, or power decreases. Additionally, high flow rates tend to elastically elongate the shape of the plasma. Unlike nitrogen plasmas exhibiting an ellipsoidal shape, helium plasmas exhibit a "dumbbell" shape.

The spectroscopy experiment provided us with an estimate for the electron temperature and the effects pressure had upon that temperature. The electron temperature is approximately 13,000°K in the atmospheric pressure region. Finally, the electron temperature decreases as pressure increases.

The computer model provided us with the importance of the recombination and ionization effects. For low pressures when recombination and ionization coefficients are negligible, the wall recombination plays a very important role in the shape of the plasma. The plasma reaches the wall. For high pressures when those coefficients are important, wall recombination becomes less important. The plasma forms an ellipsoidal shape and does not reach the wall.

CHAPTER X

RECOMMENDATIONS

Improvements can be made on future research in the areas of equipment modification, experiments, and theoretical modeling.

10.1 Equipment Modifications.

An accurate model for the plasma region must account for the flow pattern (i.e. the velocity profile). A major area which needs to be addressed is flow in and out of the plasma. For example, does the flow by-pass or pass through the plasma discharge? If both occur, how much of the flow by-passes the discharge? To answer these questions, modification to the collars of the plasma tubes should be done. The collars should be modified such that the flow velocity contains an angular component (swirling flow). Furthermore, this modification should include an adjuster such that the axial helix interval can be varied. Additionally, a modification to the collars should include a way for an additional gas to enter. This additional gas can be used to conduct streamline and pulse change experiments.

Another important problem with modeling plasmas in a microwave resonance cavity deals with power absorption to the walls. For an efficient thruster system, power absorbed by the walls must be minimized. As seen in chapter 5, the condition of the cavity wall influences power absorption to the wall. Two main types of energy are

absorbed by the wall - radiation and convection. To minimize radiation energy to the wall, the inside wall of the cavity should act as a mirror. A mirror coating, such as silver, should reflect most of the radiation energy to the plasma.

When the investigations of analyzing the plasma region and the thruster region result in an accurate model, one should consider combining the two experiments. For example, a nozzle should be connected to the cavity system to investigate thrust and efficiency measurements. This should result in optimizing the location of the plasma relative to the nozzle.

The quartz tube provides a large unknown temperature gradient. Presently, we can estimate the outer wall temperature of the inner tube as being the temperature of the exiting air coolant. An infrared temperature probe can be used to measure an intermediate level temperature of the plasma. This temperature can be approximated to be that of the inner wall temperature.

The wall effects on a plasma are important. One such effect is wall recombination. This wall recombination affects the size and shape of the plasma. To investigate this effect, one should conduct experiments using various sizes and shapes for the confinement tube.

Finally, with part of the experimental system being automated, one should consider automating the entire system. The next step in automating the system includes connecting both the temperature probes from the calorimetry experiments and the power meters (incident and reflective) from the microwave power source to the data acquistion

system. Once this is completed, a computer program should be written to numerically analyze the data as it is being collected.

10.2 Proposed Experiments.

Several new areas of experiments should be considered. Some of them involve the equipment modifications as mentioned above. Dependent upon those modifications, the following experiments can be conducted. Flow pattern experiments can be done to determine the flow to and from the plasma as a function of the environmental variables (i.e. pressure and flow conditions). Power absorption to the walls of the mirror coated cavity should be compared to the mirrorless cavity. Simultaneous thruster and plasma experiments should be conducted. Estimates of the inner wall temperatures should be compared to changes in the environment. Finally, simultaneous experiments should be done using a completely automated system to provide more accurate data for constant environmental conditions.

Experiments which can presently be done involve power increases and gas mixtures. Increasing the power to above one kilowatt should be done. This would provide a more realistic model characterizing the dependence upon power. Finally, gas mixtures should be done starting with non-reactive binary gases. This work should continue into investigating tertiary reactive gases. This evolution of experiments may someday branch off into a new type of rocket thruster mention by Pollard[15]. This new type of thruster is a hybrid chemical / electric thruster. The reactive gases could simulate a chemical thruster with high thrust, while the non-reactive gases could simulate an electric thruster

with high impulse. This is a new concept which should seriously be considered.

10.3 Theoretical Modeling.

Given the large amount of data collected, work should be done in correlating the analyzed variables. For example, we would need a model to estimate the power distribution and plasma dimensions for a given environmental condition (i.e. pressure and flow pattern).

An initial step towards modeling the plasma region was taken in chapter eight. The weakness of that model stems form its unrealistic assumptions (constant temperature and pressure throughout the plasma discharge). A more accurate model should be developed which accounts for the non-zero temperature gradient. Additionally, because the electron is not the only important species in the plasma, the gradient profile of the other species (i.e. ions and neutrals) should be determined.

Another important model involves energy and species transfer to and from the plasma region. A model should be developed to estimate the energy and mass transport properties between the plasma and its adjoining fluid.

10.4 Recommendation List.

The following summarizes and lists the above recommendations:

1. To modify the plasma tube collars to allow experiments to be conducted for investigating flow patterns near the plasma discharge.

2. To mirror coat the resonance cavity for minimizing power absorption to the wall.

3. To combine the cavity and thruster experimental systems for analyzing the optimal location of the plasma with respect to the nozzle.

4. To use an infrared temperature probe for estimating the inner wall temperature.

5. To use different size containment tubes for investigating the wall effects upon the plasma.

6. To completely automate the experimental system so that one can conduct simultaneous experiments.

7. To conduct increased power experiments for providing data with power above one kilowatt.

8. To conduct mixture experiments for providing an expanded data base beyond pure gas experiments.

9. To correlate the given and future data for predicting power distribution and plasma dimensions.

10. To develop a theoretical model for determining the species and temperature gradients within the plasma discharge.

11. To develop a theoretical model for predicting the transport properties between the plasma and the adjacient fluid.

REFERENCES

1. CRC Press, Inc., Handbook of Chemistry and Physics, 68th ed. [1988].

2. National Research Council Panel on the Physics of Plasmas and Fluids, Plasmas and Fluids, Washington D.C., National Academy Press [1986].

3. Hellund, E.J., The Plasma State , New York, Reinhold Publishing Corp. [1961].

4. Dryden, H.L., "Power and Propulsion for the Exploration of Space," Advances in Space Research , New York Permagon Press [1964].

5. Langton, N.H., ed., Rocket Propulsion, New York, American Elsevier Publishing Co. [1970].

6. Hawley, M.C., Asmussen, J., Filpus, J.W., Whitehair, S., Hoekstra, C., Morin, T.J., Chapman, R., "A Review of Research and Development on the Microwave-Plasma Electrothermal Rocket", Journal of Propulsion and Power, Vol 5, No 6 [1989].

7. Moisson, M. and Zakrzewski, Z., "Plasmas Sustained by Surface Waves at Microwave and RF Frequencies: Experimental Investigation and Applications", Radiative Processes in Discharge Plasmas, Pletnum Press [1987].

8. Chapman, R., "Energy Distribution and Transfer in Flowing Hydrogen Microwave Plasmas." Ph.D. Dissertation, Michigan State University [1986].

9. Bennett, C., and Myers, J., Momentum, Heat, and Mass Transfer, 2nd ed., McGraw-Hill, Inc., New York [1974].

10. Hoekstra, C.F., "Investigations of Energy Transport Properties in High Pressure Microwave Plasmas." M.S. Thesis, Michigan State University [1988].

11. Eddy, T.L., "Low Pressure Plasma Diagnostic Methods," AIAA/ASME/SAE/ASEE 25th Joint Propulsion Conference [1989].

12. Eddy, T.L., and Sedghinasab, A., "The Type and Extent of Non-LTE in Argon Arcs at 0.1 - 10 Bar," IEEE Transactions on Plasma Science, Vol 16, No 4 [1988].

13. Cho, K.Y., and Eddy, T.L., "Collisional-Radiative Modeling with Multi-Temperature Thermodynamic Models," Journal Quant. Spectrosc. Radiat. Transfer, Vol 41, No 4 [1989].

14. Eddy, T.L., "Electron Temperature Determination in LTE and Non-LTE Plasmas," Journal Quant. Spectrosc. Radiat. Transfer , Vol 33, No 3 [1985].

15. Pollard, J.E., and Cohen, R.B., Hybrid Electric Chemical Propulsion, Report SD-TR-89-24, Air Force Systems Command [1989].

16. Stone, J.R., Recent Advances in Low Thrust Propulsion Technology, NASA Technical Memorandum 100959 [1988].

17. Sovey, J.S., Zana, L.M., and Knowles, S.C., Electromagnetic Emission Experiences Using Electric Propulsion Systems - A Survey, NASA Technical Memorandum 100120 [1987].

18. Hawkins, C.E., and Nakanishi, S., Free Radical Propulsion Concept, NASA Technical Memorandum 81770 [1981].

19. Aston, G., and Brophy, J.R., "A Detailed Model of Electrothermal Propulsion Systems," AIAA/ASME/SAE/ASEE 25th Joint Propulsion Conference [1989].

20. Beattie, J.R., and Penn, J.P., "Electric Propulsion - National Capability," AIAA/ASME/SAE/ASEE 25th Joint Propulsion Conference [1989].

21. Stone, J.R., and Bennet, G.L., The NASA Low Thrust Propulsion Program, NASA Technical Memorandum 102065 [1989].

22. Morin, T.J., "Collision Induced Heating of a Weakly Ionized Dilute Gas in Steady Flow," Ph.D. Dissertation, Michigan State University [1985].

23. Carr, M.B., "Life Support Systems," Military Posture - FY 1985, Joint Chiefs of Staff [1985].

24. Whitehair, S.J., "Experimental Development of a Microwave Electrothermal Thruster," Ph.D. Dissertation, Michigan State University [1986].

25. Halliday, D., and Resnick, R., Physics, New York, John Wiley and Sons [1978].

26. Samaras, D.G., Theory of Ion Flow Dynamics, Englewood Cliffs, N.J., Prentice-Hall, Inc. [1962].

27. Mason, E.A., and McDonald, E.W., Transport Properties of Ions in Gases, New York, John Wiley and Sons [1988].

28. Cherrington, B.E., Gaseous Electronics and Gas Lasers, New York, Pergamon Press [1979].

29. Cambel, A.B., Plasma Physics and Magnetofluid Mechanics, New York, McGraw Hill Book Company, Inc. [1963].

30. Panofsky, W.K.H., and Phillips, M., Classical Electricity and Magnetism, 2nd ed., Reading, Massachusetts, Addison-Wesly Publishing Co. [1962].

31. Johnson, L.W., and Ross,R.D., Numericai Analysis, 2nd ed., Phillipines, Addison-Wesley Publishing Co. [1982].

32. Mueller, J., and Micci, M., "Investigation of Propagation Mechanism and Stabilization of a Microwave Heated Plasma," AIAA/ASME/SAE/ASEE 25th Joint Propulsion Conference [1989].

33. Atwater, H.A., Introduction to Microwave Theory, New York, McGraw Hill Book Company [1962].

34. Goodger, E.M., Principles of Spaceflight Propulsion, Oxford, Pergamon Press [1970].

35. Jahn, R.G., Physics of Electric Propulsion, New York, McGraw Hill Book Company [1968].

36. Davis, H.F., and Snider, A.D., Vector Analysis, Dubuque, Iowa, Wm. C. Brown Publishers [1988].

37. Kreyszig, E., Advanced Engineering Mathematics, New York, John Wiley & Sons [1988].

38. Bromberg, J.P., Physical Chemistry, Boston, Allyn and Bacon [1980].

39. Nicholson, D.R., Introduction to Plasma Theory, New York, John Wiley & Sons [1983].

40. McDaniel, E.W., Collision Phenomena in Ionized Gases, New York, John Wiley & Sons [1964].

41. Haraburda, S., and Hawley, M., "Investigations of Microwave Plasmas (Applications in Electrothermal Thruster Systems)," AIAA/ASME/SAE/ASEE 25th Joint Propulsion Conference [1989].

APPENDIX A

MATHEMATICS

A.1 Introduction.

The following appendix highlights the vector operations, phasor transformations (from time domain), and series solutions / orthoganalility used in this thesis. Only cartesian and cylindrical coordinates will be discussed. It is noted that spherical coordinates can be used, but are not used in this paper.

A.2 Vector Operations[36].

The following expressions and equations are used throughout the presentation of this thesis:

Cartesian Coordinate Vector:

$$\bar{E} = E_x\hat{x} + E_y\hat{y} + E_z\hat{z} \qquad A.1$$

Cylindrical Coordinate Vector:

$$\bar{E} = E_r\hat{r} + E_\theta\hat{\theta} + E_z\hat{z} \qquad A.2$$

Vector Addition:

$$\bar{E} + \bar{H} = (E_x + H_x)\hat{x} + (E_y + H_y)\hat{y} + (E_z + H_z)\hat{z} \qquad A.3$$

Scalar Vector Multiplication:

$$\sigma\bar{E} = \sigma E_x\hat{x} + \sigma E_y\hat{y} + \sigma E_z\hat{z} \qquad A.4$$

Vector Dot Product:

$$\bar{E} \cdot \bar{H} = E_xH_x + E_yH_y + E_zH_z \qquad A.5$$

Vector Cross Product:

$$\bar{E} \times \bar{H} = (E_yH_z - E_zH_y)\hat{x} + (E_zH_x - E_xH_z)\hat{y} + (E_xH_y - E_yH_x)\hat{z} \qquad A.6$$

Gradient of a function:

$$\nabla f(x,y,z) = \frac{\partial f}{\partial x}\hat{x} + \frac{\partial f}{\partial y}\hat{y} + \frac{\partial f}{\partial z}\hat{z} \qquad A.7$$

$$\nabla f(r,\theta,z) = \frac{\partial f}{\partial r}\hat{r} + \frac{\partial f}{r\,\partial\theta}\hat{\theta} + \frac{\partial f}{\partial z}\hat{z} \qquad A.8$$

Divergence of a Vector:

$$\nabla\cdot\bar{E}(x,y,z) = \frac{\partial E_x}{\partial x} + \frac{\partial E_y}{\partial y} + \frac{\partial E_z}{\partial z} \qquad A.9$$

$$\nabla\cdot\bar{E}(r,\theta,z) = \frac{\partial (rE_r)}{r\,\partial r} + \frac{\partial E_\theta}{r\,\partial\theta} + \frac{\partial E_z}{\partial z} \qquad A.10$$

Curl of a Vector:

$$\nabla\times\bar{E}(x,y,z) = \left(\frac{\partial E_z}{\partial y} - \frac{\partial E_y}{\partial z}\right)\hat{x} + \left(\frac{\partial E_x}{\partial z} - \frac{\partial E_z}{\partial x}\right)\hat{y} + \left(\frac{\partial E_y}{\partial x} - \frac{\partial E_x}{\partial y}\right)\hat{z} \qquad A.11$$

$$\nabla\times\bar{E}(r,\theta,z) = \left(\frac{\partial E_z}{r\partial\theta} - \frac{\partial E_\theta}{\partial z}\right)\hat{r} + \left(\frac{\partial E_r}{\partial z} - \frac{\partial E_z}{\partial r}\right)\hat{\theta} + \frac{1}{r}\left(\frac{\partial (rE_\theta)}{\partial r} - \frac{\partial E_r}{\partial\theta}\right)\hat{z} \qquad A.12$$

Laplacian of a function:

$$\nabla^2 f(x,y,z) = \nabla\cdot(\nabla f) = \frac{\partial^2 f}{\partial x^2} + \frac{\partial^2 f}{\partial y^2} + \frac{\partial^2 f}{\partial z^2} \qquad A.13$$

$$\nabla^2 f(r,\theta,z) = \frac{\partial}{r\ \partial r}\left(\frac{r\ \partial f}{\partial r}\right) + \frac{\partial^2 f}{r^2\ \partial\theta^2} + \frac{\partial^2 f}{\partial z^2} \qquad A.14$$

A.3 Phasor Transformation.

Phasors are defined as transformation of a differential or integral of a time dependant function into an algebraic expression. To accomplish this, one must rewrite the time domain function as the real component of a complex phase domain function.

Let:

$$f(t) = \cos(\omega t) \qquad A.15$$

Rewritten as real component of complex phase domain function:

$$f(t) = \mathrm{Re}\left[\cos(\omega t) + j\ \sin(\omega t)\right] \qquad A.16$$

Differential

Differential equation:

$$\frac{d\ f(t)}{dt} = \mathrm{Re}\left[\frac{d\ \cos(\omega t)}{dt} + \frac{d\ [j\ \sin(\omega t)]}{dt}\right] \qquad A.16$$

$$\frac{d\ f(t)}{dt} = \mathrm{Re}\left[-\omega\ \sin(\omega t) + j\omega\ \cos(\omega t)\right] \qquad A.17$$

$$\frac{d\ f(t)}{dt} = -\omega\ \sin(\omega t) \qquad A.18$$

Define Differential Phasor:

$$\boxed{\frac{d}{dt} = j\omega} \qquad \text{A.19}$$

Substitution:

$$\frac{d\ f(t)}{dt} = j\omega\ f(t) \qquad \text{A.20}$$

$$\frac{d\ f(t)}{dt} = j\omega\ \mathrm{Re}\left[\cos(\omega t) + j\ \sin(\omega t)\right] \qquad \text{A.21}$$

$$\frac{d\ f(t)}{dt} = \mathrm{Re}\left[j\omega\ \cos(\omega t) - \omega\ \sin(\omega t)\right] \qquad \text{A.22}$$

$$\frac{d\ f(t)}{dt} = -\omega\ \sin(\omega t) \qquad \text{A.23}$$

Integral

Integral Equation:

$$\int f(t)\ dt = \mathrm{Re}\left[\int \cos(\omega t)\ dt + \int j\ \sin(\omega t)\ dt\right] \qquad \text{A.24}$$

$$\int f(t)\ dt = \mathrm{Re}\left[\frac{\sin(\omega t)}{\omega} - \frac{j\ \cos(\omega t)}{\omega}\right] \qquad \text{A.25}$$

$$\int f(t)\ dt = \frac{\sin(\omega t)}{\omega} \qquad \text{A.26}$$

Define Integral Phasor:

$$\boxed{\int dt = \frac{1}{j\omega} = \frac{-j}{\omega}} \qquad \text{A.27}$$

Substitution:

$$\int f(t)\,dt = \frac{1}{j\omega}\,\mathrm{Re}\left[\cos(\omega t) + j\sin(\omega t)\right] \qquad A.28$$

$$\int f(t)\,dt = \mathrm{Re}\left[\frac{\cos(\omega t)}{j\omega} + \frac{\sin(\omega t)}{\omega}\right] \qquad A.29$$

$$\int f(t)\,dt = \frac{\sin(\omega t)}{\omega} \qquad A.30$$

A.4 Series Solutions and Orthoganality[37].

A series solution method is used to calculate the solution of special kinds of higher order differential equations. For this thesis, only the Bessel differential equation is used. Orthoganality is used for calculation the coefficients of the solution. Bessel functions and certain types of trigonometric series are orthoganal.

Bessel's Differential Equation:

$$x^2\frac{d^2y}{dx^2} + x\frac{dy}{dx} + (x^2 - \psi_1^2)\,y = 0 \qquad A.31$$

Series Solution (Frobenius Method) to equation A.31:

$$y(x) = \sum_{m=0}^{\infty} a_m\, x^{m+\psi} \qquad A.32$$

Obvious Solution for ψ :

$$\psi = \pm\,\psi_1 \qquad A.33$$

Define Bessel Function of First Kind:

$$J_{\psi}(x) = x^{\psi} \sum_{m=0}^{\infty} \frac{(-1)^m x^{2m}}{2^{2m+\psi}\, m!\, (\psi+m)!} \qquad \text{A.34}$$

Substitution for ψ :

$$y(x) = \sum_{n=0}^{\infty} \left[C_n J_{\psi_1}(\alpha_n x) + D_n J_{-\psi_i}(\alpha_n x) \right] \qquad \text{A.35}$$

Solutions for C_n and D_n can be calcuiated from the properties of orthoganality.

Define Inner Product of Two Functions:

$$\langle f(x), g(x) \rangle = \int f(x)\, g(x)\, dx \qquad \text{A.36}$$

Inner Product of Orthoganal Functions:

$$\langle f(x), g(x) \rangle = 0 \quad \text{for} \quad f(x) \neq g(x) \qquad \text{A.37}$$

Rewriting y(x):

$$y(x) = C_1 f(x) + C_2 g(x) + \cdots \qquad \text{A.38}$$

To solve for C_1, one must multiply each side by f(x) and a

weight function, w(x), and integrate over the domain of the function.

$$\int w(x)f(x)y(x)dx = \int C_1 w(x)f(x)f(x)dx + \int C_2 w(x)f(x)g(x)dx + \cdots \quad A.39$$

By orthoganality of the series:

$$\int w(x)\ f(x)\ y(x) \ = \ \int C_1 w(x)\ f(x)\ f(x)\ dx \ + \ 0 \quad A.40$$

Rearranging the terms:

$$C_1 \ = \ \frac{\int w(x)\ f(x)\ y(x)\ dx}{\int w(x)\ f(x)\ f(x)\ dx} \quad A.41$$

Some useful integrals of Bessel functions[37]:

$$\int x^n J_{n-1}(x)\ dx = x^n J_n(x) + C_1 \quad A.42$$

$$\int J_{n+1}(x)\ dx = \int J_{n-1}(x)\ dx - 2J_n(x) \quad A.43$$

$$\int x^{-n} J_{n+1}(x)\ dx = -x^{-n} J_n(x) + C_1 \quad A.44$$

$$\int_0^R x\ J_n^2(x)\ dx = \frac{R^2}{2} J_{n+1}^2(R) \quad A.45$$

A.5 Useful Vector Properties[39].

The following are several useful vector relationships which become very helpful when solving vector related equations such as Maxwell's equations for electromagnetics.

$$\bar{A} \cdot (\bar{B} \times \bar{C}) = (\bar{A} \times \bar{B}) \cdot \bar{C} = \bar{B} \cdot (\bar{C} \times \bar{A}) \quad A.46$$

$$\bar{A} \times (\bar{B} \times \bar{C}) = (\bar{A} \cdot \bar{C})\,\bar{B} - (\bar{A} \cdot \bar{B})\,\bar{C} \qquad \text{A.47}$$

$$(\bar{A} \times \bar{B}) \cdot (\bar{C} \times \bar{D}) = (\bar{A} \cdot \bar{C})\,(\bar{B} \cdot \bar{D}) - (\bar{A} \cdot \bar{D})\,(\bar{B} \cdot \bar{C}) \qquad \text{A.48}$$

$$\nabla (f\,g) = f\,\nabla g + g\,\nabla f \qquad \text{A.49}$$

$$\nabla \cdot (f\,\bar{A}) = f\,\nabla \cdot \bar{A} + \bar{A} \cdot \nabla f \qquad \text{A.50}$$

$$\nabla \times (f\,\bar{A}) = f\,\nabla \times \bar{A} + \nabla f \times \bar{A} \qquad \text{A.51}$$

$$\nabla^2 \bar{A} = \nabla\,(\nabla \cdot \bar{A}) - \nabla \times (\nabla \times \bar{A}) \qquad \text{A.52}$$

$$\nabla \times \nabla f = \nabla \cdot (\nabla \times \bar{A}) = 0 \qquad \text{A.53}$$

APPENDIX B

COMPUTER PROGRAM

The following is the computer program used for calculating the normalized electron density for chapter eight.

```
      PROGRAM ARMY1
*****************************************************************
*                                                               *
*     PROGRAM:  Runge Kutta Solution for Electron Diffusion     *
*        NAME:  Scott S. Haraburda                              *
*        DATE:  1 January 1990                                  *
*DESCRIPTION: This program is designed to estimate electron     *
*           concentration gradient within the plasma region     *
*           using the fifth order Runge Kutta numerical method  *
*           using variable step size control.  This control is  *
*           accomplished using an absolute error test.          *
*                                                               *
*   VARIABLES:HSTART - The Initial Step Size for the Program.   *
*             HMIN   - The Minimum Step Size for the Program.   *
*             HMAX   - The Maximum Step Size for the Program.   *
*             RTOL   - The Relative Tolerance Level.            *
*             RERR   - The Relative Error for a Given Step.     *
*             Q      - The Initial N Value in the Interval.     *
*             R      - The Latter N Value in the Interval.      *
*             RQ     - The Value of R at Point Q.               *
*             RR     - The Value of R at Point R.               *
*             NQ     - The Value of N at Point Q.               *
*             NR     - The Value of N at Point R.               *
*             DT     - The Given Step Size for the Program      *
*             ROLD   - The Old Value of R.                      *
*             RNEW   - The New Value of R.                      *
*             NOLD   - The Old Value of N.                      *
*             NNEW   - The New Value of N.                      *
*             GAMMA  - The Calculated Fractional Step Size      *
*             IFLAG  - The Termination and Write Flag.          *
*             RK1-6  - The Runge Kutta Functions.               *
*             NK1-6  - The Runge Kutta Functions.               *
*             EST    - The Estimated Error.                     *
*             A1-5   - The Runge Kutta Coefficients for New     *
*             R1-6   - The Runge Kutta Coefficients for EST.    *
*             I      - The Loop Integer for Main Program.       *
*             IR     - The Collision Rate Frequency Value       *
*             RECOMB - The Recombination Rate Frequency Value   *
*             REST   - The Estimated Value for R.               *
```

```
*              NEST    - The Estimated Value for N.              *
*              NT      - The intermediate New Value of N.        *
*              RT      - The Intermediate New Value of R.        *
*                                                                *
******************************************************************
      INTEGER I, IFLAG
      REAL HSTART,HMIN,HMAX,RTOL,RERR,Q,R,DT,RECOMB,IR,REST,
     +     NERR,NEST
      DOUBLE PRECISION RQ, RR, NQ, NR
      OPEN (9, FILE = 'ARMY1', STATUS = 'NEW')
1     PRINT *, 'Input the Recombination Coefficient [RECOMB]:'
      READ *, RECOMB
      PRINT *, 'Input the Collision Frequency [IR]:'
      READ *, IR
      PRINT *, 'Input the Initial Derivative Value [NQ]:'
      READ *, NQ
      PRINT *, 'Do You Want the Results Saved [1-yes, 0-no]?'
      READ *, IFLAG
      HSTART = 0.01
      HMIN = 1E-6
      RTOL = 1E-6
      HMAX = 0.01
      R = 1.
      RQ = 0.
      DT = 0.01
      PRINT 75
      PRINT 100, R, NQ, RQ, R, R, HSTART
      Q = 1.
      IF (IFLAG .EQ. 1) WRITE (UNIT = 9, FMT = *) Q, RQ
      DO 5 I = 1,99
        R =  1. - (I - 1) * DT
        Q = 1. - I * DT
        CALL DESOLV (Q,R,NQ,NR,RQ,RR,RTOL,HSTART,HMIN,HMAX,
     +               IFLAG,NERR,RERR,RECOMB,IR)
        IF (IFLAG .EQ. 3) GOTO 10
        PRINT 100, Q, NR, RR, NERR, RERR, HSTART
        IF (IFLAG .EQ. 1) WRITE (UNIT = 9, FMT = *) Q, RR
        NQ = NR
        RQ = RR
5     CONTINUE
      IF (IFLAG .EQ. 0) GOTO 1
      GOTO 50
10    PRINT *,'Algorithm failed.  Last point was [R,NOLD,ROLD]:'
      PRINT *, Q, NR, RR
50    CONTINUE
75    FORMAT (//,T5,'r',T14,'N(r)',T28,'R(r)',T39,'N Rel Err',
     +        T53,'R Rel Err',T66,'HSTART',/,73(1H-))
100   FORMAT (T2,F5.2,T9,E12.5,T23,E12.5,T37,E12.5,T51,E12.5,
     +        T65,F7.4)
      CLOSE (9)
      END
```

```
      SUBROUTINE RKF (NOLD, NNEW, ROLD, RNEW, NEST, REST, INC,
     +                RECOMB, IR, R)
*****************************************************************
*                                                               *
*  The Runge Kutta fourth / fifth order method to estimate      *
*  the next value of N(r) & R(r) and their estimated error.     *
*                                                               *
*****************************************************************
      INTEGER I, IFLAG
      REAL NEST,REST,INC,NK1,NK2,NK3,NK4,NK5,NK6,Q,R,DT,IR,
     +     RK1,RK2,RK3,RK4,RK5,RK6,RECOMB,RTOL,RERR,NERR,RN
      DOUBLE PRECISION ROLD,RNEW,NOLD,NNEW,NT,RT
*****************************************************************
*                                                               *
*     Define the Runge Kutta coefficients.                      *
*                                                               *
*****************************************************************
      B21 = 1. / 4.
      B22 = 3. / 8.
      B23 = 12. / 13.
      B31 = 3. / 32.
      B32 = 9. / 32.
      B41 = 1932. / 2197.
      B42 = -7200. / 2197.
      B43 = 7296. / 2197.
      B51 = 439. / 216.
      B52 = -8.
      B53 = 3680. / 513.
      B54 = -845. / 4104.
      B61 = -8. / 27.
      B62 = 2.
      B63 = -3544 / 2565.
      B64 = 1859. / 4104.
      B65 = -11. / 40.
      A1 = 25. / 216.
      A3 = 1408. / 2565.
      A4 = 2197. / 4104.
      A5 = -1. / 5.
      R1 = 1. / 360.
      R3 = -128. / 4275.
      R4 = -2197. / 75240.
      R5 = 1. / 50.
      R6 = 2. / 55.
      NT = NOLD
      RT = ROLD
```

```
*****************************************************************
*                                                               *
*      Begin the Runge Kutta numerical analysis.                *
*                                                               *
*****************************************************************
      RN = R
      NK1 = -NT/RN + RECOMB*RT*RT - IR*RT
      RK1 = NT
      NT = NOLD + INC * B21 * NK1
      RT = ROLD + INC * B21 * RK1
      RN = R + INC * B21
      NK2 = -NT/RN + RECOMB*RT*RT - IR*RT
      RK2 = NT
      NT = NOLD + INC * (B31*NK1 + B32*NK2)
      RT = ROLD + INC * (B31*RK1 + B32*RK2)
      RN = R + INC * B22
      NK3 = -NT/RN + RECOMB*RT*RT - IR*RT
      RK3 = NT
      NT = NOLD + INC * (B41*NK1 + B42*NK2 + B43*NK3)
      RT = ROLD + INC * (B41*RK1 + B42*RK2 + B43*RK3)
      RN = R + INC * B23
      NK4 = -NT/RN + RECOMB*RT*RT - IR*RT
      RK4 = NT
      NT = NOLD + INC * (B51*NK1+B52*NK2+B53*NK3+B54*NK4)
      RT = ROLD + INC * (B51*RK1+B52*RK2+B53*RK3+B54*RK4)
      RN = R + INC
      NK5 = -NT/RN + RECOMB*RT*RT - IR*RT
      RK5 = NT
      NT = NOLD+INC*(B61*NK1+B62*NK2+B63*NK3+B64*NK4+B65*NK5)
      RT = ROLD+INC*(B61*RK1+B62*RK2+B63*RK3+B64*RK4+B65*RK5)
      NNEW = NOLD + INC * (A1*NK1 + A3*NK3 + A4*NK4 + A5*NK5)
      RNEW = ROLD + INC * (A1*RK1 + A3*RK3 + A4*RK4 + A5*RK5)
      RN = R + INC / 2.
      NK6 = -NT/RN + RECOMB*RT*RT - IR*RT
      RK6 = NT
      NEST = R1*NK1 + R3*NK3 + R4*NK4 + R5*NK5 + R6*NK6
      REST = R1*RK1 + R3*RK3 + R4*RK4 + R5*RK5 + R6*RK6
      RETURN
      END
```

```
      SUBROUTINE GAMCAL (Q,R,NOLD,ROLD,NEST,REST,RTOL,GAMMA)
*****************************************************************
*                                                               *
* The method to evaluate the necessary step size for the        *
* given tolerance levels and precalculated estimated error.    *
* The mixed control is evaluated here using both the relat.     *
* and absolute tolerances.                                      *
*                                                               *
*****************************************************************
      DOUBLE PRECISION NOLD,ROLD
      REAL T1,T2,ABSEST,NEST,REST,Q,R,RTOL
      IF (NEST .NE. 0.) THEN
        T1 = ABS (NOLD / NEST)
      ELSE
        T1 = 1E30
      ENDIF
      IF (REST .NE. 0.) THEN
        T2 = ABS (ROLD / REST)
      ELSE
        T2 = 1E30
      ENDIF
      ABSEST = MIN (T1,T2)
*****************************************************************
*                                                               *
* Calculate the gamma value for the variable step algorithm.    *
*                                                               *
*****************************************************************
      IF (ABSEST .EQ. 0.) GOTO 1
      GAMMA = (RTOL * ABSEST / (R - Q)) ** 0.25
      RETURN
1     T1 = MAX (NEST,REST,RTOL/10)
      GAMMA = (RTOL * RTOL / (T1 * (R - Q))) ** 0.25
      RETURN
      END
```

```
      SUBROUTINE DESOLV (Q,R,NQ,NR,RQ,RR,RTOL,HSTART,HMIN,
     +                   HMAX,IFLAG,NERR,RERR,RECOMB,IR)
*****************************************************************
*                                                               *
* The main subroutine combining the Runge Kutta algorithm       *
* along with the variable step size calculation for a given*
* interval [Q,R].  Minimum and Maximum step sizes are neede*
* This subroutine is terminated if the calculated step size*
* is less than the minimum step size provided.                  *
*                                                               *
*****************************************************************
      INTEGER IFLAG
      REAL Q,R,HSTART,HMIN,HMAX,RTOL,RERR,NERR,NEXT,REST,
     +     HOLD,DT,T,NEST,RECOMB,IR
      DOUBLE PRECISION NQ,NR,RQ,RR,ROLD,RNEW,NNEW,NOLD
      HOLD = HSTART
      T = R
      NOLD = NQ
      ROLD = RQ
*****************************************************************
*                                                               *
*  Using given parameters, the new value and required step      *
*  size is calculated.                                          *
*                                                               *
*****************************************************************
1     CALL RKF (NOLD,NNEW,ROLD,RNEW,NEST,REST,HOLD,RECOMB,IR,T)
      CALL GAMCAL (Q,T,NOLD,ROLD,NEST,REST,RTOL,GAMMA)
      HNEW = (0.8) * GAMMA * HOLD
      IF (GAMMA .GE. 1.) GOTO 2
      IF (HNEW .LT. HOLD/10.) HNEW = HOLD / 10.
      IF (HNEW .LT.HMIN) GOTO 3
      HOLD = HNEW
      GOTO 1
*****************************************************************
*                                                               *
*     Calculated new value for R is acceptable, and next        *
*     parameters are established.                               *
*                                                               *
*****************************************************************
2      IF (HNEW .LT. HMIN) GOTO 3
       IF (HNEW .GT. 5.*HOLD) HNEW = 5. * HOLD
       IF (HNEW .GT. HMAX) HNEW = HMAX
       IF (T-HOLD .LE. Q) GOTO 4
       T = T - HOLD
       HOLD = HNEW
       NOLD = NNEW
       ROLD = RNEW
       GOTO 1
```

```
*****************************************************************
*                                                               *
*      Algorithm failure flag and last values are set.          *
*                                                               *
*****************************************************************
3       IFLAG = 3
        R = T
        NR = NOLD
        RR = ROLD
        RETURN
*****************************************************************
*                                                               *
*  Computation of final step in interval, along with the        *
*  relative and absolute errors (of that final step).           *
*                                                               *
*****************************************************************
4       CONTINUE
        HSTART = HNEW
        HOLD = T-Q
        CALL RKF (NOLD,NNEW,ROLD,RNEW,NEST,REST,HOLD,RECOMB,IR,T)
        NR = NNEW
        RR = RNEW
        IF (RR .EQ. 0.) THEN
          RERR = 1.
        ELSE
          RERR = ABS(REST / RR)
        ENDIF
        IF (NR .EQ. 0.) THEN
          NERR = 1.
        ELSE
          NERR = ABS(NEST / NR)
        ENDIF
        RETURN
        END
```